

Synchronization frequency analysis and stochastic simulation of multisite flood flows based on the complicated vine-copula structure

Xinting Yu, [Yue-Ping Xu](#), Yuxue Guo, Siwei Chen, [Haiting Gu*](#)

Institute of Water Science and Engineering, Civil Engineering and Architecture, Zhejiang University, Hangzhou, 310058, China

Correspondence to: [Haiting Gu \(ght000@zju.edu.cn\)](mailto:ght000@zju.edu.cn)

Abstract: Accurately modeling and predicting flood flows across multiple sites within a watershed presents significant challenges due to potential issues of insufficient accuracy and excessive computational demands in existing methodologies. In response to these challenges, this study introduces a novel approach centered around the use of vine copula models, termed RDV-Copula (Reduced-dimension vine copula construction approach). The core of this methodology lies in its ability to integrate and extract complex data information before constructing the copula function, thus preserving the intricate spatial-temporal connections among multiple sites while substantially reducing the vine copula's complexity. This study performs a synchronization frequency analysis using the devised copula models, offering valuable insights into flood encounter probabilities. Additionally, the innovative approach undergoes validation by comparison with three benchmark models, which vary in dimensions and nature of variable interactions. Furthermore, the study conducts stochastic simulations, exploring both unconditional and conditional scenarios across different vine copula models. Applied in the Shifeng Creek watershed, China, the findings reveal that vine copula models are superior in capturing complex variable relationships, demonstrating significant spatial interconnectivity crucial for flood risk prediction in heavy rainfall events. Interestingly, the study observes that expanding the model's dimensions does not inherently enhance simulation precision. The RDV-Copula method not only captures comprehensive information effectively but also simplifies the vine copula model by reducing its dimensionality and complexity. This study contributes to the field of hydrology by offering a refined method for analyzing and simulating multisite flood flows.

29 1 Introduction

30 Floods are the most frequent natural disaster, inflicting substantial economic losses, environmental
31 degradation and human casualties (Teng et al., 2017). As ~~is~~-reported by Centre for Research on the
32 Epidemiology of Disasters (CRED), floods represented 45.6% of worldwide natural disasters in 2022,
33 affecting an average of 57.1 million people annually (CRED,2023). The data also indicated a 4.76%
34 increase in flood occurrences in 2022 compared to the annual average from 2002 to 2021(CRED,2023).
35 Therefore, it is very meaningful and essential to analyze flooding and achieve flood risk control. At the
36 watershed scale, flood risk is primarily influenced by rainfall patterns and interconnections among sub-
37 watersheds. Large floods often result from the merging of floods from multiple sub-watersheds~~Large~~
38 ~~floods often result from the amalgamation of floods from multiple sub-watersheds~~ (Prohaska and Ilic,
39 2010). Concurrent flood events cause runoff from various sources to merge, forming large floods that
40 pose threats to downstream regions. As a result, analyzing the runoff at various sites not only provides a
41 better understanding of the flood characteristics within the watershed, but also contributes to the
42 development of flood control programs to avoid flood risks.

43 There are currently many techniques for analyzing hydrological variables. Common univariate
44 methods include statistical analyses such as frequency analysis (Stedinger et al., 1993), extreme value
45 theory (Coles, 2001), and time series analysis methods like the Autoregressive Integrated Moving
46 Average (ARIMA) model (Box et al., 2013). However, univariate analyses often fall short in accurately
47 estimating the risks associated with extreme events due to their inability to account for the
48 interdependence of variables (Khan et al., 2023). This oversight can lead to significant underestimation
49 or overestimation of risks, particularly given the inherent relationships among variables within a
50 catchment. To address the complexity of these relationships across multiple variables, researchers have
51 turned to multivariate analysis techniques. Methods such as Autoregressive (AR) models are utilized for
52 analyzing temporal correlations (Box et al., 2013), while spatial relationships can be examined using
53 techniques like geostatistical methods (Isaaks and Srivastava, 1989), spatial regression models (Bekker
54 and Wansbeek, 2001), Copula functions (Sklar, 1959) and Bayesian hierarchical models (Gelman et al.,
55 2013). However, these methods have their limitations. AR models, while effective for temporal analysis,
56 do not account for spatial dependencies. Geostatistical methods and spatial regression models focus
57 primarily on spatial relationships but may struggle with temporal dynamics. Bayesian hierarchical

58 models can handle complex dependencies but often involve high computational demands and require
59 substantial prior information. In contrast, copula functions offer substantial advantages when dealing
60 with multivariate spatial-temporal relationships. They provide a flexible framework for modeling
61 dependencies between variables without assuming a specific marginal distribution, allowing for a more
62 accurate representation of complex interdependencies. Later adopted in hydrology by De Michele and
63 Salvadori (2003), copula functions link multidimensional probability distribution functions to their one-
64 dimensional margins, preserving both the dependence structure and the distinct distribution
65 characteristics of random variables (Tosunoglu et al., 2020). Copula functions ~~is~~are widely applied in
66 hydrological fields, including the joint frequency analysis (Liu et al., 2018; Zhang et al., 2021), water
67 resources management (Gao et al., 2018; Nazeri Tahroudi et al., 2022), wetness-dryness encountering
68 (Wang et al., 2022; Zhang et al., 2023), flood risk assessment (Li et al., 2022; Tosunoglu et al., 2020;
69 Zhong et al., 2021) , water quality analysis (Yu et al., 2020; Yu and Zhang, 2021), precipitation model
70 (Gao et al., 2020; Nazeri Tahroudi et al., 2023; Tahroudi et al., 2022) and so on.

71 Despite the broad application of conventional copula functions to create joint distributions for
72 multiple variables, their capacity to accurately represent high-dimensional realities is constrained. This
73 limitation arises from their reliance on a single parameter to describe correlations and a simplistic
74 approach to model the dependence structure between variables (Aas et al., 2009; Daneshkhah et al., 2016).
75 To overcome these limitations, Bedford and Cooke (2002) proposed a reliable way called Vine Copula
76 to construct complex multivariate models with high dependency. Vine copula construction relies
77 exclusively on the principle of breaking down the complete multivariate density into a series of simple,
78 foundational components through conditional independence or pair-copula constructs. There are two
79 main types of vine structures: C-Vine and D-Vine (Brechmann and Schepsmeier, 2013). The former
80 presents star-shaped configurations, while the latter displays path-like structures, providing enhanced
81 flexibility in constructing the joint distribution of multiple variables by enabling the use of different types
82 of bivariate copulas for each pair, thus accommodating a diverse range of dependency structures (Aas et
83 al., 2009; Çekin et al., 2020).

84 Vine copulas are increasingly applied in hydrological studies to model complex relationships among
85 multiple variables. For instance, Ahn (2021) developed a D-vine copula-based model to estimate flows
86 in catchments with limited or partial gauging, focusing on the temporal relationship of runoff at a specific

87 site. This model employed a six-dimensional copula structure centered around annual runoff, using
88 conditional simulation to compensate for missing data. Wang et al. (2022) explored the joint distribution
89 of multi-inflows to assess wetness-dryness conditions, highlighting spatial interconnections across three
90 water systems but ignoring the temporal influences within each system on the overall assessment. Unlike
91 the above studies, Xu et al. (2022) developed a stepwise and dynamic C-vine copula-based conditional
92 model (SDCVC) to incorporate the non-stationarity into a monthly streamflow prediction. This model
93 synthesizes the temporal and spatial relationships at multiple sites, developing a four-dimensional C-vine
94 copula for dual-site monthly streamflow forecasts. The term "four dimensions" relates to the categories
95 of variables involved, such as rainfall, downstream station streamflow, among others. Integrating
96 temporal and spatial relationships in copula construction allows for a more comprehensive data inclusion,
97 facilitating enhanced modeling of complex inter-variable relationships. However, challenges arise as the
98 number of sites or the analysis period extends, leading to increased complexity and dimensionality of the
99 copula function. This complexity can complicate the copula structure's determination ~~copula's structure~~
100 ~~determination~~, inflate computational demands during parameter fitting, and potentially diminish the
101 accuracy of stochastic simulations. To bridge this gap, this study aims to propose a new approach to
102 achieve dimensionality reduction while ensuring the complete access of spatial-temporal relationships
103 for multiple sites. The primary focus is to filter effective information to fully incorporate runoff data from
104 each site and mitigate the complexity of the vine copula function, thereby preventing poor model fitting
105 due to increased computational effort.

106 Moreover, understanding the spatial and temporal relationships of runoff across multiple sites within
107 a catchment is essential for effective flood control and water resources management. Synchronization
108 probability analysis and stochastic simulation of streamflow sequences play a pivotal role in these
109 processes (Chen et al., 2015). The terminology used to describe the encounter situations of wetness and
110 dryness varies; an asynchronous event refers to a scenario where such encounters do not occur
111 simultaneously, whereas both wetness-wetness and dryness-dryness encounters are considered
112 synchronous events. These encounters exist not only in diversion projects and multi-source water supply
113 systems, but also in main streams and tributaries at a watershed scale. They offer invaluable insights into
114 the spatial and temporal distribution of water resources, aiding in the preparation for anticipated future
115 events (Szilagyi et al., 2006). Copula-based simulation was first discussed in the study of Bedford and

116 Cooke (2001;2002). Subsequently, as more studies have been conducted, copula-based modeling and
117 simulation models for hydrological variables have demonstrated high performance (Gao et al., 2021;
118 Huang et al., 2018; Tahroudi et al., 2022). Utilizing stochastic simulation to generate sets of runoff
119 sequences from multiple sites not only allows for a more progressive test of the effectiveness of the vine
120 copula function in fitting the relationship, but also provides a data base for flood control scheduling in
121 making decisions.

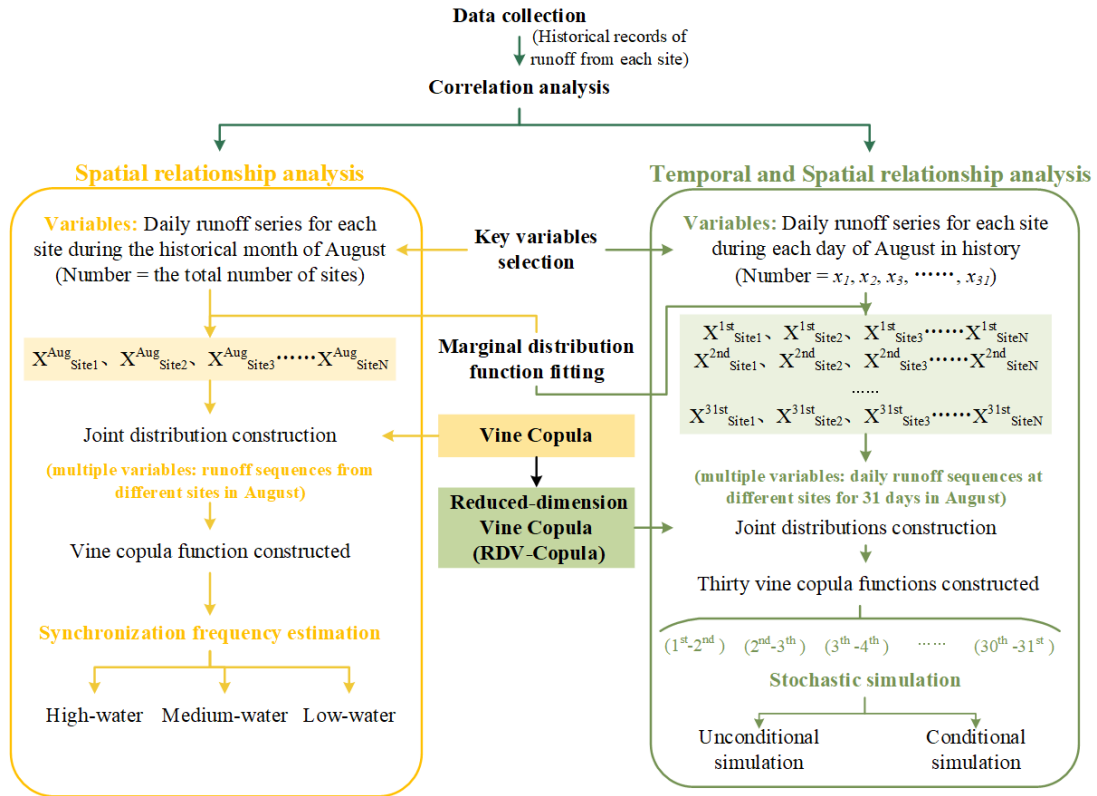
122 The basic task of this study is to construct the relationship functions of runoff across multiple sites
123 within a catchment using the vine copula. By leveraging the copula model, the frequency of flood
124 encounters for multiple runoffs is calculated to further analyze the intrinsic spatial and temporal
125 relationship characteristics. Addressing the challenge of dimensionality disaster caused by excessive
126 variables, this study proposes a novel approach to reduce the dimensionality by filtering the effective
127 information under the premise of fully incorporating the runoff information from each site. This approach
128 makes it possible to access the spatial and temporal relationships of runoff from multiple sites in the
129 catchment more accurately and efficiently. In addition, more reality-oriented simulation results can be
130 obtained, which provide statistical support for flood control and scheduling decision-making.

131 This paper is structured as follows: Section 2 outlines the proposed methodology's framework.
132 Section 3 presents the application of this methodology through a case study. The results are detailed in
133 Section 4, while Section 5 provides a thorough analysis and discussion of the results. Finally, Section 6
134 concludes the paper by summarizing the principal conclusions.

135 **2 Methodology**

136 The framework of this study is shown in Figure 1. This Section focuses on constructing and applying
137 multivariate joint distribution functions based on the vine copula function. It is divided into two cases:
138 one considering only spatial relations and the other combining spatial and temporal relations. Utilizing
139 the data characteristics, it describes how to build a vine copula function based on multiple variables and
140 details the processes of synchronization frequency analysis and stochastic simulation with the
141 constructed vine copula function. Additionally, it presents a new approach called the reduced-dimension
142 vine copula (RDV-Copula).

Joint distribution among multiple variables by vine copula function



143

144 **Figure 1. Framework of proposed methodology**

145 2.1 Joint distribution of multiple variables

146 Before identifying the dependence relationships among multi-variables, their correlations need to be
 147 analyzed and judged. Kendall's correlation coefficient, a nonparametric statistic, serves to measure the
 148 correlation degree between two variables, making it suitable for nonlinear relationships and categorical
 149 variables. In this study, vine copula functions are constructed to achieve synchronization frequency and
 150 stochastic simulation of multiple streamflow sequences. To more accurately simulate the temporal and
 151 spatial relationships, the correlations among multi-site streamflow series are determined by calculating
 152 the Kendall correlation coefficients.

153 2.1.1 Marginal distribution function

154 To build the dependence structure of hydrological variables using copulas, it is essential to determine the
 155 marginal distribution of each variable first. Given that the marginal distribution function for each
 156 characteristic variable is not predetermined and the skewness of their probability distributions varies
 157 (Zhong et al., 2021), it becomes crucial to consider multiple marginal distribution functions as candidates.

158 In this study, a comprehensive comparison is conducted among 12 commonly utilized distributions
 159 (Tosunoğlu, 2018), including Gamma distribution (gamma), Exponential distribution (exp), Pearson-III
 160 distribution (p3), Generalized extreme value distribution (gev), Inverse gaussian distribution (invgauss),
 161 Normal distribution (norm), Logistic distribution (logis), Log-normal distribution (lnorm), Log-logistic
 162 distribution (llogis), Generalized pareto distribution (gpd), Weibull distribution (weibull) and Gumbel
 163 distribution (gumbel). According to the goodness-of-fit test and AIC minimum criterion, the optimal
 164 distribution functions are selected as the marginal functions of the characteristic variables. The specific
 165 details of different distributions, such as the probability distribution function and the respective
 166 parameters, are displayed in Appendix A.

167 **2.1.2 Vine copula function theory**

168 Copula functions, first introduced in 1959, represent a multivariate joint probability distribution function
 169 within the unit square $[0, 1]$, featuring uniform marginal distributions. According to Sklar's theorem
 170 (Sklar, 1959), for a multivariate random variable $x_1, x_2, x_3, \dots, x_d$, there exist marginal distributions
 171 $u_1 = f_1(x_1), u_2 = f_2(x_2), u_3 = f_3(x_3), \dots, u_d = f_d(x_d)$ and joint distribution $f(x_1, x_2, x_3, \dots, x_d)$,
 172 then there exists a copula function C_θ such that

$$173 f(x_1, x_2, x_3, \dots, x_d) = C_\theta[f_1(x_1), f_2(x_2), \dots, f_d(x_d)] = C_\theta(u_1, u_2, \dots, u_d) \quad (1)$$

174 If $f_1(x_1), f_2(x_2), \dots, f_d(x_d)$ are continuous functions, then C is unique. θ represents an
 175 explicit parameter to the function.

176 The multivariate conditional density function can be represented as:

$$177 f(x|v) = C_{xv_j|v_{-j}}(F(x|v_{-j}), F(v_j|v_{-j})) f(x|v_{-j}) \quad (2)$$

178 where v_j denotes a component of the n -dimensional vector v , while v_{-j} denotes the $(n-1)$ -dimensional
 179 vector with v_j removed.

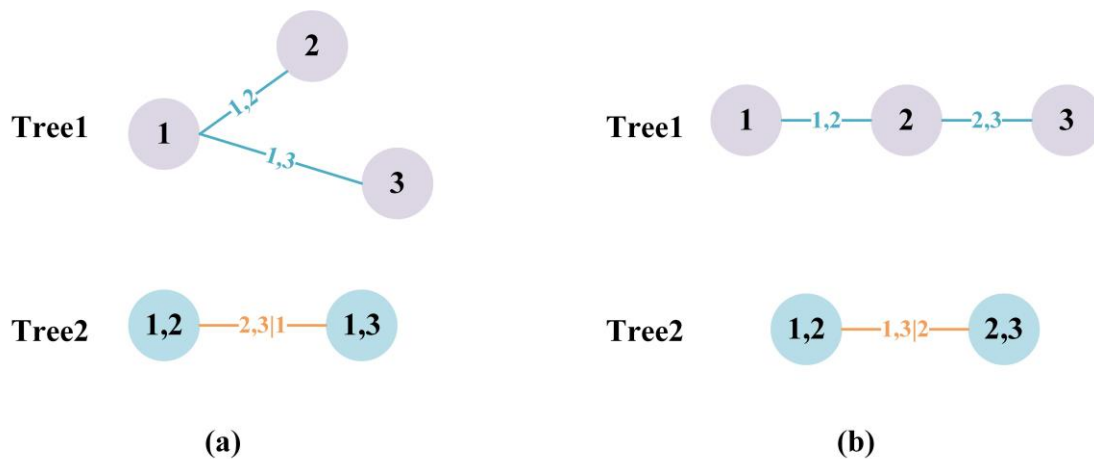
180 The term $f(x|v)$ in each conditional density function can be denoted as:

$$181 F(x|v) = \frac{\partial C_{xv_j|v_{-j}}(F(x|v_{-j}), F(v_j|v_{-j}))}{F(v_j|v_{-j})} \quad (3)$$

182 The copula function, essentially, acts as a transformation function that connects the joint distribution
 183 of multiple variables to the marginal distributions. There are a number of alternative copula families that
 184 can be selected for the construction of modeling dependence, such as Gaussian copula, t-copula, Clayton
 185 copula, Gumbel copula, Frank copula and so on. However, the construction of high-dimensional copula

186 functions is often constrained by parameter limitations and computationally demanding. Bedford and
 187 Cooke (2002) introduced a more advanced and flexible alternative method of constructing the
 188 dependence structure called Vine Copula. Also later called pair-copula construction by Aas et al. (2009),
 189 vine copulas decompose the joint density function into a cascade of building blocks of the bivariate
 190 copulas. Assuming that there are d variables given to us, it is possible by this method to decompose the
 191 d -dimensional joint distribution into $d(d - 1)/2$ pair copulas densities. In vine copula structure, the
 192 vine consists of a series of trees, nodes, and edges. The trees represent the layers. Each layer contains
 193 several nodes and the connections between the nodes are called the edges. The nodes in the first tree
 194 represent the marginal distributions of each variable. Each edge represents a pair-copula joint distribution
 195 function of two adjacent nodes. The edges in each tree, except the last tree, are used as nodes in the next
 196 tree. There are two subsets of regular vines in commonly use: canonical vines (C-vines) and drawable
 197 vines (D-vines). Both types of vine-copula have their own specific way of decomposing the density
 198 function.

199 ~~C-vine is suitable for structures with a key variable that has a significant correlation with the~~
 200 ~~remaining other variables. However, in D-vine structure, each node is linked to at most two edges. In the~~
 201 C-vine copula structure, each tree features a central node that is connected to all other edges, as illustrated
 202 in Figure 2(a). C-vine is suitable for structures with a key variable that has a significant correlation with
 203 the remaining other variables. In contrast, in the D-vine copula structure, each node is connected to no
 204 more than two edges, as depicted in Figure 2(b). The order of dependencies between variables can be
 205 determined by one after the other. The expressions for the n -dimensional joint probability density of C-
 206 vine and D-vine are shown in Equations (4) and (5).



207

208 Figure 2. The vine structures for the given order of 3 variables in (a) the C-vine copula and (b) the D-
 209 vine copula

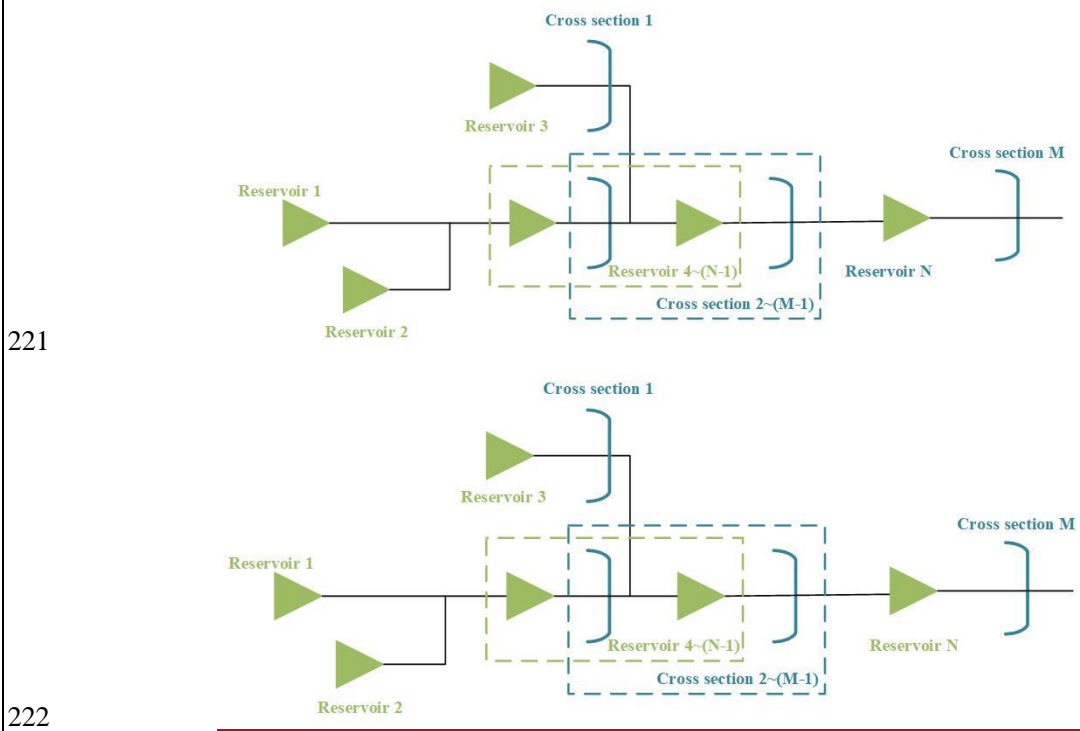
210 $f(x_1, \dots, x_d) = \left[\prod_{j=1}^{d-1} \prod_{i=1}^{d-j} c_{j,j+1|1,\dots,j-1} \right] \cdot \left[\prod_{k=1}^d f_k(x_k) \right]$ (C-vine) (4)

211 $f(x_1, \dots, x_d) = \left[\prod_{j=1}^{d-1} \prod_{i=1}^{d-j} c_{i,(i+j)|(i+1),\dots,(i+j-1)} \right] \cdot \left[\prod_{k=1}^d f_k(x_k) \right]$ (D-vine) (5)

212 where $c(\cdot)$ refers to the bivariate copula with index i running over the edges for each tree and index j
 213 identifying the trees, $f_k(x_k)$ denotes the marginal density.

214 **2.2 Estimation of inflow synchronization frequency**

215 A distinct advantage of the copula method lies in its precision in analyzing inflow encounter probabilities
 216 and conditional probabilities. In this study, a synchronization event is defined as the simultaneous
 217 occurrence of inflows of similar magnitudes from multiple sites. We categorize the flow into three levels:
 218 high, medium, and low. The frequencies associated with high-water and low-water events are set as $P_h =$
 219 37.5% and $P_l = 62.5\%$. It is assumed that there is a generalized reservoir group scheduling system, as
 220 shown in Figure 32. The system encompasses N reservoirs and M flood control cross sections.



221
 222
 223 **Figure 32. Schematic diagram of the generalized system in the catchment**

224 We can generalize all reservoirs and cross-sections to multiple sites within the watershed system.
 225 Each of these sites may be exposed to incoming flows when rainfall occurs. Let X_{ph} and X_{pl} be the

226 amounts of water corresponding to P_h and P_l , respectively. $X_i > X_{ph}$ corresponds to high-water (H),
 227 $X_i < X_{pl}$ corresponds to low-water (L), and $X_{pl} < X_i < X_{ph}$ corresponds to medium-water (M), where
 228 X_i denotes the inflow of day i .

229 Let the inflows of the different sites be represented by $X^1, X^2, X^3, \dots, X^{N+M}$.
 230 $X_{ph}^1, X_{ph}^2, X_{ph}^3, \dots, X_{ph}^{N+M}$ represent the amounts of inflow corresponding to the high-water of these
 231 different sites respectively. Meanwhile, $X_{pl}^1, X_{pl}^2, X_{pl}^3, \dots, X_{pl}^{N+M}$ represent the amounts of inflow
 232 corresponding to the low-water of these different sites respectively. The marginal distribution functions
 233 are $u^1, u^2, u^3, \dots, u^{N+M}$, respectively. Specifically, $u_{ph}^1, u_{ph}^2, u_{ph}^3, \dots, u_{ph}^{N+M}$ denote the marginal
 234 distribution functions corresponding to the high-water inflow amounts $X_{ph}^1, X_{ph}^2, X_{ph}^3, \dots, X_{ph}^{N+M}$,
 235 capturing the probabilistic behavior of the inflows during high-water conditions at each site. Similarly,
 236 $u_{pl}^1, u_{pl}^2, u_{pl}^3, \dots, u_{pl}^{N+M}$ represent the marginal distribution functions for the low-water inflow amounts
 237 $X_{pl}^1, X_{pl}^2, X_{pl}^3, \dots, X_{pl}^{N+M}$, describing the inflow behavior during low-water conditions at these sites.

238 The number of possible inflow-state combinations increases with the number of sites, directly tied
 239 to the three distinct states (High/Medium/Low) identified for each site. For instance, with just two sites,
 240 there are nine unique combinations. The number of combinations expands to 27 for three sites, 81 for
 241 four sites, and 243 for five sites. The pattern continues similarly for additional sites. Take the
 242 combinations of four sites as an example, following the copula theory, $P(X^1 < x^1, X^2 < x^2) =$
 243 $f(u^1, u^2) = C(u^1, u^2)$ and $P(X > x) = 1 - P(X < x)$, the probability formulas of synchronization
 244 are derived as below.

245 (1) The probability of synchronized high-water is as follows:

$$\begin{aligned}
 & P(X^1 > X_{ph}^1, X^2 > X_{ph}^2, X^3 > X_{ph}^3, X^4 > X_{ph}^4) = 1 - u_{ph}^1 - u_{ph}^2 - u_{ph}^3 - u_{ph}^4 \\
 & + C(u_{ph}^1, u_{ph}^2) + C(u_{ph}^1, u_{ph}^3) + C(u_{ph}^1, u_{ph}^4) + C(u_{ph}^2, u_{ph}^3) + C(u_{ph}^2, u_{ph}^4) \\
 & + C(u_{ph}^3, u_{ph}^4) - C(u_{ph}^1, u_{ph}^2, u_{ph}^3) - C(u_{ph}^1, u_{ph}^2, u_{ph}^4) - C(u_{ph}^1, u_{ph}^3, u_{ph}^4) \\
 & - C(u_{ph}^2, u_{ph}^3, u_{ph}^4) + C(u_{ph}^1, u_{ph}^2, u_{ph}^3, u_{ph}^4)
 \end{aligned} \tag{6}$$

247 (2) The probability of synchronized medium-water is as follows:

$$\begin{aligned}
 & P = (X_{pl}^1 < X^1 < X_{ph}^1, X_{pl}^2 < X^2 < X_{ph}^2, X_{pl}^3 < X^3 < X_{ph}^3, X_{pl}^4 < X^4 < X_{ph}^4) \\
 & = C(u_{ph}^1, u_{ph}^2, u_{ph}^3, u_{ph}^4) - C(u_{ph}^1, u_{ph}^2, u_{ph}^3, u_{pl}^4) - C(u_{ph}^1, u_{ph}^2, u_{pl}^3, u_{ph}^4) \\
 & - C(u_{ph}^1, u_{pl}^2, u_{ph}^3, u_{ph}^4) - C(u_{pl}^1, u_{ph}^2, u_{ph}^3, u_{ph}^4) + C(u_{ph}^1, u_{ph}^2, u_{pl}^3, u_{pl}^4) \\
 & + C(u_{ph}^1, u_{pl}^2, u_{pl}^3, u_{pl}^4) + C(u_{pl}^1, u_{ph}^2, u_{pl}^3, u_{pl}^4) + C(u_{pl}^1, u_{pl}^2, u_{pl}^3, u_{ph}^4) \\
 & + C(u_{pl}^1, u_{pl}^2, u_{pl}^3, u_{pl}^4) + C(u_{pl}^1, u_{pl}^2, u_{ph}^3, u_{ph}^4) - C(u_{ph}^1, u_{pl}^2, u_{pl}^3, u_{pl}^4) \\
 & - C(u_{pl}^1, u_{ph}^2, u_{pl}^3, u_{pl}^4) - C(u_{pl}^1, u_{pl}^2, u_{pl}^3, u_{pl}^4) - C(u_{pl}^1, u_{pl}^2, u_{pl}^3, u_{ph}^4) \\
 & + C(u_{pl}^1, u_{pl}^2, u_{pl}^3, u_{pl}^4)
 \end{aligned} \tag{7}$$

249 (3) The probability of synchronized low-water is as follows:

250
$$P(X^1 < X_{pl}^1, X^2 < X_{pl}^2, X^3 < X_{pl}^3, X^4 < X_{pl}^4) = C(u_{pl}^1, u_{pl}^2, u_{pl}^3, u_{pl}^4) \quad (8)$$

251 **2.3 Stochastic simulation based on RDV-Copula functions**

252 **2.3.1 Reduced-dimension vine copula construction approach (RDV-Copula) for multi-variate**

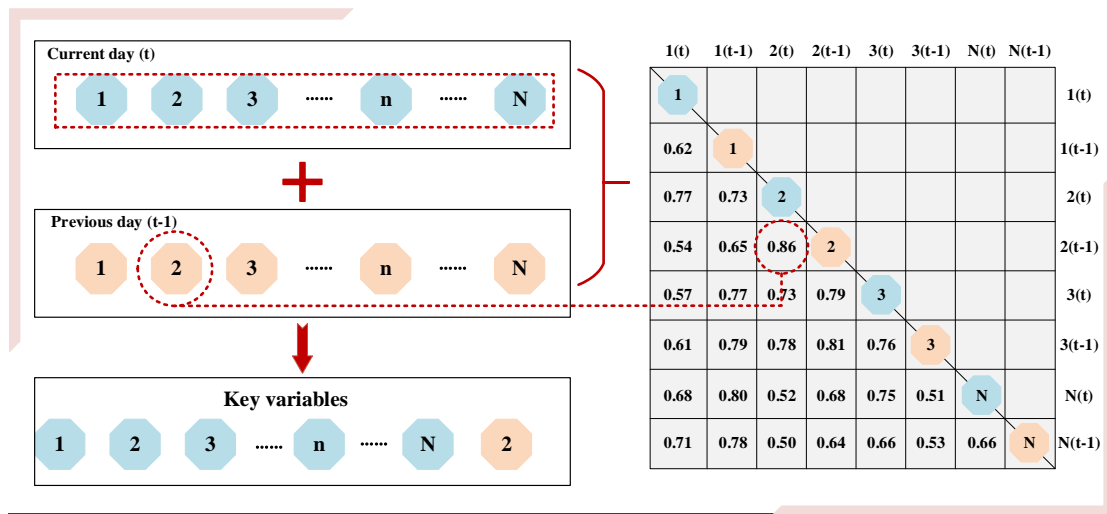
253 To construct joint distribution functions for multiple variables that encapsulate both temporal and spatial
 254 relationships, it is essential to incorporate a comprehensive range of information to efficiently capture
 255 the interconnections among variables.

256 Using the flow at N points within a catchment as an example, the relationships among the flows
 257 are analyzed. Given that these points reside within the same geographical region, it's highly likely that
 258 they are spatially related and the strength of the relationship is negatively correlated with spatial distance.
 259 Additionally, each site exhibits temporal correlations, such as the relationship between today's flow and
 260 that of the previous day(s), although for simplicity, this analysis assumes relevance only between
 261 consecutive days' flows. Incorporating both temporal and spatial dimensions into the analysis implies
 262 that for " N " sites, there should ideally be " $N + N$ " variables considered in constructing the copula
 263 function. As the number of sites grows, it simultaneously elevates the dimensionality of the copula,
 264 leading to increasingly complex structures. This complexity not only escalates computational efforts but
 265 also presents significant challenges in accurately fitting the model. To address this issue, our study
 266 introduces a novel methodology termed the Reduced-Dimension Vine Copula Construction Approach
 267 (RDV-Copula). This strategy aims to ~~extract~~ distill essential spatial-temporal information, thereby
 268 reducing the vine copula function's dimensionality to simplify the model structure.

269 The primary goal of this approach is to pinpoint the crucial variables necessary for effectively and
 270 efficiently representing the spatial-temporal relationships among different sites. The process begins by
 271 identifying variables to capture spatial relationships, under the assumption that the spatial relationships
 272 remain stable over short periods. Consequently, the current day's flows across all sites are selected as
 273 spatial variables, totaling N . Subsequently, the Kendall correlation coefficient between the current and
 274 previous day's flows is computed for each site, with the values ranked in descending order. The site with
 275 the highest Kendall coefficient is deemed the most temporally correlated, and its previous day's flow is
 276 also chosen as a key variable for the vine copula construction. Flows from the previous day at other sites
 277 are excluded from being key variables. Ultimately, this approach selects " $N + 1$ " key variables,

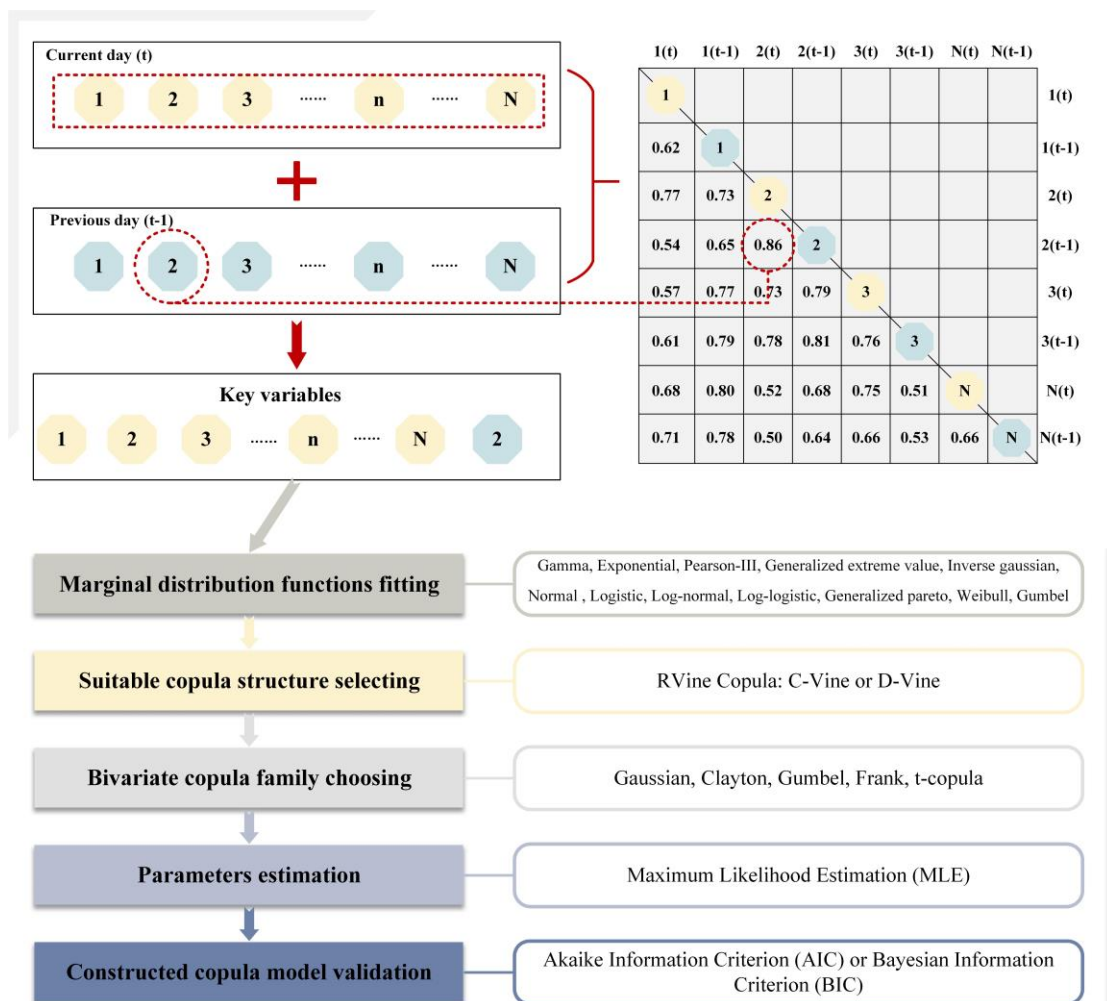
278 achieving an effective representation of spatial-temporal relationships while minimizing variable count.

279 The schematic diagram of the process is shown in Figure 43.



280

281 **Figure 3. Schematic diagram of the RDV Copula method**



282

283 **Figure 4. Schematic diagram of the RDV-Copula method**

284 After identifying the "N+1" key variables, the marginal distribution function for each variable is
285 determined, selecting the most appropriate distribution (e.g., Normal, Gamma) based on the
286 statistical characteristics of each variable. Using these marginal distributions, a suitable copula
287 structure is then selected, such as C-Vine or D-Vine, depending on the nature of dependencies among
288 the key variables. Next, for each pair of variables in the chosen vine structure, the most appropriate
289 bivariate copula family (e.g., Gaussian, Clayton, Gumbel) is selected to accurately capture their
290 dependencies. Subsequently, parameters for each selected pair-copula are estimated sequentially
291 using methods like Maximum Likelihood Estimation (MLE). Finally, the constructed copula model
292 is validated using statistical criteria such as the Akaike Information Criterion (AIC) or Bayesian
293 Information Criterion (BIC).

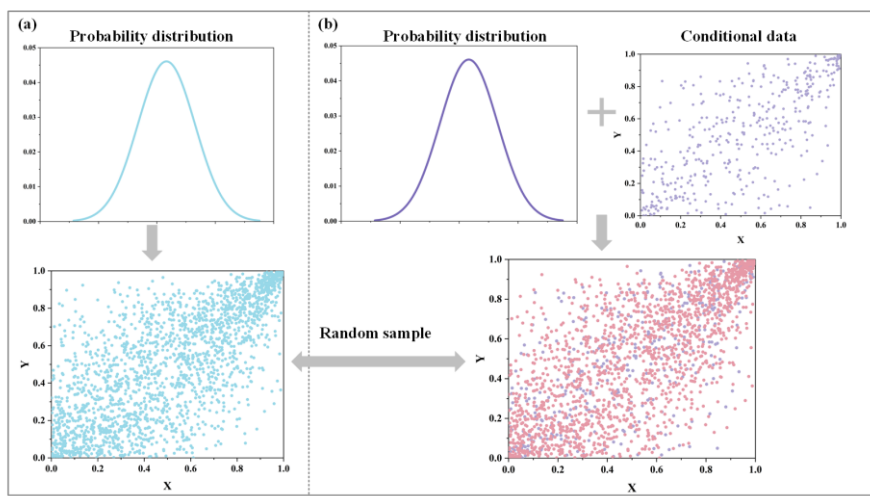
295 **2.3.2 Stochastic simulation**

296 Simulation methods for multivariate stochastic processes are categorized into two main types:
297 unconditional and conditional simulations, as delineated by Wu et al. (2015). ~~The core distinction~~
298 ~~between these two simulation methods hinges on whether certain data points are pre-determined at the~~
299 ~~time of simulation. The key difference between these two simulation methods lies in whether specific~~
300 ~~data points are known in advance before generating the simulation.~~ Figure 54(a) and (b) illustrate the
301 unconditional simulation and the conditional simulation, respectively.

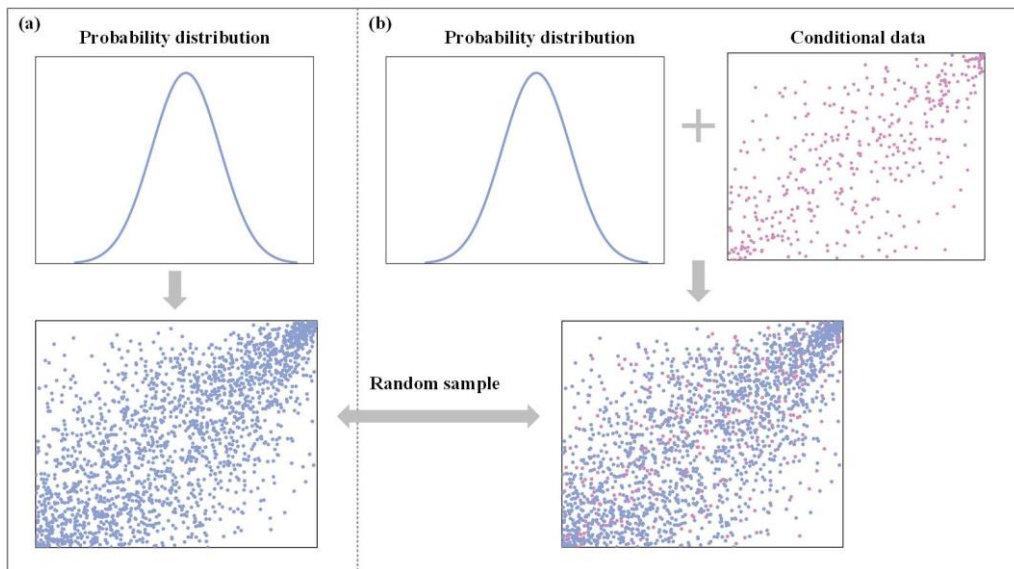
302 Unconditional simulation (Figure 5(a)): ~~This simulation approach generates stochastic samples~~
303 ~~solely based on the probability distribution of the dataset, without any prior knowledge of data states. All~~
304 ~~sample data are produced simultaneously through stochastic simulation, with each data point being in an~~
305 ~~unknown state prior to the simulation. This approach generates random samples based solely on the~~
306 ~~marginal probability distribution, without incorporating any existing data constraints. The probability~~
307 ~~distribution is shown in the upper-left plot, and random samples are generated simultaneously, resulting~~
308 ~~in the scatter plot below. The generated samples, represented by blue points, illustrate the joint variability~~
309 ~~according to their predefined marginal distributions. Since no prior information is used, each data point~~
310 ~~is in an unknown state before the simulation.~~

311 Conditional simulation (Figure 5(b)): ~~Conversely, conditional simulation operates under the premise~~
312 ~~that data at specific locations are already known. These known data points are then used to generate~~

313 ~~random samples, with the complete set of samples being produced based on both the probability~~
 314 ~~distribution of the data and the conditions set by the known variables. This method allows for a tailored~~
 315 ~~simulation that incorporates pre-existing data insights. In this scenario, the simulation takes into account~~
 316 ~~pre-existing data conditions. The marginal probability distribution is displayed in the top-center plot,~~
 317 ~~while the known conditional data is shown in the upper-right scatter plot (in pink). These known data~~
 318 ~~points act as a constraint for generating new random samples. The resulting scatter plot below (blue and~~
 319 ~~pink points) demonstrates how the conditional samples are influenced by both the marginal distribution~~
 320 ~~and the specified conditions of the known data. This method allows for a tailored simulation that~~
 321 ~~incorporates pre-existing data insights.~~



322



323

324 **Figure 54. Schematic diagram for generating random simulation samples (a) unconditional simulation (b)**

325 **conditional simulation**

326

327 Based on the presentation of each section in detail above, it can be generalized that stochastic
328 simulation based on the RDV-Copula function needs to go through the following steps.

329 Step 1: Collect as much historical data as possible.

330 Step 2: Correlation analysis is conducted on the collected data by calculating the Kendall's
331 coefficient.

332 Step 3: According to the method of filtering key variables proposed in Subsection 2.3.1, the
333 representative key variables are extracted based on the correlation relationship among multiple variables.

334 Step 4: Marginal distribution functions are fitted to the historical data series of the screened key
335 variables.

336 Step 5: Based on the proposed RDV-Copula approach, the joint distribution function of multi-site
337 runoff sequences is constructed with consideration of spatial-temporal relationships.

338 Step 6: The stochastic simulation sequences of runoff are generated by performing unconditional
339 stochastic simulation and conditional stochastic simulation based on the constructed vine copula
340 functions with different structures.

341 **3 Case study**

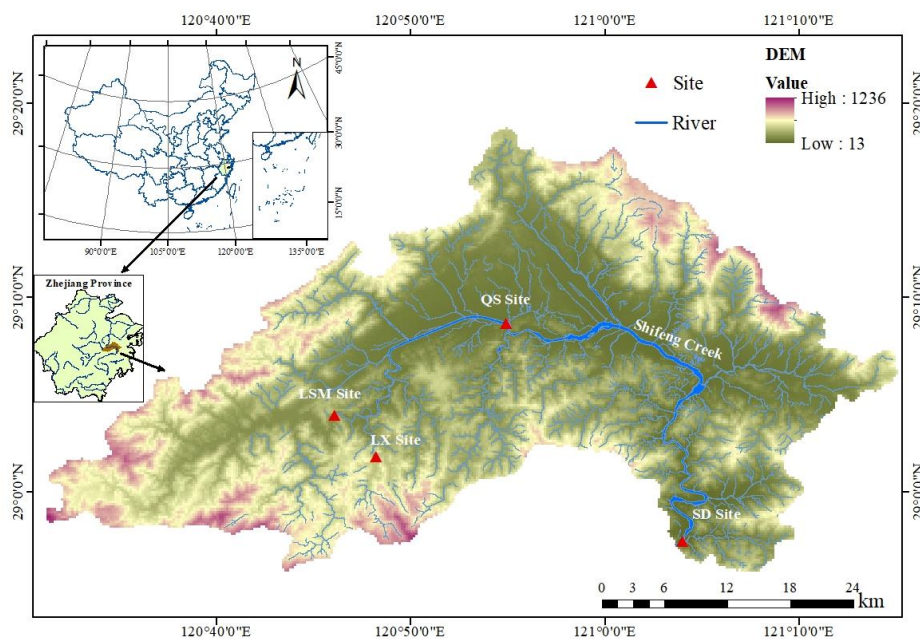
342 **3.1 Study area and data description**

343 This study applies its methodology to a case study focusing on constructing spatial-temporal
344 relationships within the Shifeng Creek area, located in the Jiaojiang River catchment in Eastern China.

345 The Jiaojiang River ranks as the third largest river in Zhejiang Province. As the primary tributary of the
346 Jiaojiang River basin and the principal watercourse in Tiantai County, Shifeng Creek plays a significant
347 role. Rainfall distribution in the Shifeng Creek catchment is notably uneven throughout the year, with a
348 substantial portion, approximately 70 to 80%, occurring from March to September. The remaining 20 to
349 30% of yearly rainfall is distributed over the other months. The period from July to September is
350 particularly marked by intense storms and rainfall, largely influenced by the Pacific subtropical high-
351 pressure system and the frequent occurrence of typhoons, contributing about 35% of the annual total
352 precipitation, with amounts ranging from 400 to 600mm.

353 The objective of this study is to delineate the spatial-temporal relationships of inflows within the

354 catchment during August, a flood-prone month, to enhance flood pattern understanding and support
 355 effective flood management strategies. In the Shifeng Creek region, there are many important hydraulic
 356 structures and critical control cross-sections. This study focuses on four major sites within the Shifeng
 357 Creek catchment: the Lishimen Reservoir (LSM) site, the Longxi Reservoir (LX) site, along with the
 358 Qianshan (QS) cross-section site and the Shaduan (SD) cross-section site. ~~These sites are strategically~~
 359 ~~located along the upper, middle, and lower stretches of Shifeng Creek, facilitating a comprehensive~~
 360 ~~analysis of the entire catchment and flood characteristics of Shifeng Creek.~~ These four sites were selected
 361 for their strategic importance within the Shifeng Creek catchment, covering the upper, middle, and lower
 362 reaches. The Lishimen (LSM) and Longxi (LX) reservoirs, both in the upper reaches, are vital for flood
 363 control, regulating inflows to reduce downstream flood risks. The Qianshan (QS) cross-section, in the
 364 middle reaches, and the Shaduan (SD) cross-section, in the lower reaches, serve as key flood control
 365 points. Analyzing flows at these sites enables better coordination of reservoir operations and prevents
 366 flood peak convergence, enhancing overall flood management. To achieve this, daily runoff data of
 367 August, covering a span from 2000 to 2020, ~~have been were~~ compiled. This dataset encompasses inflows
 368 for the LSM and LX reservoir sites, as well as flow data for the QS and SD cross-sections. The geographic
 369 positioning of Shifeng Creek is depicted in Figure 65.



370
 371 **Figure 65. Map of location of Shifeng Creek**

372 3.2 Numerical experiments setup

373 3.2.1 Synchronization frequency analysis based on spatial relationship

374 In this study, we employ the vine copula function to construct the joint distribution of runoff across four
375 sites, aiming to analyze the synchronization frequency of floods in August, a month identified as having
376 a high risk of flooding. The variables under consideration include the inflow from these four sites,
377 denoted as LSM-Aug, LX-Aug, QS-Aug, and SD-Aug. Our initial step involves calculating the Kendall
378 coefficients among these variables to assess their interdependencies. Following the methodology outlined
379 in Subsection 2.1.1, we determine the marginal distribution functions of the four variables through a
380 fitting test. Subsequently, based on the marginal distribution function of each variable, the joint
381 distribution function of four variables is constructed. The parameters of the vine copula are estimated via
382 the maximum likelihood method, with the Akaike Information Criterion (AIC) serving as the selection
383 criterion to ensure optimal model fit. Upon passing the fitting test, we identify the most appropriate vine
384 copula structure to accurately model the relationships among the variables.

385 With the four-dimensional vine copula function established, we proceed to calculate and analyze
386 the synchronization frequency of inflows as described in Subsection 2.2. The inflows at the four sites are
387 symbolized as LSM, LX, QS, and SD, with high-water and low-water inflow amounts represented as
388 X_{ph} , Y_{ph} , Z_{ph} , W_{ph} and X_{pl} , Y_{pl} , Z_{pl} and W_{pl} , respectively. The marginal distribution functions are
389 denoted as u , v , r and s .

390 Considering the three potential states (High/Medium/Low) at each site, a total of 81 possible inflow-
391 state combinations are identified. ~~Among these, the combinations [X-H, Y-H, Z-H, W-H], [X-M, Y-M,~~
392 ~~Z-M, W-M], and [X-L, Y-L, Z-L, W-L] are classified as synchronous, while the remainder are deemed~~
393 ~~asynchronous.~~ For ease of presentation, H, M, and L are then used as abbreviations for High, Medium,
394 and Low. Among the 81 combinations, the combinations [X-H, Y-H, Z-H, W-H], [X-M, Y-M, Z-M, W-
395 M], and [X-L, Y-L, Z-L, W-L] are classified as synchronous high-water, synchronous medium-water,
396 synchronous low-water, respectively, while the remainder are deemed asynchronous. The calculation
397 equations can be ~~provided refereneed~~ in Appendix B.

398 **3.2.2 Various vine copulas construction based on spatial-temporal relationships and stochastic**
399 **simulation**

400 To enhance the vine copula function's accuracy, it's imperative to integrate the temporal dimension into
401 its construction. In this section, the vine copula functions are developed on a daily basis, encompassing
402 a series of 31 copula models corresponding to each day of August, from the 1st to the 31st. Consequently,
403 both Kendall correlation analysis and the fitting of marginal distribution functions must be independently
404 conducted for the data spanning these 31 days. Following this preliminary analysis, 31 distinct
405 relationship functions are constructed, each tailored to the specific type of vine copula identified for each
406 day.

407 **3.2.2.1 RDV-Copula function construction**

408 Given that all four sites are situated within the Shifeng Creek watershed, their spatial interconnectivity
409 is inherent and can be leveraged in constructing a vine copula function. Additionally, the results of the
410 correlation analysis indicate that the correlation between the current day's runoff and the previous day's
411 runoff is the highest. While the data from two days ago no longer has much influence on the current day's
412 runoff data, so it can be excluded from the critical variable selection. Considering only the previous day's
413 contribution in the time dimension can effectively represent the time correlation while avoiding
414 unnecessary dimension increase. ~~due to the persisting effects of rainfall, the flow at any given site is also~~
415 ~~temporally linked to its previous day's flow. To encapsulate this temporal correlation, the~~This study
416 integrates the inflows from the four sites over two consecutive days. The inflows for the current day are
417 denoted as LSM, LX, QS, and SD, while those for the previous day are labeled LSM1, LX1, QS1, and
418 SD1, respectively.

419 The methodology, as detailed in Subsection 2.3, initiates by analyzing the current day's inflows at
420 the four sites to establish their spatial relationships. The subsequent step involves identifying the site
421 with the most significant correlation to its preceding day's inflow, which is then used as a ~~as a~~ variable
422 to represent the temporal relationship on that day. For instance, analysis between August 1st and 2nd
423 reveals that the LSM site had the highest correlation with its prior day's flow compared to the other sites.
424 Taking the construction of the copula function relationship between August 1st and August 2nd as an
425 example, the analysis reveals that the LSM site has the highest correlation with its previous day's flow
426 compared to the other three sites. As a result, a total of five key variables are determined for this

427 relationship set, including LSM, LX, QS, SD, and LSM1, effectively encompassing both temporal and
428 spatial correlations while streamlining the variable dimensions within the copula.

429 Due to the fundamental difference in structure between C-vine and D-vine copula, this study
430 constructs five-dimensional RDV-Copula functions based on these two types, respectively, labeled as
431 RDV-Cvine and RDV-Dvine. These two types of models should first be evaluated against each other on
432 various indexes, including AIC, BIC, and Loglik, to ascertain the most suitable five-dimensional RDV-
433 Copula structure. ~~This chosen structure~~ The RDV-Copula structure with better index values is then further
434 compared with other copula functions to validate its efficacy.

435 3.2.2.2 Benchmark copula functions construction

436 To validate the effectiveness of the RDV-Copula approach, this study compares it against a series of
437 benchmark copula functions. These benchmarks are constructed by applying various combinations of
438 multiple variables and stochastic simulation approaches to the existing data, resulting in vine copula
439 models of differing dimensions. The specifics of these vine copula models are summarized as follows
440 and illustrated in Figure 76.

441 **Benchmark 1:**

442 Focuses solely on spatial correlations, utilizing inflows at the four sites on the current day (LSM-
443 LX-QS-SD) to create a four-dimensional vine copula. Simulations are conducted unconditionally.

444 **Benchmark 2:**

445 Incorporates both spatial and temporal correlations, including inflows at the four sites for both the
446 current and previous day (LSM-LX-QS-SD-LSM1-LX1-QS1-SD1), resulting in an eight-dimensional
447 vine copula. This model also employs unconditional simulation.

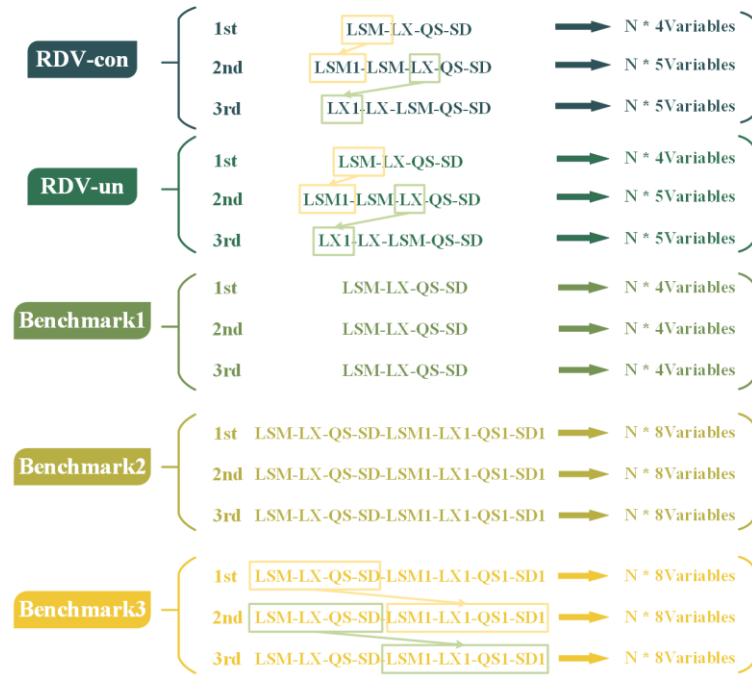
448 **Benchmark 3:**

449 Like Benchmark 2, this model considers both spatial and temporal correlations using the same set
450 of key variables (LSM-LX-QS-SD-LSM1-LX1-QS1-SD1), thereby forming an eight-dimensional vine
451 copula. However, it differs in its application of conditional simulation, assuming the previous day's runoff
452 as a known condition to simulate the current day's flows.

453 To further detail the distinctions in stochastic simulation approaches, the RDV-Copula functions are
454 bifurcated into two categories:

455 **RDV-un/ RDV-con:**

456 Both models account for spatial and temporal correlations by incorporating inflows at the four sites
 457 on the current day and the inflow at one site from the previous day (LSM-LX-QS-SD-X1), creating a
 458 five-dimensional vine copula. The variable “X” represents the site with the strongest temporal connection.
 459 The “RDV-un” employs unconditional simulation, while “RDV-con” utilizes conditional simulation.



460

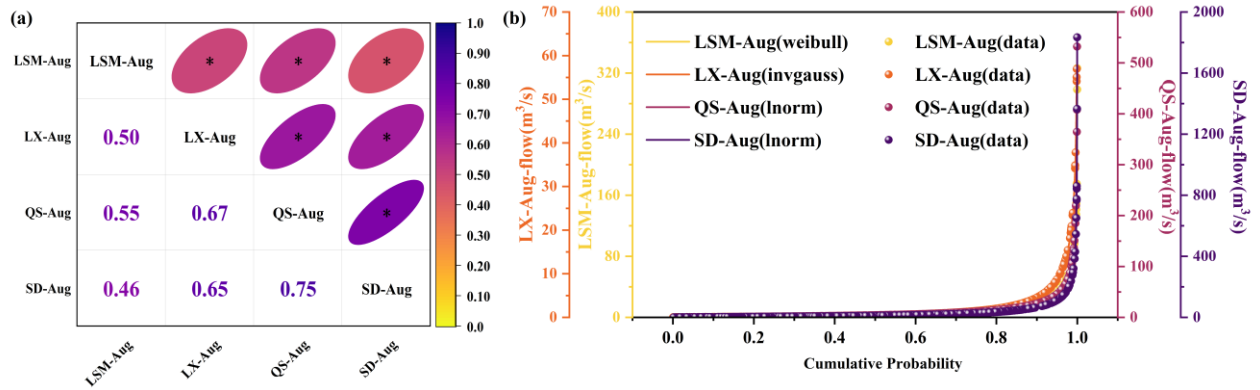
461 **Figure 76. Five different vine copula models**

462 4 Results

463 4.1 Synchronization frequency analysis

464 Prior to performing a synchronization frequency analysis on multiple variables, it is imperative to
 465 conduct a correlation analysis to verify the presence of spatial correlations among them. Following the
 466 approach outlined in Subsection 2.1, this study begins with a correlation analysis of the daily runoff in
 467 August at the four selected sites, utilizing Kendall coefficients to quantify their interconnections. The
 468 results of this analysis, demonstrating the correlation among the four variables, are shown in Figure 87(a).
 469 The "*" on the ellipse means that the correlation passes the significance test of $\alpha = 0.05$. Subsequent
 470 to identifying correlation, the next step involves determining the marginal distributions for these
 471 variables. Figure 87(b) displays the results of this process, showcasing both the plots of the fitted
 472 marginal distributions for the four variables and the actual data distribution, thereby laying the

473 groundwork for a comprehensive understanding of the data's distribution characteristics.



474 **Figure 87. (a) Results of correlation analysis for daily runoff at multiple sites (b) Cumulative probability**
 475 **distribution of the preferred marginal distribution function**

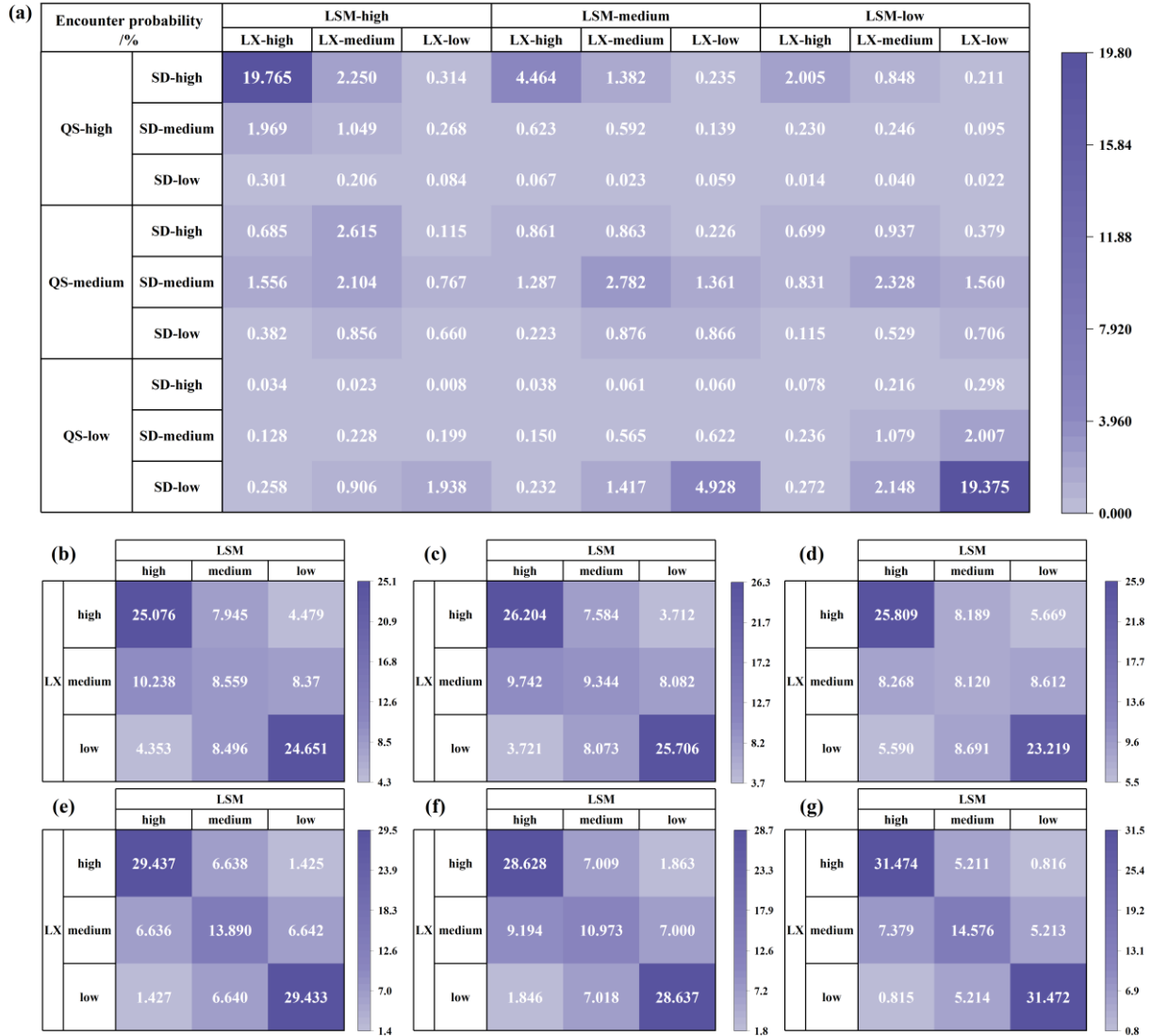
476 Figure 87 demonstrates that the correlations among the four study variables have all passed the
 477 significance test ($p \leq 0.05$), with the QS and SD sites exhibiting the strongest correlations. This is
 478 closely followed by the spatial connections between the LX site and both QS and SD sites, with
 479 correlation coefficients of 0.67 and 0.65, respectively. The correlations involving the LSM site and the
 480 other three sites are relatively low, reflecting a reduction in spatial correlation with increasing distance.
 481 In terms of runoff distribution, the LSM site's runoff adheres to the Weibull distribution (weibull), while
 482 the runoff at the LX site fits the Inverse Gaussian distribution (invgauss), and the runoffs at both QS and
 483 SD sites align with the Log-normal distribution (lnorm). Building on the vine copula function
 484 methodology outlined in Subsection 2.1.2, we have developed a four-dimensional vine copula function
 485 using these variables. The function's structure, alongside the estimated parameters, is detailed in Table 1.

486 **Table 1 Four-dimensional vine copula structure and parameters**

Tree	edge	family	rotation	parameters	tau	loglik
	1,3	bb7	0	2.2, 1.1	0.54	296
1	2,3	t	0	0.86, 6.51	0.66	433
	3,4	t	0	0.92,2.69	0.74	636
2	1,4 3	frank	0	-1.3	-0.15	15
	2,4 3	Bb1	180	0.13, 1.10	0.15	25
3	12 43	bb7	180	1.07, 0.21	0.13	24

487 Upon the construction of four-dimensional vine copula function, the synchronization frequency

488 analysis can be expanded. Using the approach detailed in Subsection 2.2, we obtained 81 encounter
 489 probabilities reflecting potential inflow scenarios at four sites: high-water, medium-water, and low-water.
 490 Figure 98(a) shows these 81 probabilities in detail. Figures 98(b)-(g) present aggregated views, focusing
 491 on nine combinations representing two of the four variables in each of their three states.



492 **Figure 98.** Encounter probabilities for the multiple sites (a) LSM-LX-QS-SD (b) LSM-LX (c) LSM-QS (d)
 493 LSM-SD (e) LS-QS (f) LX-SD (g) QS-SD

494 As observed in Figure 98, the cumulative probability of synchronization across all four sites
 495 simultaneously stands at 41.92%, encompassing three scenarios: (1) LSM-high, LX-high, QS-high, SD-
 496 high (2) LSM-medium, LX-medium, QS-medium, SD-medium (3) LSM-low, LX-low, QS-low, SD-low.
 497 Any two of these sites also demonstrate a very strong synchronization between them, with probabilities
 498 nearing 60%. **The obvious dark colored blocks in the graph indicate the high probabilities of being the**

499 ~~high water or the low water concurrently. The obvious dark-colored blocks in the graph indicate the high~~
500 ~~probabilities of being in high-water or low-water states concurrently.~~ Among these, the strongest
501 synchronization occurs between the QS and SD sites, reaching a probability of 77.52%. This is closely
502 followed by the LX site's synchronization with both QS and SD sites, at probabilities of 72.76% and
503 68.24%, respectively. ~~While the LSM site's synchronization probabilities with the other sites are~~
504 ~~comparatively lower, they still exceed 50%, recorded at 58.29% with the LX site, 61.25% with the QS~~
505 ~~site, and 57.15% with the SD site.~~ While the LSM site's synchronization probabilities with the other sites
506 are comparatively lower, they still exceed 50%, with values of 58.29% for the LX site, 61.25% for the
507 QS site, and 57.15% for the SD site. This analysis underscores the clear spatial correlation among the
508 four sites and highlights the critical importance of monitoring high-water synchronization. This is
509 because such a case of simultaneous high water at multiple sites can easily induce flooding and pose a
510 risk to the downstream. By analyzing the relationship of flow among multiple sites in advance and
511 clarifying the probability of synchronization, it would be more conducive to the formulation of flood
512 control and scheduling strategies to reduce the probability of flood encounters and protect the safety of
513 the downstream.

514 **4.2 Construction of joint distributions of multi-site daily inflows**

515 **4.2.1 Correlation analysis**

516 Correlation analysis serves as an efficient tool for quickly identifying and quantifying the correlations
517 among multiple variables. Following the methodology outlined in Subsection 2.1, this study incorporates
518 both temporal and spatial correlations in its analysis. To achieve this, historical runoff data from four key
519 sites, along with the previous day's runoff data at each site, were used, resulting in a set of eight variables
520 for the correlation analysis. The results of the analysis are presented in Figure 109. Due to the large
521 amount of information, only part of the correlation results is shown here. The complete set of results is
522 available in Appendix C.



523 **Figure 109.** Partial results of correlation analysis for daily runoff at multiple sites (LSM, LX, QS, SD
 524 represent the runoff sequences of current day, while LSM1, LX1, QS1, SD1 represent the runoff sequences
 525 of previous day)

526 Figure 109 illustrates the Kendall correlation coefficients between pairs of variables. The intensity
 527 of colors correlates with the strength of positive correlation, with darker shades signifying a correlation
 528 coefficient closer to 1. The "*" on the ellipse means that the correlation passes the significance test of
 529 $\alpha = 0.05$. This figure uncovers a marked positive correlation among the runoff series at the LSM, LX,
 530 QS, and SD sites, with approximately 93% of these correlations meeting the significance threshold. This
 531 finding indicates that there is an obvious spatial correlation among the four locations. Notably, the QS
 532 and SD sites exhibit the strongest spatial correlation, with an average coefficient in August of 0.74,
 533 closely followed by the LX reservoir's correlation with the QS and SD sections at 0.67 and 0.63,
 534 respectively. In comparison, the LSM reservoir's runoff shows relatively lower correlations with the other
 535 sites, averaging 0.48 with LX site, 0.55 with QS site, and 0.45 with SD site in August.

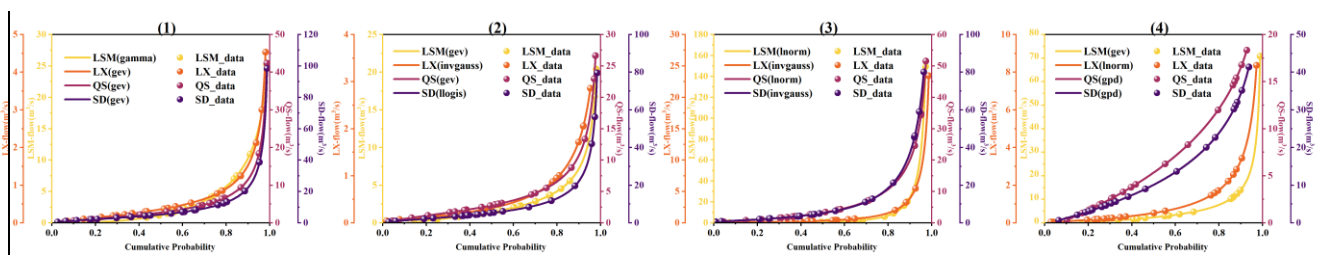
536 Upon analyzing the temporal correlation of runoff at each site for adjacent days within August
 537 (denoted as LSM-LSM1, LX-LX1, QS-QS1, SD-SD1), it becomes evident that temporal correlations are

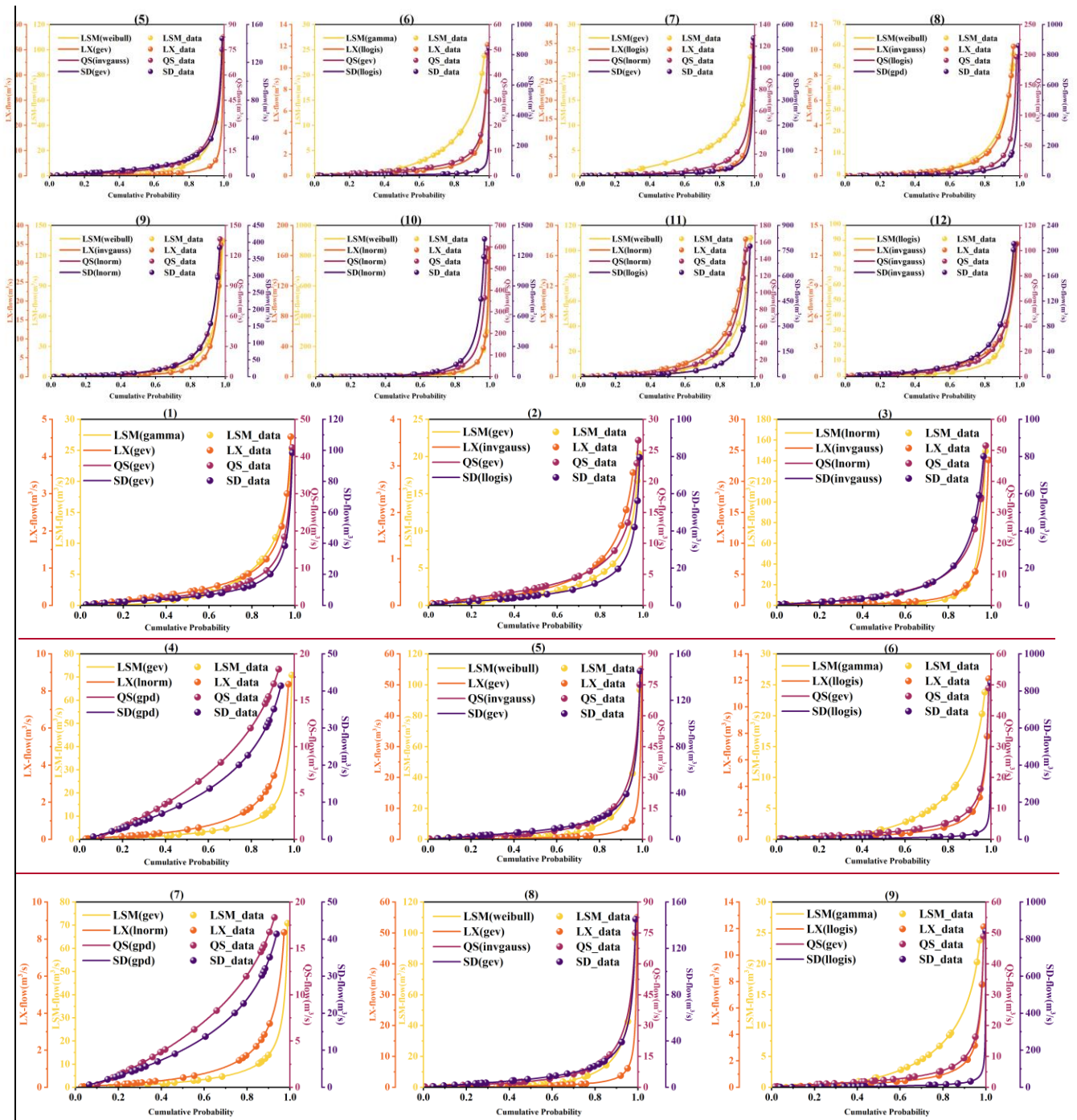
538 significant and should not be overlooked. Particularly in early August, these correlations register at a
 539 notably high level, suggesting more frequent flooding during this period. The LSM site demonstrates a
 540 standout temporal correlation, averaging 0.72 in August, indicative of a strong link between the current
 541 and previous day's runoff. The other sites display slightly lower, yet significant, temporal correlations:
 542 LX at 0.65, QS at 0.65, and SD at 0.67. When these temporal correlations are considered alongside the
 543 spatial ones, it's evident that LSM's temporal correlation surpasses its spatial correlation with other sites.

544 These correlation analysis results solidly confirm both spatial and temporal correlations among the
 545 four sites, laying a foundational basis for advancing with the construction of a copula structural model.

546 4.2.2 Fitting of marginal distribution of each runoff

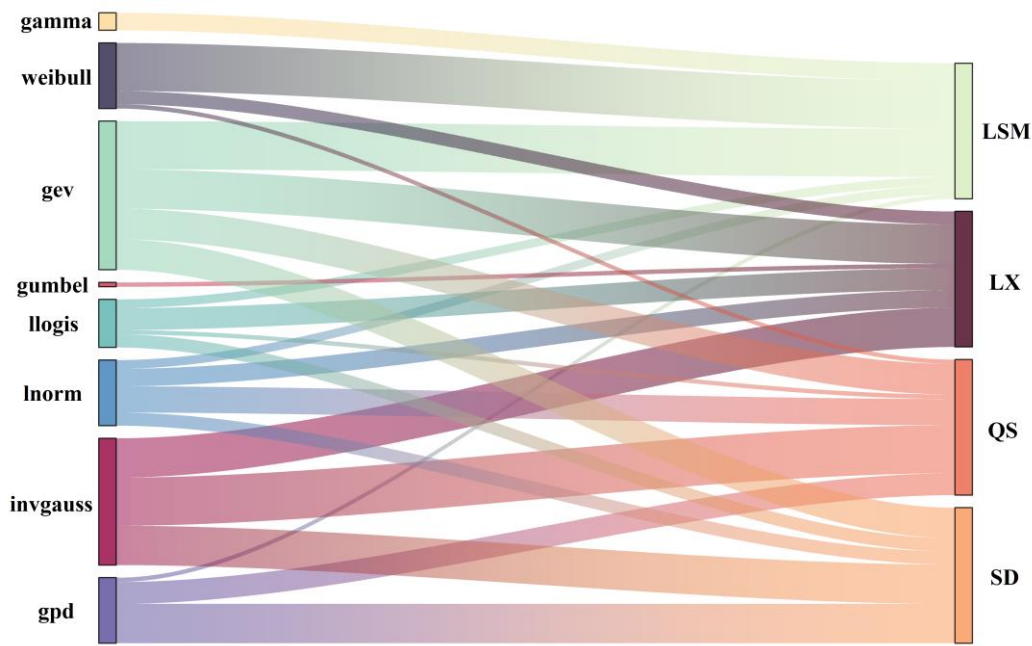
547 In this study, twelve distinct distribution functions were utilized to model the daily runoff at four sites
 548 throughout August. To assess the goodness-of-fit of these distributions, the Kolmogorov-Smirnov (K-S)
 549 test, with a significance level of 0.05, was employed. Following a successful significance test, the Akaike
 550 Information Criterion (AIC) minimum method was applied to evaluate and determine the optimal
 551 marginal distribution for each dataset. Figure 11-10 shows the preferred marginal distribution functions
 552 for each variable over the 31 days of August. This figure contrasts the actual historical data points against
 553 the curves of the fitted functions, offering a visual representation of the fitting accuracy. The specific
 554 marginal distribution functions chosen for each variable, along with their parameters for each day, are
 555 comprehensively listed in Appendix D. Figure 10-11 notably illustrates how well these selected marginal
 556 distribution functions match the actual data for all four variables from the 1st to the 12th of August. The
 557 chosen marginal distribution functions for the entire month are detailed in Figure D1. Furthermore, the
 558 figure's legend explicitly details the types of fitting functions employed for each variable, providing a
 559 clear and comprehensive overview of the distributional characteristics.





560 **Figure 411.** Cumulative probability distribution of the preferred marginal distribution function for
 561 runoff on each day throughout 1st-12th-9th in August

562 The distribution of the corresponding marginal distribution functions for the four variables over the
 563 31 days in August is summarized in Figure 412.

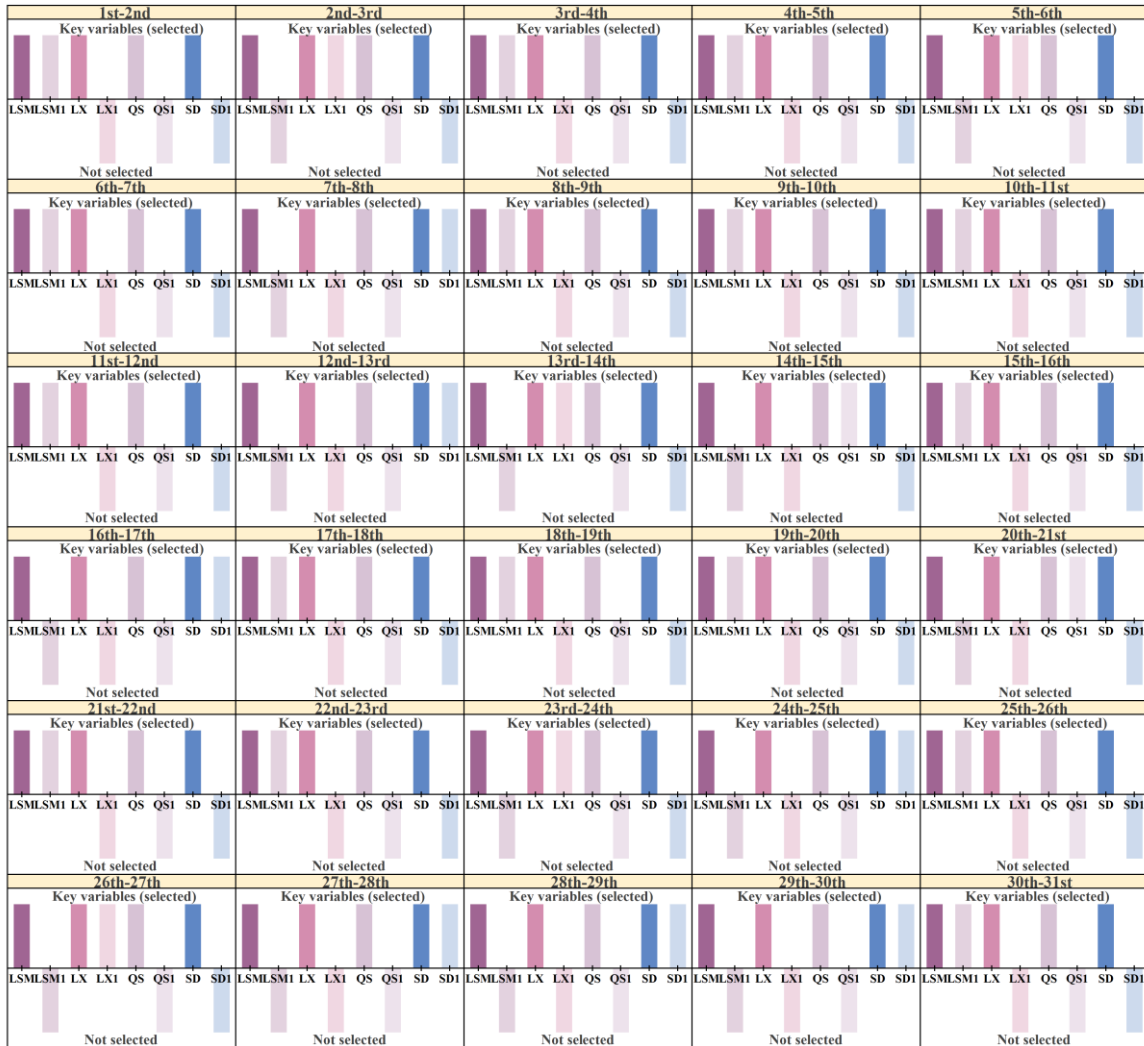


564
565 **Figure 4-12.** Distribution of the preferred marginal distribution function for the daily series of flows at
566 **LSM, LX, QS and SD site in August**

567 Figure 4-12 shows that most streamflow series follow the “gev” distribution (27.52%) and the
568 “invgauss” distribution (23.39%). Relatively few streamflow series follow the “weibull”, “llogis”,
569 “lnorm”, and “gpd” distributions, and only a very small number follow the “gamma” and “gumbel”
570 distributions. Additionally, 71% of the runoff sequences at the LSM site follow the “weibull” and “gev”
571 distributions, each accounting for 35.5%. The runoff sequences at the LX site, the QS site, and the SD
572 site predominantly follow the “gev” and “invgauss” distributions, accounting for 29.03% and 29.03% at
573 the LX site, 22.58% and 35.48% at the QS site, and 22.58% and 29.03% at the SD site, respectively.
574 Meanwhile, nearly 30% of the runoff sequences at the SD site also follow the “gpd” distribution.

575 4.2.3 Construction of RDV-Copula function

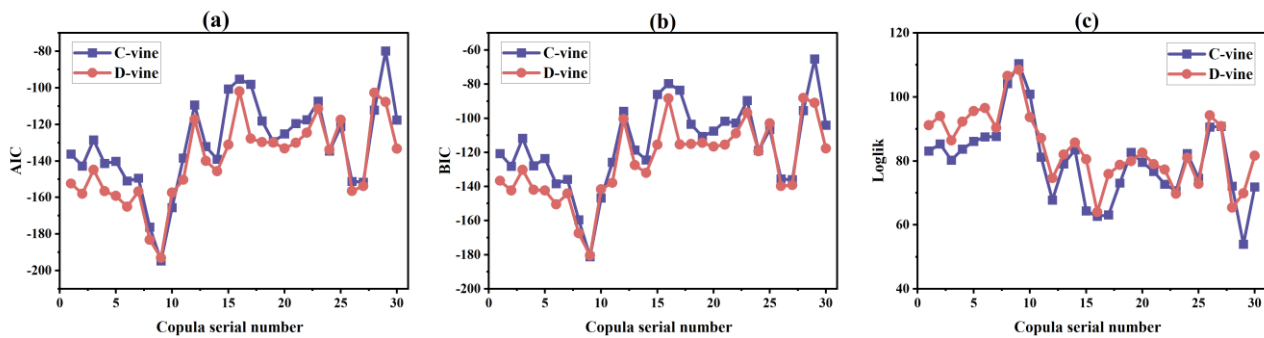
576 Following the identification of each variable's marginal distribution, the next step involves selecting the
577 appropriate copula structures to construct the vine copula models among the multiple variables. Utilizing
578 the RDV-Copula function construction approach described in Section 3.2.2.1, we identified the sites
579 exhibiting the highest temporal correlation for each day in August, based on our correlation analysis
580 results. The variables chosen for each specific day are illustrated in Figure 4-13.



581 **Figure 1213.** Key factors in the five-dimensional vine copula structure constructed in two adjacent days
 582 (LSM, LX, QS, SD represent the runoff sequences of current day, while LSM1, LX1, QS1, SD1 represent the
 583 runoff sequences of previous day)

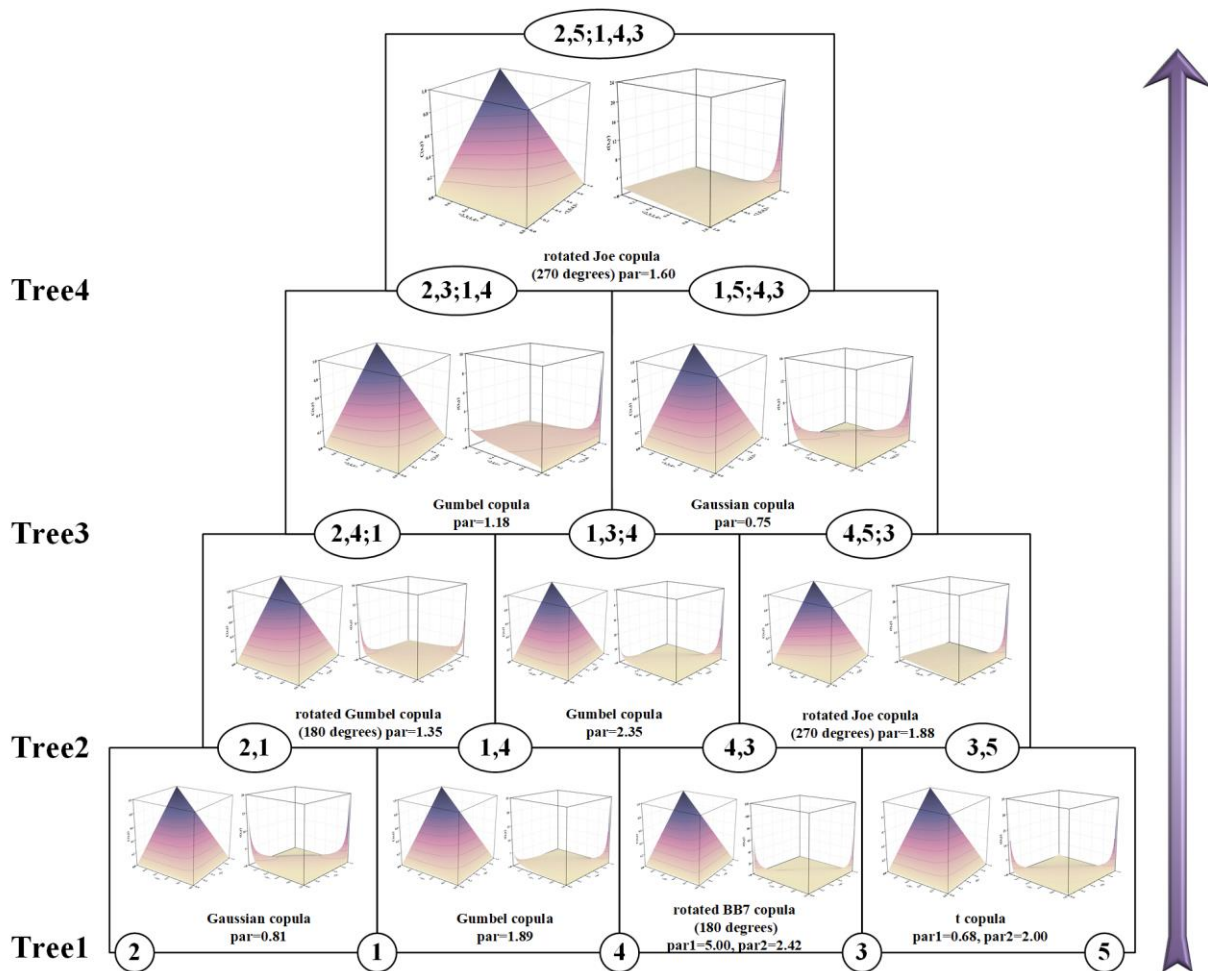
584 Prior to selecting a specific copula function for modeling, it is essential to decide on the type of
 585 copula to be employed. Among the options, C-vine and D-vine structures stand out for their common use
 586 in various applications. In this study, we constructed both C-vine and D-vine copula structures for the set
 587 of multiple variables under consideration. To evaluate the efficacy of these structures, metrics such as
 588 the Akaike Information Criterion (AIC), Bayesian Information Criterion (BIC), and Log-Likelihood
 589 (Loglik) values were utilized and computed, with the results presented in Figure 1314. The AIC and BIC
 590 values reveal that, for the majority of cases, the D-vine copula structures exhibit significantly lower
 591 values compared to those of the C-vine structures. Lower values in these criteria suggest a model's better

592 performance and fit. Moreover, the comparison of log-likelihood values also showed that D-vine
 593 structures typically yielded lower values than their C-vine counterparts. Consequently, the D-vine copula
 594 structure was identified as more effective and suitable for modeling the intricate relationships among the
 595 variables in this study. Therefore, the RDV-Copula and other benchmark copula models were designed
 596 using the D-vine structure.



597 **Figure 4.14.** Comparison of the performance of RDV-Copula models for C-vine and D-vine (a) AIC (b)
 598 BIC (c) Loglik

599 A large number of copula families were utilized to model the joint distributions, such as Gaussian
 600 copula, Gumbel copula, t copula and so on. Following the guidance of AIC criteria, the most suitable
 601 pair-copula for each connection within every tree was selected. After fitting the goodness of the copula
 602 functions, we employed the maximum likelihood method to estimate the parameters. As an illustrative
 603 example, the copula structure for August 1st-2nd is shown in Figure 4.15. This figure not only reveals
 604 the best-fit copula family for each pair of adjacent nodes but also the estimated parameters. The nodes,
 605 labeled 1 through 5, represent LSM, LX, QS, SD, and X1, which indicates the site with the highest
 606 temporal correlation on that day, respectively. In this instance, X1 corresponds to LSM1. It is important
 607 to note that the specific choice of X1 might vary from day to day, as further elaborated in Figure 4.13.
 608 In Figure 4.15, each pair of subfigures situated between nodes shows two aspects of the bi-dimensional
 609 copula function for those nodes. The first subfigure presents the joint probability plot, while the second
 610 illustrates the joint probability density plot.

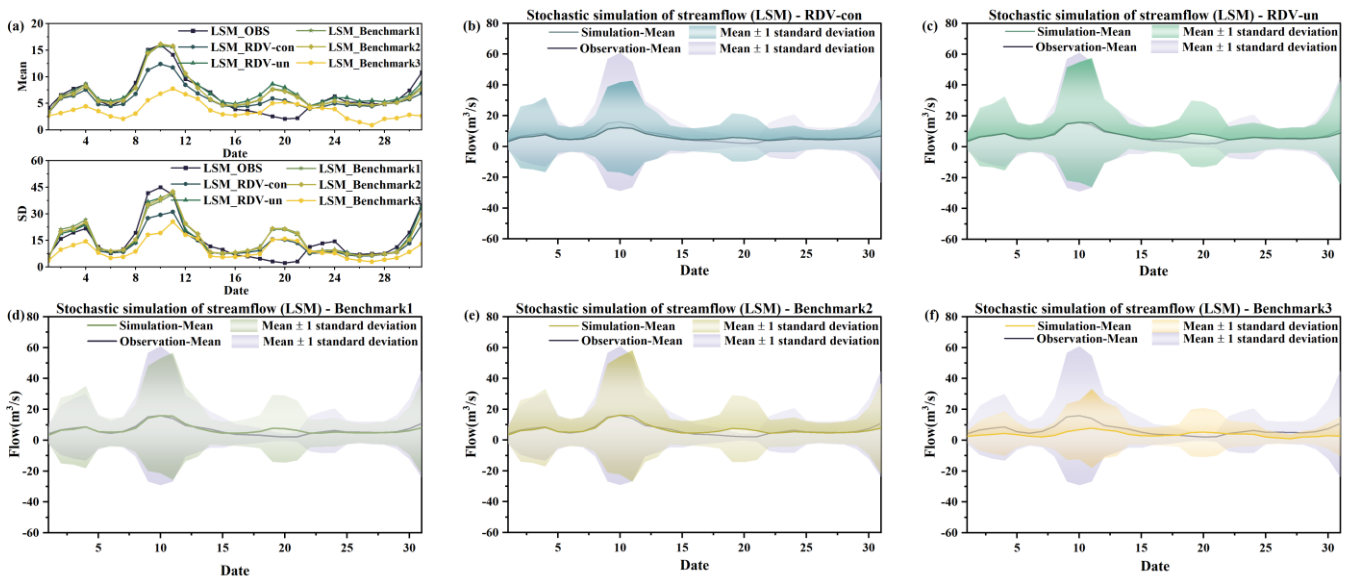


611 Figure 4.15. Structure of the five-dimensional D-vine copula model for August 1st -2nd (Nodes 1–5 represent
 612 LSM, LX, QS, SD, and LSM1; The plots between each two nodes are schematic plots of the corresponding
 613 copula function, with joint probability plot on the left and joint probability density plot on the right.)

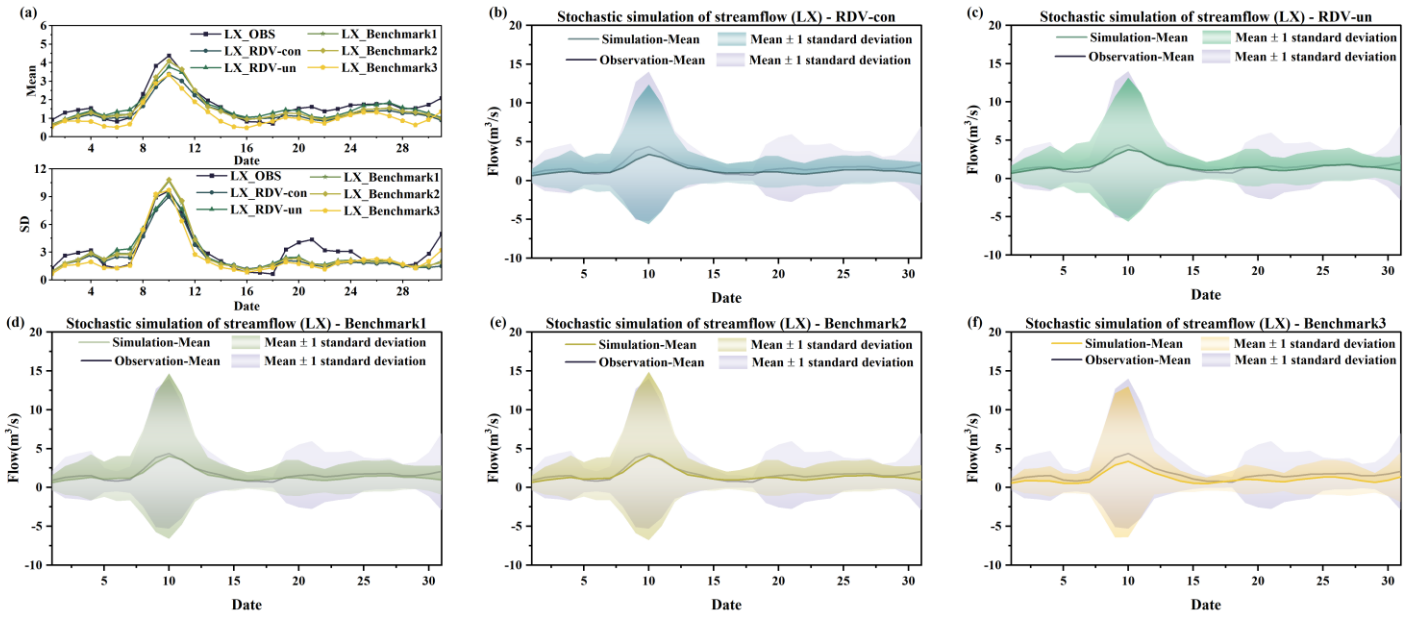
614 4.3 Stochastic simulation results of runoff from multiple sites

615 To validate the models and facilitate a comparative analysis of different vine copula functions, the
 616 following work was carried out. Initially, the constructed copula structure and the results from parameter
 617 estimation were incorporated into a simulation process, generating 20,000 sets of random runoff
 618 scenarios for each day in August. Considering August's susceptibility to flooding and the typical
 619 continuity of rainfall events, it's highly likely that runoff on consecutive days is temporally correlated.
 620 Therefore, comparing only the mean and standard deviation of runoff simulated for individual days might
 621 not fully capture the model's simulation efficacy. In this context, the study calculated the mean and
 622 standard deviation for the current day by considering the simulated flows of both the preceding and
 623 following days. Ultimately, after the exclusion of outliers from the 20,000 sets of simulated runoff

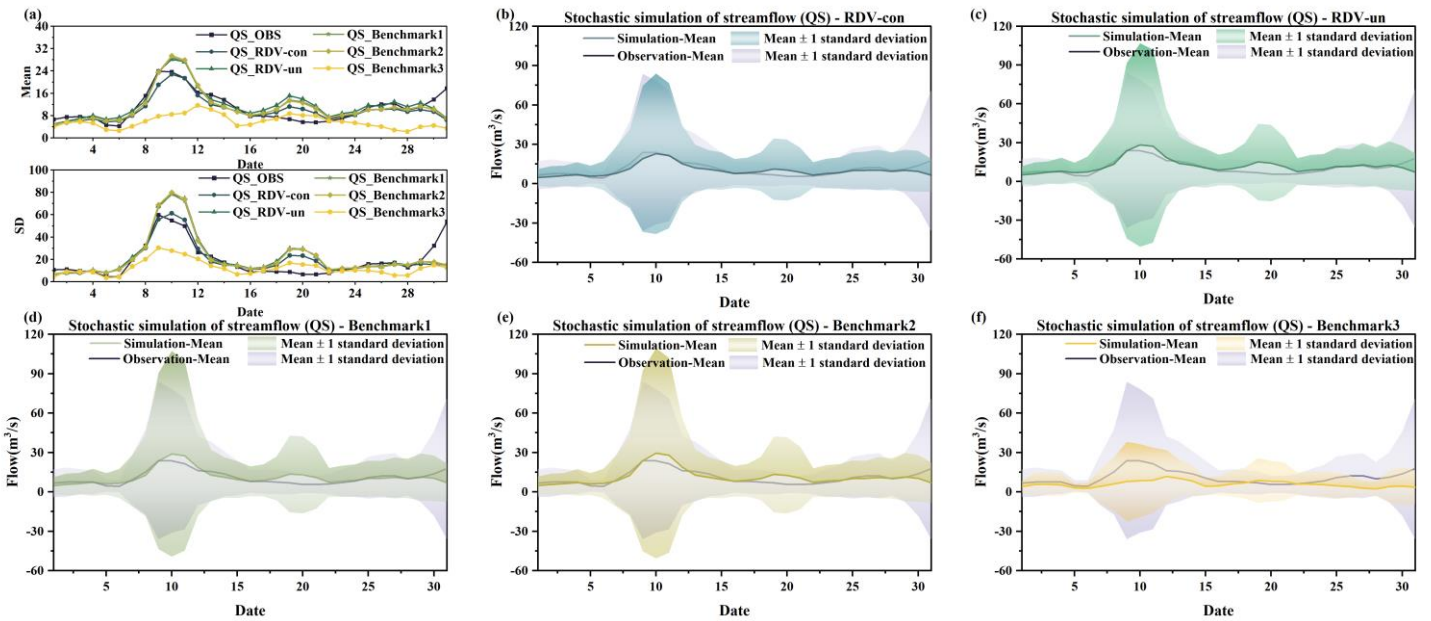
624 scenarios, the average of the mean and standard deviation calculated from these three days' simulated
 625 flows will be used as the mean and standard deviation for the current day. The runoff simulation results
 626 for the four locations (LSM, LX, QS, and SD) are presented in Figures 1516, 1617, 17-18 and 1819,
 627 respectively. Notably, in each figure, subfigure (a) displays the mean values and standard deviations from
 628 the simulation results for the five copula structures, allowing these results to be compared against
 629 historical observations for a nuanced evaluation of the simulation's performance. Subfigures(b), (c), (d),
 630 (e) and (f) represent the simulation results for five different sets of copula structures (RDV-con, RDV-
 631 un, Benchmark1, Benchmark2 and Benchmark3) respectively. The solid line in the figure is the mean of
 632 the simulation results and the shaded area represents the uncertainty (± 1 standard deviation) of the
 633 simulation.



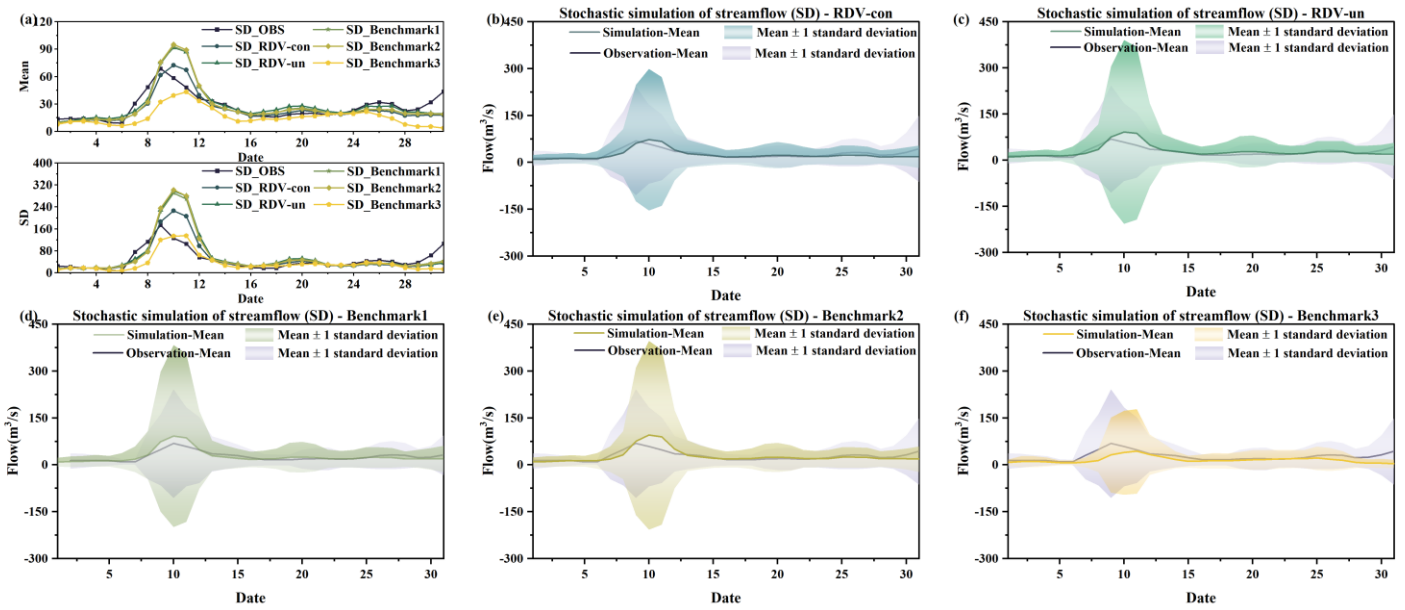
634 **Figure 1516.** Comparison of the actual observed series with simulation results of four copula structures at
 635 LSM site (a) comparison of daily runoff mean values and standard deviation (b) simulation results of RDV-
 636 con (c) simulation results of RDV-un (d) simulation results of Benchmark1 (e) simulation results of
 637 Benchmark2 (f) simulation results of Benchmark3



638 **Figure 16**. Comparison of the actual observed series with simulation results of four copula structures at
 639 LX site (a) comparison of daily runoff mean values and standard deviation (b) simulation results of RDV-
 640 con (c) simulation results of RDV-un (d) simulation results of Benchmark1 (e) simulation results of
 641 Benchmark2 (f) simulation results of Benchmark3



642 **Figure 17**. Comparison of the actual observed series with simulation results of four copula structures at
 643 QS site (a) comparison of daily runoff mean values and standard deviation (b) simulation results of RDV-
 644 con (c) simulation results of RDV-un (d) simulation results of Benchmark1 (e) simulation results of
 645 Benchmark2 (f) simulation results of Benchmark3



646 **Figure 1819.** Comparison of the actual observed series with simulation results of four copula structures at
 647 SD site (a) comparison of daily runoff mean values and standard deviation (b) simulation results of RDV-
 648 con (c) simulation results of RDV-un (d) simulation results of Benchmark1 (e) simulation results of
 649 Benchmark2 (f) simulation results of Benchmark3

650 From four figures, it is evident that the simulation results of RDV-Copula, Benchmark1 and
 651 Benchmark2 are comparatively more accurate. The mean values and standard deviations from these
 652 simulations closely match the actual observed runoff, particularly for simulations involving smaller flow
 653 magnitudes, where the accuracy aligns more precisely with the actual values. Although the RDV-Copula
 654 results are consistent with the benchmark models, they do not exhibit a marked advantage for smaller
 655 flows. However, in scenarios involving larger flows, such as those at the SD site, RDV-Copulas
 656 outperform other models, highlighting their superiority in capturing the characteristics of larger inflow
 657 events. This analysis suggests that for smaller flows, models focusing solely on spatial relationships
 658 suffice to capture the critical interrelationships among variables. In contrast, for larger flows, neglecting
 659 the influence of temporal correlations can lead to substantial inaccuracies in the simulation results,
 660 suggesting that larger flows are more significantly influenced by adjacent day's flows. Comparing the
 661 four figures, we can also find that the simulation results at LX location consistently exhibit high accuracy,
 662 with the simulation results basically covering the actual observations. This suggests that the constructed
 663 copula models can easily extract the historical correlations and simulate them, particularly in smaller
 664 flow magnitudes.

665 However, the Benchmark3 model's performance is notably less effective among the five models.
666 This suboptimal performance can be attributed to two main factors. Firstly, the complexity of the eight-
667 dimensional copula function, which involves a diverse combination of "trees," "nodes," and various types
668 of parameters, poses significant challenges in accurately extracting the relationship characteristics among
669 the four sites. Secondly, the conditional simulation approach of Benchmark3, which relies on the previous
670 day's flow at the four sites as a known condition for simulation, is highly susceptible to the accuracy of
671 these initial conditions. If the simulation results for the previous day contain significant errors, these
672 inaccuracies are likely to propagate through the simulation, leading to compounded errors in the entire
673 results. Another noteworthy point is that the simulation results on the August 10th, 20th and 31st are not
674 quite consistent with historical conditions. This is because the runoff on these three days has been at a
675 low level for most of the time over a number of years in history. It is therefore a rather exceptional
676 phenomenon that a major flood event occurred on these particular dates in just one year. Specifically, the
677 data recorded on these dates (August 10, 2009, August 31, 2011, and August 20, 2014) indicate unusually
678 high runoff, which significantly exceeds their respective historical averages. Such an occurrence presents
679 a challenge for the simulations, as it requires accurately capturing and replicating these atypically high
680 flow values within the model.

681 Comparing the two types of simulations of RDV-Copula, it can be found that the performances of
682 the simulation results of RDV-un and RDV-con are similarly well for LSM and LX sites. However, in
683 the simulation of QS and SD sites, RDV-con shows an obvious superiority compared to RDV-un. This
684 illustrates the better generalization of conditional simulation for such complex structure with spatial-
685 temporal relationships. In contrast to the unconditional simulation, RDV-con can better utilize the
686 temporal correlation to improve the accuracy of the simulation. Meanwhile, since it is different from the
687 conditional simulation of the eight-dimensional vine copula (Benchmark2), RDV-con successfully
688 reduces the cumulative error caused by the excessive dimensionality.

689 In summary, for the relational construction and stochastic simulation of flows across varying
690 magnitudes, RDV-Copula and Benchmark2 emerge as more suitable, particularly when considering the
691 influences of both temporal and spatial correlations. However, the use of an eight-dimensional copula
692 function in Benchmark2 introduces significant computational demands and adds complexity to the
693 problem. RDV-Copula is favored for its effective integration of temporal and spatial correlations, while

694 also simplifying the copula structure, thereby streamlining the problem-solving process and enhancing
695 computational efficiency.

696 5 Discussion

697 For variables with interdependencies, the copula function, increasingly popular in contemporary studies,
698 extracts spatial-temporal relationships from their marginal distributions. Vine copulas are notably
699 effective in modeling complex dependencies among variables, as they offer substantial flexibility. This
700 capability is exemplified in the work of Pereira and Veiga (2018), who developed a multivariate
701 conditional model using D-vine copulas for simulating periodic streamflow scenarios, emphasizing the
702 structured arrangement of variables to capture monthly flow dependencies. This and numerous other
703 studies (Nazeri Tahroudi et al., 2022; Wang et al., 2018, 2019; Wang and Shen, 2023a) underscored the
704 effectiveness of vine copulas in capturing dependencies among variables with differing marginal
705 distributions.

706 The synchronous probability analysis of multi-site runoff shows that the vine copula model can be
707 used to provide a good fit to the dependencies among variables obeying different marginal distributions.
708 Similar conclusions have been obtained in other studies (Qian et al., 2022; Ren et al., 2020; Wei et al.,
709 2023). In the study of Xu et al. (2022), the multivariate Copula model was implemented to evaluate the
710 synchronous–asynchronous characteristics for hydrological probabilities for the multiple water sources.
711 The simultaneous probabilistic analysis of multi-site runoff provides an understanding of the flood
712 characteristics of the catchment leading to better flood control and prevention.

713 For high-dimensional variable dependency analysis, the structure of the vine copula is extremely
714 complicated to construct. Depending on the number of hydrometric stations, Wang and Shen (2023b)
715 established ~~the~~-7-dimensional regular vine (R-vine) copula models to depict the complex and diverse
716 ~~dependene~~ dependencies. To tackle the problem above, in their study, the corresponding vine structure
717 was specified by the vine structure array that can reflect the sequence of tributaries flowing into the main
718 stream and the spatial locations of different hydrometric stations. The performance of the ultimate
719 simulation results was favorable, but it did not incorporate the temporal connection of the variables for
720 each hydrometric station. If considered, it would lead to an exponential increase in the dimensionality of
721 the variable. The RDV-Copula method proposed in this study aims to minimize the dimensionality of the

722 copula model while extracting the effective information of spatial-temporal relationships. The evaluation
723 criterion of high-performance stochastic simulation is that the simulated series can preserve the statistical
724 characteristics of the observed records (Hao and Singh, 2013). As shown in Figure [15-16](#) - [1819](#), different
725 vine copula structures have a large impact on the results of stochastic simulations. The simulation results
726 of the four-dimensional and five-dimensional vine copula models are relatively closer to the actual
727 historical values. ~~Although the eight dimensional vine copula model takes more variables into account,~~
728 ~~including both temporal and spatial correlation, the model is too complicated due to many variables,~~
729 ~~which makes the simulation less efficient on the contrary.~~ Although the eight-dimensional vine copula
730 model considers both temporal and spatial correlations, its complexity reduces simulation efficiency due
731 to the large number of variables. This illustrates that when performing multi-site runoff simulations, it is
732 not better for the vine copula function to consider as many variables as possible. Compared to the four-
733 dimensional copula structure that only considers spatial relations, the five-dimensional copula structure
734 can better fit the characteristics of high flows, which is especially evident in the simulation results of QS
735 and SD points. This is due to the fact that high flows in flood season mostly originate from continuous
736 heavy rainfall, which implies that the temporal connection is not negligible for capturing the flow
737 characteristics.

738 Consequently, the approach introduced in this study effectively integrates all pertinent information
739 for multi-site runoff simulations while reducing the complexity of the vine copula function. This
740 methodology strikes a critical balance between detailed representation and practicality in model
741 complexity, enhancing the applicability of the simulations.

742 **6 Conclusions**

743 This study introduced an innovative approach designed to capture the spatial-temporal relationships
744 across multiple sites while simplifying the computational complexity inherent in vine copula functions.
745 By computing Kendall correlation coefficients, we assessed the interconnections among various sites.
746 Utilizing the approach proposed, we pinpointed the key variables for the construction of the vine copula
747 model, fitted the marginal distribution functions for multiple variables, and constructed the RDV-Copula
748 functions considering the spatial-temporal relationships. Subsequent to this, a synchronization frequency
749 analysis based on the copula model was executed to delve deeper into the characteristics of the watershed.

750 To gauge the efficacy of this method, three benchmark vine copula models, each predicated on different
751 dimensions and variable relationships, were constructed. Stochastic simulations were then employed to
752 generate arrays of daily inflow sequences over a typical flood month, with both conditional and
753 unconditional simulation methods being critically compared. Key findings are summarized below.

754 (1) The results of our study demonstrated that, within the Shifeng Creek watershed, the synchronization
755 probability among the four sites reaches up to 41.92%, with the average synchronization probability
756 between any two sites hitting 65.87%. This strong spatial connectivity indicates a potential for heavy
757 rainfall events to exacerbate flooding risks downstream.

758 (2) This study revealed that increasing model dimensions does not inherently improve simulation
759 outcomes. The high-dimensional copula function, while it can capture more information on the
760 variables, also makes the structure more complicated. The RDV-Copula method not only ensures
761 comprehensive data integration but also diminishes the complexity and dimensionality of the vine
762 copula function, showcasing an optimal balance between information accuracy and model simplicity.

763 (3) ~~The~~ Conditional simulation is a double-edged sword. In comparison to unconditional simulation,
764 for temporally correlated runoff sequences, conditional simulation can better follow the properties
765 of prior conditions. However, with an increase in the copula's dimensionality, relying on previously
766 simulated runoff as a basis for current day predictions can accumulate errors, reducing the overall
767 simulation accuracy.

768 In summary, our proposed approach can effectively consolidate relevant spatial-temporal
769 information for multisite runoff simulations, striking a critical balance between detailed representation
770 and practical model complexity. This methodology enhances the applicability of vine copula models for
771 analyzing and managing flood risks. The results obtained using this method can provide valuable decision
772 support for flood control and scheduling, effectively mitigating flood risk.

773

774 **Appendix A**

775 **Table A1 Common hydrological distribution functions**

Distribution name	Probability distribution function	Parameters
-------------------	-----------------------------------	------------

Gamma distribution (gamma)	$f(x) = \frac{x^{k-1}}{\alpha^k \Gamma(k)} \exp\left[-\frac{x}{\alpha}\right]$	k - shape parameter ($k > 0$) α - scale parameter ($\alpha > 0$)
Exponential distribution (exp)	$f(x) = \begin{cases} \lambda \exp(-\lambda x), & x \geq 0 \\ 0, & x < 0 \end{cases}$	λ - rate parameter
Pearson-III distribution (p3)	$f(x) = \frac{\beta^\alpha}{\Gamma(\alpha)} (x - \gamma)^{\alpha-1} e^{-\beta(x-\gamma)}$	α - shape parameter ($\alpha > 0$) β - scale parameter ($\beta > 0$) γ - location parameter
Generalized extreme value distribution (gev)	$f(x) = \exp\left\{-\left(1 + \xi \frac{x - \mu}{\alpha}\right)^{\frac{1}{\xi}}\right\}$	α - scale parameter ($\alpha > 0$) μ - location parameter ξ - shape parameter
Inverse gaussian distribution (invgauss)	$f(x) = \sqrt{\frac{\lambda}{2\pi x^3}} \exp\left\{-\frac{\lambda(x - \mu)^2}{2\mu^2 x}\right\}$	μ - mean (location parameter) λ - shape parameter
Normal distribution (norm)	$f(x) = \frac{1}{\sqrt{2\pi}\sigma} \exp\left(-\frac{(x - \mu)^2}{2\sigma^2}\right)$	μ - location parameter σ - scale parameter
Logistic distribution (logis)	$f(x) = \frac{e^{-(x-\mu)/\gamma}}{\gamma(1 + e^{-(x-\mu)/\gamma})^2}$	μ - location parameter γ - shape parameter ($\gamma > 0$)
Log-normal distribution (lnorm)	$f(x) = \begin{cases} \frac{1}{x\sqrt{2\pi}\sigma} \exp\left[-\frac{1}{2\sigma^2}(\ln x - \mu)^2\right], & x > 0 \\ 0, & x \leq 0 \end{cases}$	μ - location parameter σ - scale parameter
Log-logistic distribution (llogis)	$f(x) = \frac{\left(\frac{\beta}{\alpha}\right) \frac{x^{\beta-1}}{\alpha}}{\left[1 + \left(\frac{x}{\alpha}\right)^\beta\right]^2}, x > 0$	α - scale parameter ($\alpha > 0$) β - shape parameter ($\beta > 0$) μ - location parameter
Generalized pareto distribution (gpd)	$f(x) = \frac{1}{\sigma} \left(1 + k \frac{(x - \mu)}{\sigma}\right)^{-1-1/k}$	σ - scale parameter k - shape parameter
Weibull distribution (weibull)	$f(x) = \frac{k}{\alpha} \left(\frac{x - \gamma}{\alpha}\right)^{k-1} \exp\left[-\left(\frac{x - \gamma}{\alpha}\right)^k\right]$	k - shape parameter ($k > 0$) α - scale parameter ($\alpha > 0$) γ - location parameter
Gumbel distribution (gumbel)	$f(x) = \frac{1}{\sigma} \exp\left(-\frac{x - \mu}{\sigma} - \exp\left(-\frac{x - \mu}{\sigma}\right)\right)$	μ - location parameter σ - scale parameter

777 **Appendix B**

778 The probability formulas for the 81 combinations are presented as follows.

779 (1) The probability of Type [X-H, Y-H, Z-H, W-H] is as follows:

$$\begin{aligned}
& P(X > X_{ph}, Y > Y_{ph}, Z > Z_{ph}, W > W_{ph}) = 1 - u_{ph} - v_{ph} - r_{ph} - s_{ph} \\
& + C(u_{ph}, v_{ph}) + C(u_{ph}, r_{ph}) + C(u_{ph}, s_{ph}) + C(v_{ph}, r_{ph}) + C(v_{ph}, s_{ph}) \\
& + C(r_{ph}, s_{ph}) - C(u_{ph}, v_{ph}, r_{ph}) - C(u_{ph}, v_{ph}, s_{ph}) - C(u_{ph}, r_{ph}, s_{ph}) \\
& - C(v_{ph}, r_{ph}, s_{ph}) + C(u_{ph}, v_{ph}, r_{ph}, s_{ph})
\end{aligned}$$

781 (2) The probability of Type [X-M, Y-M, Z-M, W-M] is as follows:

$$\begin{aligned}
& P(X_{pl} < X < X_{ph}, Y_{pl} < Y < Y_{ph}, Z_{pl} < Z < Z_{ph}, W_{pl} < W < W_{ph}) \\
& = C(u_{ph}, v_{ph}, r_{ph}, s_{ph}) - C(u_{ph}, v_{ph}, r_{ph}, s_{pl}) - C(u_{ph}, v_{ph}, r_{pl}, s_{ph}) \\
& - C(u_{ph}, v_{pl}, r_{ph}, s_{ph}) - C(u_{pl}, v_{ph}, r_{ph}, s_{ph}) + C(u_{ph}, v_{ph}, r_{pl}, s_{pl}) \\
& + C(u_{ph}, v_{pl}, r_{ph}, s_{pl}) + C(u_{pl}, v_{ph}, r_{ph}, s_{pl}) + C(u_{ph}, v_{pl}, r_{pl}, s_{ph}) \\
& + C(u_{pl}, v_{ph}, r_{pl}, s_{ph}) + C(u_{pl}, v_{pl}, r_{ph}, s_{ph}) - C(u_{ph}, v_{pl}, r_{pl}, s_{pl}) \\
& - C(u_{pl}, v_{ph}, r_{pl}, s_{pl}) - C(u_{pl}, v_{pl}, r_{ph}, s_{pl}) - C(u_{pl}, v_{pl}, r_{pl}, s_{ph}) \\
& + C(u_{pl}, v_{pl}, r_{pl}, s_{pl})
\end{aligned}$$

783 (3) The probability of Type [X-L, Y-L, Z-L, W-L] is as follows:

$$P(X < X_{pl}, Y < Y_{pl}, Z < Z_{pl}, W < W_{pl}) = C(u_{pl}, v_{pl}, r_{pl}, s_{pl})$$

785 (4) The probability of Type [X-L, Y-H, Z-H, W-H] is as follows:

$$\begin{aligned}
& P(X < X_{pl}, Y > Y_{ph}, Z > Z_{ph}, W > W_{ph}) = u_{pl} - C(u_{pl}, v_{ph}) - C(u_{pl}, r_{ph}) \\
& - C(u_{pl}, s_{ph}) + C(u_{pl}, v_{ph}, r_{ph}) + C(u_{pl}, v_{ph}, s_{ph}) + C(u_{pl}, r_{ph}, s_{ph}) \\
& - C(u_{pl}, v_{ph}, r_{ph}, s_{ph})
\end{aligned}$$

787 (5) The probability of Type [X-H, Y-L, Z-H, W-H] is as follows:

$$\begin{aligned}
& P(X > X_{ph}, Y < Y_{pl}, Z > Z_{ph}, W > W_{ph}) = v_{pl} - C(u_{ph}, v_{pl}) - C(v_{pl}, r_{ph}) \\
& - C(v_{pl}, s_{ph}) + C(u_{ph}, v_{pl}, r_{ph}) + C(u_{ph}, v_{pl}, s_{ph}) + C(v_{pl}, r_{ph}, s_{ph}) \\
& - C(u_{ph}, v_{pl}, r_{ph}, s_{ph})
\end{aligned}$$

789 (6) The probability of Type [X-H, Y-H, Z-L, W-H] is as follows:

$$\begin{aligned}
& P(X > X_{ph}, Y > Y_{ph}, Z < Z_{pl}, W > W_{ph}) = r_{pl} - C(u_{ph}, r_{pl}) - C(v_{ph}, r_{pl}) \\
& - C(r_{pl}, s_{ph}) + C(u_{ph}, v_{ph}, r_{pl}) + C(u_{ph}, r_{pl}, s_{ph}) + C(v_{ph}, r_{pl}, s_{ph}) \\
& - C(u_{ph}, v_{ph}, r_{pl}, s_{ph})
\end{aligned}$$

791 (7) The probability of Type [X-H, Y-H, Z-H, W-L] is as follows:

$$\begin{aligned}
& P(X > X_{ph}, Y > Y_{ph}, Z > Z_{ph}, W < W_{pl}) = s_{pl} - C(u_{ph}, s_{pl}) - C(v_{ph}, s_{pl}) \\
& - C(r_{ph}, s_{pl}) + C(u_{ph}, v_{ph}, s_{pl}) + C(u_{ph}, r_{ph}, s_{pl}) + C(v_{ph}, r_{ph}, s_{pl}) \\
& - C(u_{ph}, v_{ph}, r_{ph}, s_{pl})
\end{aligned}$$

793 (8) The probability of Type [X-M, Y-H, Z-H, W-H] is as follows:

$$\begin{aligned}
& P(X_{pl} < X < X_{ph}, Y > Y_{ph}, Z > Z_{ph}, W > W_{ph}) = u_{ph} - u_{pl} - C(u_{ph}, v_{ph}) \\
& - C(u_{ph}, r_{ph}) - C(u_{ph}, s_{ph}) + C(u_{pl}, v_{ph}) + C(u_{pl}, r_{ph}) + C(u_{pl}, s_{ph}) \\
794 \quad & + C(u_{ph}, v_{ph}, r_{ph}) + C(u_{ph}, v_{ph}, s_{ph}) + C(u_{ph}, r_{ph}, s_{ph}) - C(u_{pl}, v_{ph}, r_{ph}) \\
& - C(u_{pl}, v_{ph}, s_{ph}) - C(u_{pl}, r_{ph}, s_{ph}) - C(u_{ph}, v_{ph}, r_{ph}, s_{ph}) \\
& + C(u_{pl}, v_{ph}, r_{ph}, s_{ph})
\end{aligned}$$

795 (9) The probability of Type [X-H, Y-M, Z-H, W-H] is as follows:

$$\begin{aligned}
& P(X > X_{ph}, Y_{pl} < Y < Y_{ph}, Z > Z_{ph}, W > W_{ph}) = v_{ph} - v_{pl} - C(u_{ph}, v_{ph}) \\
& - C(v_{ph}, r_{ph}) - C(v_{ph}, s_{ph}) + C(u_{ph}, v_{pl}) + C(v_{pl}, r_{ph}) + C(v_{pl}, s_{ph}) \\
796 \quad & + C(u_{ph}, v_{ph}, r_{ph}) + C(u_{ph}, v_{ph}, s_{ph}) + C(v_{ph}, r_{ph}, s_{ph}) - C(u_{ph}, v_{pl}, r_{ph}) \\
& - C(u_{ph}, v_{pl}, s_{ph}) - C(v_{pl}, r_{ph}, s_{ph}) - C(u_{ph}, v_{ph}, r_{ph}, s_{ph}) \\
& + C(u_{ph}, v_{pl}, r_{ph}, s_{ph})
\end{aligned}$$

797 (10) The probability of Type [X-H, Y-H, Z-M, W-H] is as follows:

$$\begin{aligned}
& P(X > X_{ph}, Y > Y_{ph}, Z_{pl} < Z < Z_{ph}, W > W_{ph}) = r_{ph} - r_{pl} - C(u_{ph}, r_{ph}) \\
& - C(v_{ph}, r_{ph}) - C(r_{ph}, s_{ph}) + C(u_{ph}, r_{pl}) + C(v_{ph}, r_{pl}) + C(r_{pl}, s_{ph}) \\
798 \quad & + C(u_{ph}, v_{ph}, r_{ph}) + C(u_{ph}, r_{ph}, s_{ph}) + C(v_{ph}, r_{ph}, s_{ph}) - C(u_{ph}, v_{ph}, r_{pl}) \\
& - C(u_{ph}, r_{pl}, s_{ph}) - C(v_{ph}, r_{pl}, s_{ph}) - C(u_{ph}, v_{ph}, r_{ph}, s_{ph}) \\
& + C(u_{ph}, v_{ph}, r_{pl}, s_{ph})
\end{aligned}$$

799 (11) The probability of Type [X-H, Y-H, Z-H, W-M] is as follows:

$$\begin{aligned}
& P(X > X_{ph}, Y > Y_{ph}, Z > Z_{ph}, W_{pl} < W < W_{ph}) = s_{ph} - s_{pl} - C(u_{ph}, s_{ph}) \\
& - C(v_{ph}, s_{ph}) - C(r_{ph}, s_{ph}) + C(u_{ph}, s_{pl}) + C(v_{ph}, s_{pl}) + C(r_{ph}, s_{pl}) \\
800 \quad & + C(u_{ph}, v_{ph}, s_{ph}) + C(u_{ph}, r_{ph}, s_{ph}) + C(v_{ph}, r_{ph}, s_{ph}) - C(u_{ph}, v_{ph}, s_{pl}) \\
& - C(u_{ph}, r_{ph}, s_{pl}) - C(v_{ph}, r_{ph}, s_{pl}) - C(u_{ph}, v_{ph}, r_{ph}, s_{ph}) \\
& + C(u_{ph}, v_{ph}, r_{ph}, s_{pl})
\end{aligned}$$

801 (12) The probability of Type [X-L, Y-L, Z-H, W-H] is as follows:

$$\begin{aligned}
802 \quad & P(X < X_{pl}, Y < Y_{pl}, Z > Z_{ph}, W > W_{ph}) = C(u_{pl}, v_{pl}) - C(u_{pl}, v_{pl}, r_{ph}) \\
& - C(u_{pl}, v_{pl}, s_{ph}) + C(u_{pl}, v_{pl}, r_{ph}, s_{ph})
\end{aligned}$$

803 (13) The probability of Type [X-L, Y-H, Z-L, W-H] is as follows:

$$\begin{aligned}
804 \quad & P(X < X_{pl}, Y > Y_{ph}, Z < Z_{pl}, W > W_{ph}) = C(u_{pl}, r_{pl}) - C(u_{pl}, v_{ph}, r_{pl}) \\
& - C(u_{pl}, r_{pl}, s_{ph}) + C(u_{pl}, v_{ph}, r_{pl}, s_{ph})
\end{aligned}$$

805 (14) The probability of Type [X-L, Y-H, Z-H, W-L] is as follows:

$$\begin{aligned}
806 \quad & P(X < X_{pl}, Y > Y_{ph}, Z > Z_{ph}, W < W_{pl}) = C(u_{pl}, s_{pl}) - C(u_{pl}, v_{ph}, s_{pl}) \\
& - C(u_{pl}, r_{ph}, s_{pl}) + C(u_{pl}, v_{ph}, r_{ph}, s_{pl})
\end{aligned}$$

807 (15) The probability of Type [X-H, Y-L, Z-L, W-H] is as follows:

$$\begin{aligned}
808 \quad & P(X > X_{ph}, Y < Y_{pl}, Z < Z_{pl}, W > W_{ph}) = C(v_{pl}, r_{pl}) - C(u_{ph}, v_{pl}, r_{pl}) \\
& - C(v_{pl}, r_{pl}, s_{ph}) + C(u_{ph}, v_{pl}, r_{pl}, s_{ph})
\end{aligned}$$

809 (16) The probability of Type [X-H, Y-L, Z-H, W-L] is as follows:

$$\begin{aligned}
810 \quad & P(X > X_{ph}, Y < Y_{pl}, Z > Z_{ph}, W < W_{pl}) = C(v_{pl}, s_{pl}) - C(u_{ph}, v_{pl}, s_{pl}) \\
& - C(v_{pl}, r_{ph}, s_{pl}) + C(u_{ph}, v_{pl}, r_{ph}, s_{pl})
\end{aligned}$$

811 (17) The probability of Type [X-H, Y-H, Z-L, W-L] is as follows:

812
$$P(X > X_{ph}, Y > Y_{ph}, Z < Z_{pl}, W < W_{pl}) = C(r_{pl}, s_{pl}) - C(u_{ph}, r_{pl}, s_{pl})$$

$$-C(v_{ph}, r_{pl}, s_{pl}) + C(u_{ph}, v_{ph}, r_{pl}, s_{pl})$$

813 (18) The probability of Type [X-M, Y-L, Z-H, W-H] is as follows:

814
$$P(X_{pl} < X < X_{ph}, Y < Y_{pl}, Z > Z_{ph}, W > W_{ph}) = C(u_{ph}, v_{pl}) - C(u_{pl}, v_{pl})$$

$$-C(u_{ph}, v_{pl}, r_{ph}) - C(u_{ph}, v_{pl}, s_{ph}) + C(u_{pl}, v_{pl}, r_{ph}) + C(u_{pl}, v_{pl}, s_{ph})$$

$$+C(u_{ph}, v_{pl}, r_{ph}, s_{ph}) - C(u_{pl}, v_{pl}, r_{ph}, s_{ph})$$

815 (19) The probability of Type [X-L, Y-M, Z-H, W-H] is as follows:

816
$$P(X < X_{pl}, Y_{pl} < Y < Y_{ph}, Z > Z_{ph}, W > W_{ph}) = C(u_{pl}, v_{ph}) - C(u_{pl}, v_{pl})$$

$$-C(u_{pl}, v_{ph}, r_{ph}) - C(u_{pl}, v_{ph}, s_{ph}) + C(u_{pl}, v_{pl}, r_{ph}) + C(u_{pl}, v_{pl}, s_{ph})$$

$$+C(u_{pl}, v_{ph}, r_{ph}, s_{ph}) - C(u_{pl}, v_{pl}, r_{ph}, s_{ph})$$

817 (20) The probability of Type [X-M, Y-H, Z-L, W-H] is as follows:

818
$$P(X_{pl} < X < X_{ph}, Y > Y_{ph}, Z < Z_{pl}, W > W_{ph}) = C(u_{ph}, r_{pl}) - C(u_{pl}, r_{pl})$$

$$-C(u_{ph}, v_{ph}, r_{pl}) - C(u_{ph}, r_{pl}, s_{ph}) + C(u_{pl}, v_{ph}, r_{pl}) + C(u_{pl}, r_{pl}, s_{ph})$$

$$+C(u_{ph}, v_{ph}, r_{pl}, s_{ph}) - C(u_{pl}, v_{ph}, r_{pl}, s_{ph})$$

819 (21) The probability of Type [X-L, Y-H, Z-M, W-H] is as follows:

820
$$P(X < X_{pl}, Y > Y_{ph}, Z_{pl} < Z < Z_{ph}, W > W_{ph}) = C(u_{pl}, r_{ph}) - C(u_{pl}, r_{pl})$$

$$-C(u_{pl}, v_{ph}, r_{ph}) - C(u_{pl}, r_{ph}, s_{ph}) + C(u_{pl}, v_{ph}, r_{pl}) + C(u_{pl}, r_{pl}, s_{ph})$$

$$+C(u_{pl}, v_{ph}, r_{ph}, s_{ph}) - C(u_{pl}, v_{ph}, r_{pl}, s_{ph})$$

821 (22) The probability of Type [X-M, Y-H, Z-H, W-L] is as follows:

822
$$P(X_{pl} < X < X_{ph}, Y > Y_{ph}, Z > Z_{ph}, W < W_{pl}) = C(u_{ph}, s_{pl}) - C(u_{pl}, s_{pl})$$

$$-C(u_{ph}, v_{ph}, s_{pl}) - C(u_{ph}, r_{ph}, s_{pl}) + C(u_{pl}, v_{ph}, s_{pl}) + C(u_{pl}, r_{ph}, s_{pl})$$

$$+C(u_{ph}, v_{ph}, r_{ph}, s_{pl}) - C(u_{pl}, v_{ph}, r_{ph}, s_{pl})$$

823 (23) The probability of Type [X-L, Y-H, Z-H, W-M] is as follows:

824
$$P(X < X_{pl}, Y > Y_{ph}, Z > Z_{ph}, W_{pl} < W < W_{ph}) = C(u_{pl}, s_{ph}) - C(u_{pl}, s_{pl})$$

$$-C(u_{pl}, v_{ph}, s_{ph}) - C(u_{pl}, r_{ph}, s_{ph}) + C(u_{pl}, v_{ph}, s_{pl}) + C(u_{pl}, r_{ph}, s_{pl})$$

$$+C(u_{pl}, v_{ph}, r_{ph}, s_{ph}) - C(u_{pl}, v_{ph}, r_{ph}, s_{pl})$$

825 (24) The probability of Type [X-H, Y-M, Z-L, W-H] is as follows:

826
$$P(X > X_{ph}, Y_{pl} < Y < Y_{ph}, Z < Z_{pl}, W > W_{ph}) = C(v_{ph}, r_{pl}) - C(v_{pl}, r_{pl})$$

$$-C(u_{ph}, v_{ph}, r_{pl}) - C(v_{ph}, r_{pl}, s_{ph}) + C(u_{ph}, v_{pl}, r_{pl}) + C(v_{pl}, r_{pl}, s_{ph})$$

$$+C(u_{ph}, v_{ph}, r_{pl}, s_{ph}) - C(u_{ph}, v_{pl}, r_{pl}, s_{ph})$$

827 (25) The probability of Type [X-H, Y-L, Z-M, W-H] is as follows:

828
$$P(X > X_{ph}, Y < Y_{pl}, Z_{pl} < Z < Z_{ph}, W > W_{ph}) = C(v_{pl}, r_{ph}) - C(v_{pl}, r_{pl})$$

$$-C(u_{ph}, v_{pl}, r_{ph}) - C(v_{pl}, r_{ph}, s_{ph}) + C(u_{ph}, v_{pl}, r_{pl}) + C(v_{pl}, r_{pl}, s_{ph})$$

$$+C(u_{ph}, v_{pl}, r_{ph}, s_{ph}) - C(u_{ph}, v_{pl}, r_{pl}, s_{ph})$$

829 (26) The probability of Type [X-H, Y-M, Z-H, W-L] is as follows:

830
$$P(X > X_{ph}, Y_{pl} < Y < Y_{ph}, Z > Z_{ph}, W < W_{pl}) = C(v_{ph}, s_{pl}) - C(v_{pl}, s_{pl})$$

$$-C(u_{ph}, v_{ph}, s_{pl}) - C(v_{ph}, r_{ph}, s_{pl}) + C(u_{ph}, v_{pl}, s_{pl}) + C(v_{pl}, r_{ph}, s_{pl})$$

$$+C(u_{ph}, v_{ph}, r_{ph}, s_{pl}) - C(u_{ph}, v_{pl}, r_{ph}, s_{pl})$$

- 831 (27) The probability of Type [X-H, Y-L, Z-H, W-M] is as follows:
- $$\begin{aligned}
& P(X > X_{ph}, Y < Y_{pl}, Z > Z_{ph}, W_{pl} < W < W_{ph}) = C(v_{pl}, s_{ph}) - C(v_{pl}, s_{pl}) \\
& - C(u_{ph}, v_{pl}, s_{ph}) - C(v_{pl}, r_{ph}, s_{ph}) + C(u_{ph}, v_{pl}, s_{pl}) + C(v_{pl}, r_{ph}, s_{pl}) \\
& + C(u_{ph}, v_{pl}, r_{ph}, s_{ph}) - C(u_{ph}, v_{pl}, r_{ph}, s_{pl})
\end{aligned}$$
- 832
- 833 (28) The probability of Type [X-H, Y-H, Z-M, W-L] is as follows:
- $$\begin{aligned}
& P(X > X_{ph}, Y > Y_{ph}, Z_{pl} < Z < Z_{ph}, W < W_{pl}) = C(r_{ph}, s_{pl}) - C(r_{pl}, s_{pl}) \\
& - C(u_{ph}, r_{ph}, s_{pl}) - C(v_{ph}, r_{ph}, s_{pl}) + C(u_{ph}, r_{pl}, s_{pl}) + C(v_{ph}, r_{pl}, s_{pl}) \\
& + C(u_{ph}, v_{ph}, r_{ph}, s_{pl}) - C(u_{ph}, v_{ph}, r_{pl}, s_{pl})
\end{aligned}$$
- 834
- 835 (29) The probability of Type [X-H, Y-H, Z-L, W-M] is as follows:
- $$\begin{aligned}
& P(X > X_{ph}, Y > Y_{ph}, Z < Z_{pl}, W_{pl} < W < W_{ph}) = C(r_{pl}, s_{ph}) - C(r_{pl}, s_{pl}) \\
& - C(u_{ph}, r_{pl}, s_{ph}) - C(v_{ph}, r_{pl}, s_{ph}) + C(u_{ph}, r_{pl}, s_{pl}) + C(v_{ph}, r_{pl}, s_{pl}) \\
& + C(u_{ph}, v_{ph}, r_{pl}, s_{ph}) - C(u_{ph}, v_{ph}, r_{pl}, s_{pl})
\end{aligned}$$
- 836
- 837 (30) The probability of Type [X-M, Y-M, Z-H, W-H] is as follows:
- $$\begin{aligned}
& P(X_{pl} < X < X_{ph}, Y_{pl} < Y < Y_{ph}, Z > Z_{ph}, W > W_{ph}) = C(u_{ph}, v_{ph}) \\
& + C(u_{pl}, v_{pl}) - C(u_{ph}, v_{pl}) - C(u_{pl}, v_{ph}) - C(u_{ph}, v_{ph}, r_{ph}) \\
& - C(u_{ph}, v_{ph}, s_{ph}) + C(u_{pl}, v_{ph}, r_{ph}) + C(u_{pl}, v_{ph}, s_{ph}) + C(u_{ph}, v_{pl}, r_{ph}) \\
& + C(u_{ph}, v_{pl}, s_{ph}) - C(u_{pl}, v_{pl}, r_{ph}) - C(u_{pl}, v_{pl}, s_{ph}) + C(u_{ph}, v_{ph}, r_{ph}, s_{ph}) \\
& - C(u_{pl}, v_{ph}, r_{ph}, s_{ph}) - C(u_{ph}, v_{pl}, r_{ph}, s_{ph}) + C(u_{pl}, v_{pl}, r_{ph}, s_{ph})
\end{aligned}$$
- 838
- 839 (31) The probability of Type [X-M, Y-H, Z-M, W-H] is as follows:
- $$\begin{aligned}
& P(X_{pl} < X < X_{ph}, Y > Y_{ph}, Z_{pl} < Z < Z_{ph}, W > W_{ph}) = C(u_{ph}, r_{ph}) \\
& + C(u_{pl}, r_{pl}) - C(u_{ph}, r_{pl}) - C(u_{pl}, r_{ph}) - C(u_{ph}, v_{ph}, r_{ph}) \\
& - C(u_{ph}, r_{ph}, s_{ph}) + C(u_{pl}, v_{ph}, r_{ph}) + C(u_{pl}, r_{ph}, s_{ph}) + C(u_{ph}, v_{ph}, r_{pl}) \\
& + C(u_{ph}, r_{pl}, s_{ph}) - C(u_{pl}, v_{ph}, r_{pl}) - C(u_{pl}, r_{pl}, s_{ph}) + C(u_{ph}, v_{ph}, r_{ph}, s_{ph}) \\
& - C(u_{pl}, v_{ph}, r_{ph}, s_{ph}) - C(u_{ph}, v_{ph}, r_{pl}, s_{ph}) + C(u_{pl}, v_{ph}, r_{pl}, s_{ph})
\end{aligned}$$
- 840
- 841 (32) The probability of Type [X-M, Y-H, Z-H, W-M] is as follows:
- $$\begin{aligned}
& P(X_{pl} < X < X_{ph}, Y > Y_{ph}, Z > Z_{ph}, W_{pl} < W < W_{ph}) = C(u_{ph}, s_{ph}) \\
& + C(u_{pl}, s_{pl}) - C(u_{ph}, s_{pl}) - C(u_{pl}, s_{ph}) - C(u_{ph}, v_{ph}, s_{ph}) \\
& - C(u_{ph}, r_{ph}, s_{ph}) + C(u_{pl}, v_{ph}, s_{ph}) + C(u_{pl}, r_{ph}, s_{ph}) + C(u_{ph}, v_{ph}, s_{pl}) \\
& + C(u_{ph}, r_{ph}, s_{pl}) - C(u_{pl}, v_{ph}, s_{pl}) - C(u_{pl}, r_{ph}, s_{pl}) + C(u_{ph}, v_{ph}, r_{ph}, s_{ph}) \\
& - C(u_{pl}, v_{ph}, r_{ph}, s_{ph}) - C(u_{ph}, v_{ph}, r_{ph}, s_{pl}) + C(u_{pl}, v_{ph}, r_{ph}, s_{pl})
\end{aligned}$$
- 842
- 843 (33) The probability of Type [X-H, Y-M, Z-M, W-H] is as follows:
- $$\begin{aligned}
& P(X > X_{ph}, Y_{pl} < Y < Y_{ph}, Z_{pl} < Z < Z_{ph}, W > W_{ph}) = C(v_{ph}, r_{ph}) \\
& + C(v_{pl}, r_{pl}) - C(v_{ph}, r_{pl}) - C(v_{pl}, r_{ph}) - C(u_{ph}, v_{ph}, r_{ph}) \\
& - C(v_{ph}, r_{ph}, s_{ph}) + C(u_{ph}, v_{pl}, r_{ph}) + C(v_{pl}, r_{ph}, s_{ph}) + C(u_{ph}, v_{ph}, r_{pl}) \\
& + C(v_{ph}, r_{pl}, s_{ph}) - C(u_{pl}, v_{ph}, r_{pl}) - C(v_{pl}, r_{pl}, s_{ph}) + C(u_{ph}, v_{ph}, r_{ph}, s_{ph}) \\
& - C(u_{ph}, v_{pl}, r_{ph}, s_{ph}) - C(u_{ph}, v_{ph}, r_{pl}, s_{ph}) + C(u_{ph}, v_{pl}, r_{pl}, s_{ph})
\end{aligned}$$
- 844
- 845 (34) The probability of Type [X-H, Y-M, Z-H, W-M] is as follows:

$$\begin{aligned}
& P(X > X_{ph}, Y_{pl} < Y < Y_{ph}, Z > Z_{ph}, W_{pl} < W < W_{ph}) = C(v_{ph}, s_{ph}) \\
& + C(v_{pl}, s_{pl}) - C(v_{ph}, s_{pl}) - C(v_{pl}, s_{ph}) - C(u_{ph}, v_{ph}, s_{ph}) \\
846 \quad & - C(v_{ph}, r_{ph}, s_{ph}) + C(u_{ph}, v_{pl}, s_{ph}) + C(v_{pl}, r_{ph}, s_{ph}) + C(u_{ph}, v_{ph}, s_{pl}) \\
& + C(v_{ph}, r_{ph}, s_{pl}) - C(u_{ph}, v_{pl}, s_{pl}) - C(v_{pl}, r_{ph}, s_{pl}) + C(u_{ph}, v_{ph}, r_{ph}, s_{ph}) \\
& - C(u_{ph}, v_{pl}, r_{ph}, s_{ph}) - C(u_{ph}, v_{ph}, r_{ph}, s_{pl}) + C(u_{ph}, v_{pl}, r_{ph}, s_{pl})
\end{aligned}$$

847 (35) The probability of Type [X-H, Y-H, Z-M, W-M] is as follows:

$$\begin{aligned}
& P(X > X_{ph}, Y > Y_{ph}, Z_{pl} < Z < Z_{ph}, W_{pl} < W < W_{ph}) = C(r_{ph}, s_{ph}) \\
& + C(r_{pl}, s_{pl}) - C(r_{ph}, s_{pl}) - C(r_{pl}, s_{ph}) - C(u_{ph}, r_{ph}, s_{ph}) \\
848 \quad & - C(v_{ph}, r_{ph}, s_{ph}) + C(u_{ph}, r_{pl}, s_{ph}) + C(v_{ph}, r_{pl}, s_{ph}) + C(u_{ph}, r_{ph}, s_{pl}) \\
& + C(v_{ph}, r_{ph}, s_{pl}) - C(u_{ph}, r_{pl}, s_{pl}) - C(v_{ph}, r_{pl}, s_{pl}) + C(u_{ph}, v_{ph}, r_{ph}, s_{ph}) \\
& - C(u_{ph}, v_{ph}, r_{pl}, s_{ph}) - C(u_{ph}, v_{ph}, r_{ph}, s_{pl}) + C(u_{ph}, v_{ph}, r_{pl}, s_{pl})
\end{aligned}$$

849 (36) The probability of Type [X-M, Y-M, Z-M, W-H] is as follows:

$$\begin{aligned}
& P(X_{pl} < X < X_{ph}, Y_{pl} < Y < Y_{ph}, Z_{pl} < Z < Z_{ph}, W > W_{ph}) \\
& = C(u_{ph}, v_{ph}, r_{ph}) - C(u_{ph}, v_{ph}, r_{pl}) - C(u_{ph}, v_{pl}, r_{ph}) - C(u_{pl}, v_{ph}, r_{ph}) \\
850 \quad & + C(u_{pl}, v_{pl}, r_{ph}) + C(u_{pl}, v_{ph}, r_{pl}) + C(u_{ph}, v_{pl}, r_{pl}) - C(u_{pl}, v_{pl}, r_{pl}) \\
& - C(u_{ph}, v_{ph}, r_{ph}, s_{ph}) + C(u_{pl}, v_{ph}, r_{ph}, s_{ph}) + C(u_{ph}, v_{pl}, r_{ph}, s_{ph}) \\
& + C(u_{ph}, v_{ph}, r_{pl}, s_{ph}) - C(u_{pl}, v_{pl}, r_{ph}, s_{ph}) - C(u_{pl}, v_{ph}, r_{pl}, s_{ph}) \\
& - C(u_{ph}, v_{pl}, r_{pl}, s_{ph}) + C(u_{pl}, v_{pl}, r_{pl}, s_{ph})
\end{aligned}$$

851 (37) The probability of Type [X-H, Y-M, Z-M, W-M] is as follows:

$$\begin{aligned}
& P(X > X_{ph}, Y_{pl} < Y < Y_{ph}, Z_{pl} < Z < Z_{ph}, W_{pl} < W < W_{ph}) \\
& = C(v_{ph}, r_{ph}, s_{ph}) - C(v_{ph}, r_{ph}, s_{pl}) - C(v_{ph}, r_{pl}, s_{ph}) - C(v_{pl}, r_{ph}, s_{ph}) \\
852 \quad & + C(v_{pl}, r_{pl}, s_{ph}) + C(v_{pl}, r_{ph}, s_{pl}) + C(v_{ph}, r_{pl}, s_{pl}) - C(v_{pl}, r_{pl}, s_{pl}) \\
& - C(u_{ph}, v_{ph}, r_{ph}, s_{ph}) + C(u_{ph}, v_{pl}, r_{ph}, s_{ph}) + C(u_{ph}, v_{ph}, r_{pl}, s_{ph}) \\
& + C(u_{ph}, v_{ph}, r_{ph}, s_{pl}) - C(u_{ph}, v_{pl}, r_{pl}, s_{ph}) - C(u_{ph}, v_{pl}, r_{ph}, s_{pl}) \\
& - C(u_{ph}, v_{ph}, r_{pl}, s_{pl}) + C(u_{ph}, v_{pl}, r_{pl}, s_{pl})
\end{aligned}$$

853 (38) The probability of Type [X-M, Y-H, Z-M, W-M] is as follows:

$$\begin{aligned}
& P(X_{pl} < X < X_{ph}, Y_{pl} < Y < Y_{ph}, Z > Z_{ph}, W_{pl} < W < W_{ph}) \\
& = C(u_{ph}, r_{ph}, s_{ph}) - C(u_{ph}, r_{ph}, s_{pl}) - C(u_{ph}, r_{pl}, s_{ph}) - C(u_{pl}, r_{ph}, s_{ph}) \\
854 \quad & + C(u_{pl}, r_{pl}, s_{ph}) + C(u_{pl}, r_{ph}, s_{pl}) + C(u_{ph}, r_{pl}, s_{pl}) - C(u_{pl}, r_{pl}, s_{pl}) \\
& - C(u_{ph}, v_{ph}, r_{ph}, s_{ph}) + C(u_{pl}, v_{ph}, r_{ph}, s_{ph}) + C(u_{ph}, v_{ph}, r_{pl}, s_{ph}) \\
& + C(u_{ph}, v_{ph}, r_{ph}, s_{pl}) - C(u_{pl}, v_{ph}, r_{pl}, s_{ph}) - C(u_{pl}, v_{ph}, r_{ph}, s_{pl}) \\
& - C(u_{ph}, v_{ph}, r_{pl}, s_{pl}) + C(u_{pl}, v_{ph}, r_{pl}, s_{pl})
\end{aligned}$$

855 (39) The probability of Type [X-M, Y-M, Z-H, W-M] is as follows:

$$\begin{aligned}
& P(X_{pl} < X < X_{ph}, Y_{pl} < Y < Y_{ph}, Z > Z_{ph}, W_{pl} < W < W_{ph}) \\
& = C(u_{ph}, v_{ph}, s_{ph}) - C(u_{ph}, v_{ph}, s_{pl}) - C(u_{ph}, v_{pl}, s_{ph}) - C(u_{pl}, v_{ph}, s_{ph}) \\
856 \quad & + C(u_{pl}, v_{pl}, s_{ph}) + C(u_{pl}, v_{ph}, s_{pl}) + C(u_{ph}, v_{pl}, s_{pl}) - C(u_{pl}, v_{pl}, s_{pl}) \\
& - C(u_{ph}, v_{ph}, r_{ph}, s_{ph}) + C(u_{pl}, v_{ph}, r_{ph}, s_{ph}) + C(u_{ph}, v_{pl}, r_{ph}, s_{ph}) \\
& + C(u_{ph}, v_{ph}, r_{ph}, s_{pl}) - C(u_{pl}, v_{pl}, r_{ph}, s_{ph}) - C(u_{pl}, v_{ph}, r_{ph}, s_{pl}) \\
& - C(u_{ph}, v_{pl}, r_{ph}, s_{pl}) + C(u_{pl}, v_{pl}, r_{ph}, s_{pl})
\end{aligned}$$

857 (40) The probability of Type [X-M, Y-M, Z-L, W-H] is as follows:

$$\begin{aligned}
& P(X_{pl} < X < X_{ph}, Y_{pl} < Y < Y_{ph}, Z < Z_{pl}, W > W_{ph}) = C(u_{ph}, v_{ph}, r_{pl}) \\
& -C(u_{ph}, v_{pl}, r_{pl}) - C(u_{pl}, v_{ph}, r_{pl}) + C(u_{pl}, v_{pl}, r_{pl}) - C(u_{ph}, v_{ph}, r_{pl}, s_{ph}) \\
& + C(u_{pl}, v_{ph}, r_{pl}, s_{ph}) + C(u_{ph}, v_{pl}, r_{pl}, s_{ph}) - C(u_{pl}, v_{pl}, r_{pl}, s_{ph})
\end{aligned}$$

859 (41) The probability of Type [X-M, Y-M, Z-H, W-L] is as follows:

$$\begin{aligned}
& P(X_{pl} < X < X_{ph}, Y_{pl} < Y < Y_{ph}, Z > Z_{ph}, W < W_{pl}) = C(u_{ph}, v_{ph}, s_{pl}) \\
& -C(u_{ph}, v_{pl}, s_{pl}) - C(u_{pl}, v_{ph}, s_{pl}) + C(u_{pl}, v_{pl}, s_{pl}) - C(u_{ph}, v_{ph}, r_{ph}, s_{pl}) \\
& + C(u_{pl}, v_{ph}, r_{ph}, s_{pl}) + C(u_{ph}, v_{pl}, r_{ph}, s_{pl}) - C(u_{pl}, v_{pl}, r_{ph}, s_{pl})
\end{aligned}$$

861 (42) The probability of Type [X-M, Y-L, Z-M, W-H] is as follows:

$$\begin{aligned}
& P(X_{pl} < X < X_{ph}, Y < Y_{pl}, Z_{pl} < Z < Z_{ph}, W > W_{ph}) = C(u_{ph}, v_{pl}, r_{ph}) \\
& -C(u_{pl}, v_{pl}, r_{ph}) - C(u_{ph}, v_{pl}, r_{pl}) + C(u_{pl}, v_{pl}, r_{pl}) - C(u_{ph}, v_{pl}, r_{ph}, s_{ph}) \\
& + C(u_{pl}, v_{pl}, r_{ph}, s_{ph}) + C(u_{ph}, v_{pl}, r_{pl}, s_{ph}) - C(u_{pl}, v_{pl}, r_{pl}, s_{ph})
\end{aligned}$$

863 (43) The probability of Type [X-M, Y-H, Z-M, W-L] is as follows:

$$\begin{aligned}
& P(X_{pl} < X < X_{ph}, Y > Y_{ph}, Z_{pl} < Z < Z_{ph}, W < W_{pl}) = C(u_{ph}, r_{ph}, s_{pl}) \\
& -C(u_{pl}, r_{ph}, s_{pl}) - C(u_{ph}, r_{pl}, s_{pl}) + C(u_{pl}, r_{pl}, s_{pl}) - C(u_{ph}, v_{ph}, r_{ph}, s_{pl}) \\
& + C(u_{pl}, v_{ph}, r_{ph}, s_{pl}) + C(u_{ph}, v_{ph}, r_{pl}, s_{pl}) - C(u_{pl}, v_{ph}, r_{pl}, s_{pl})
\end{aligned}$$

865 (44) The probability of Type [X-M, Y-H, Z-L, W-M] is as follows:

$$\begin{aligned}
& P(X_{pl} < X < X_{ph}, Y > Y_{ph}, Z < Z_{pl}, W_{pl} < W < W_{ph}) = C(u_{ph}, r_{pl}, s_{ph}) \\
& -C(u_{pl}, r_{pl}, s_{ph}) - C(u_{ph}, r_{pl}, s_{pl}) + C(u_{pl}, r_{pl}, s_{pl}) - C(u_{ph}, v_{ph}, r_{pl}, s_{ph}) \\
& + C(u_{pl}, v_{ph}, r_{pl}, s_{ph}) + C(u_{ph}, v_{ph}, r_{pl}, s_{pl}) - C(u_{pl}, v_{ph}, r_{pl}, s_{pl})
\end{aligned}$$

867 (45) The probability of Type [X-M, Y-L, Z-H, W-M] is as follows:

$$\begin{aligned}
& P(X_{pl} < X < X_{ph}, Y < Y_{pl}, Z > Z_{ph}, W_{pl} < W < W_{ph}) = C(u_{ph}, v_{pl}, s_{ph}) \\
& -C(u_{pl}, v_{pl}, s_{ph}) - C(u_{ph}, v_{pl}, s_{pl}) + C(u_{pl}, v_{pl}, s_{pl}) - C(u_{ph}, v_{pl}, r_{ph}, s_{ph}) \\
& + C(u_{pl}, v_{pl}, r_{ph}, s_{ph}) + C(u_{ph}, v_{pl}, r_{ph}, s_{pl}) - C(u_{pl}, v_{pl}, r_{ph}, s_{pl})
\end{aligned}$$

869 (46) The probability of Type [X-L, Y-M, Z-M, W-H] is as follows:

$$\begin{aligned}
& P(X < X_{pl}, Y_{pl} < Y < Y_{ph}, Z_{pl} < Z < Z_{ph}, W > W_{ph}) = C(u_{pl}, v_{ph}, r_{ph}) \\
& -C(u_{pl}, v_{pl}, r_{ph}) - C(u_{pl}, v_{ph}, r_{pl}) + C(u_{pl}, v_{pl}, r_{pl}) - C(u_{pl}, v_{ph}, r_{ph}, s_{ph}) \\
& + C(u_{pl}, v_{pl}, r_{ph}, s_{ph}) + C(u_{pl}, v_{ph}, r_{pl}, s_{ph}) - C(u_{pl}, v_{pl}, r_{pl}, s_{ph})
\end{aligned}$$

871 (47) The probability of Type [X-H, Y-M, Z-M, W-L] is as follows:

$$\begin{aligned}
& P(X > X_{ph}, Y_{pl} < Y < Y_{ph}, Z_{pl} < Z < Z_{ph}, W < W_{pl}) = C(v_{ph}, r_{ph}, s_{pl}) \\
& -C(v_{pl}, r_{ph}, s_{pl}) - C(v_{ph}, r_{pl}, s_{pl}) + C(v_{pl}, r_{pl}, s_{pl}) - C(u_{ph}, v_{ph}, r_{ph}, s_{pl}) \\
& + C(u_{ph}, v_{pl}, r_{ph}, s_{pl}) + C(u_{ph}, v_{ph}, r_{pl}, s_{pl}) - C(u_{ph}, v_{pl}, r_{pl}, s_{pl})
\end{aligned}$$

873 (48) The probability of Type [X-H, Y-M, Z-L, W-M]] is as follows:

$$\begin{aligned}
& P(X > X_{ph}, Y_{pl} < Y < Y_{ph}, Z < Z_{pl}, W_{pl} < W < W_{ph}) = C(v_{ph}, r_{pl}, s_{ph}) \\
& -C(v_{pl}, r_{pl}, s_{ph}) - C(v_{ph}, r_{pl}, s_{pl}) + C(v_{pl}, r_{pl}, s_{pl}) - C(u_{ph}, v_{ph}, r_{pl}, s_{ph}) \\
& + C(u_{ph}, v_{pl}, r_{pl}, s_{ph}) + C(u_{ph}, v_{ph}, r_{pl}, s_{pl}) - C(u_{ph}, v_{pl}, r_{pl}, s_{pl})
\end{aligned}$$

875 (49) The probability of Type [X-L, Y-M, Z-H, W-M]] is as follows:

$$\begin{aligned}
& P(X < X_{pl}, Y_{pl} < Y < Y_{ph}, Z > Z_{ph}, W_{pl} < W < W_{ph}) = C(u_{pl}, v_{ph}, s_{ph}) \\
& -C(u_{pl}, v_{pl}, s_{ph}) - C(u_{pl}, v_{ph}, s_{pl}) + C(u_{pl}, v_{pl}, s_{pl}) - C(u_{pl}, v_{ph}, r_{ph}, s_{ph}) \\
& + C(u_{pl}, v_{pl}, r_{ph}, s_{ph}) + C(u_{pl}, v_{ph}, r_{ph}, s_{pl}) - C(u_{pl}, v_{pl}, r_{ph}, s_{pl})
\end{aligned}$$

877 (50) The probability of Type [X-L, Y-H, Z-M, W-M]] is as follows:

$$878 \quad P(X < X_{pl}, Y > Y_{ph}, Z_{pl} < Z < Z_{ph}, W_{pl} < W < W_{ph}) = C(u_{pl}, r_{ph}, s_{ph}) \\ - C(u_{pl}, r_{pl}, s_{ph}) - C(u_{pl}, r_{ph}, s_{pl}) + C(u_{pl}, r_{pl}, s_{pl}) - C(u_{pl}, v_{ph}, r_{ph}, s_{ph}) \\ + C(u_{pl}, v_{ph}, r_{pl}, s_{ph}) + C(u_{pl}, v_{ph}, r_{ph}, s_{pl}) - C(u_{pl}, v_{ph}, r_{pl}, s_{pl})$$

879 (51) The probability of Type [X-H, Y-L, Z-M, W-M]] is as follows:

$$880 \quad P(X > X_{ph}, Y < Y_{pl}, Z_{pl} < Z < Z_{ph}, W_{pl} < W < W_{ph}) = C(v_{pl}, r_{ph}, s_{ph}) \\ - C(v_{pl}, r_{pl}, s_{ph}) - C(v_{pl}, r_{ph}, s_{pl}) + C(v_{pl}, r_{pl}, s_{pl}) - C(u_{ph}, v_{pl}, r_{ph}, s_{ph}) \\ + C(u_{ph}, v_{pl}, r_{pl}, s_{ph}) + C(u_{ph}, v_{pl}, r_{ph}, s_{pl}) - C(u_{ph}, v_{pl}, r_{pl}, s_{pl})$$

881 (52) The probability of Type [X-M, Y-L, Z-L, W-H] is as follows:

$$882 \quad P(X_{pl} < X < X_{ph}, Y < Y_{pl}, Z < Z_{pl}, W > W_{ph}) = C(u_{ph}, v_{pl}, r_{pl}) \\ - C(u_{pl}, v_{pl}, r_{pl}) - C(u_{ph}, v_{pl}, r_{pl}, s_{ph}) + C(u_{pl}, v_{pl}, r_{pl}, s_{ph})$$

883 (53) The probability of Type [X-L, Y-M, Z-L, W-H] is as follows:

$$884 \quad P(X < X_{pl}, Y_{pl} < Y < Y_{ph}, Z < Z_{pl}, W > W_{ph}) = C(u_{pl}, v_{ph}, r_{pl}) \\ - C(u_{pl}, v_{pl}, r_{pl}) - C(u_{pl}, v_{ph}, r_{pl}, s_{ph}) + C(u_{pl}, v_{pl}, r_{pl}, s_{ph})$$

885 (54) The probability of Type [X-L, Y-L, Z-M, W-H] is as follows:

$$886 \quad P(X < X_{pl}, Y_{pl} < Y < Y_{ph}, Z < Z_{pl}, W > W_{ph}) = C(u_{pl}, v_{pl}, r_{ph}) \\ - C(u_{pl}, v_{pl}, r_{pl}) - C(u_{pl}, v_{pl}, r_{ph}, s_{ph}) + C(u_{pl}, v_{pl}, r_{pl}, s_{ph})$$

887 (55) The probability of Type [X-M, Y-L, Z-H, W-L] is as follows:

$$888 \quad P(X_{pl} < X < X_{ph}, Y < Y_{pl}, Z > Z_{ph}, W < W_{pl}) = C(u_{ph}, v_{pl}, s_{pl}) \\ - C(u_{pl}, v_{pl}, s_{pl}) - C(u_{ph}, v_{pl}, r_{ph}, s_{pl}) + C(u_{pl}, v_{pl}, r_{ph}, s_{pl})$$

889 (56) The probability of Type [X-L, Y-M, Z-H, W-L] is as follows:

$$890 \quad P(X < X_{pl}, Y_{pl} < Y < Y_{ph}, Z > Z_{ph}, W < W_{pl}) = C(u_{pl}, v_{ph}, s_{pl}) \\ - C(u_{pl}, v_{pl}, s_{pl}) - C(u_{pl}, v_{ph}, r_{ph}, s_{pl}) + C(u_{pl}, v_{pl}, r_{ph}, s_{pl})$$

891 (57) The probability of Type [X-L, Y-L, Z-H, W-M] is as follows:

$$892 \quad P(X < X_{pl}, Y < Y_{pl}, Z > Z_{ph}, W_{pl} < W < W_{ph}) = C(u_{pl}, v_{pl}, s_{ph}) \\ - C(u_{pl}, v_{pl}, s_{pl}) - C(u_{pl}, v_{pl}, r_{ph}, s_{ph}) + C(u_{pl}, v_{pl}, r_{ph}, s_{pl})$$

893 (58) The probability of Type [X-M, Y-H, Z-L, W-L] is as follows:

$$894 \quad P(X_{pl} < X < X_{ph}, Y > Y_{ph}, Z < Z_{pl}, W < W_{pl}) = C(u_{ph}, r_{pl}, s_{pl}) \\ - C(u_{pl}, r_{pl}, s_{pl}) - C(u_{ph}, v_{ph}, r_{pl}, s_{pl}) + C(u_{pl}, v_{ph}, r_{pl}, s_{pl})$$

895 (59) The probability of Type [X-L, Y-H, Z-M, W-L] is as follows:

$$896 \quad P(X < X_{pl}, Y > Y_{ph}, Z_{pl} < Z < Z_{ph}, W < W_{pl}) = C(u_{pl}, r_{ph}, s_{pl}) \\ - C(u_{pl}, r_{pl}, s_{pl}) - C(u_{pl}, v_{ph}, r_{ph}, s_{pl}) + C(u_{pl}, v_{ph}, r_{pl}, s_{pl})$$

897 (60) The probability of Type [X-L, Y-H, Z-L, W-M] is as follows:

$$898 \quad P(X < X_{pl}, Y > Y_{ph}, Z < Z_{pl}, W_{pl} < W < W_{ph}) = C(u_{pl}, r_{pl}, s_{ph}) \\ - C(u_{pl}, r_{pl}, s_{pl}) - C(u_{pl}, v_{ph}, r_{pl}, s_{ph}) + C(u_{pl}, v_{ph}, r_{pl}, s_{pl})$$

899 (61) The probability of Type [X-H, Y-M, Z-L, W-L] is as follows:

$$900 \quad P(X > X_{ph}, Y_{pl} < Y < Y_{ph}, Z < Z_{pl}, W < W_{pl}) = C(v_{ph}, r_{pl}, s_{pl}) \\ - C(v_{pl}, r_{pl}, s_{pl}) - C(u_{ph}, v_{ph}, r_{pl}, s_{pl}) + C(u_{ph}, v_{pl}, r_{pl}, s_{pl})$$

- 901 (62) The probability of Type [X-H, Y-L, Z-M, W-L] is as follows:
902
$$P(X > X_{ph}, Y < Y_{pl}, Z_{pl} < Z < Z_{ph}, W < W_{pl}) = C(v_{pl}, r_{ph}, s_{pl})$$

$$-C(v_{pl}, r_{pl}, s_{pl}) - C(u_{ph}, v_{pl}, r_{ph}, s_{pl}) + C(u_{ph}, v_{pl}, r_{pl}, s_{pl})$$
- 903 (63) The probability of Type [X-H, Y-L, Z-L, W-M] is as follows:
904
$$P(X > X_{ph}, Y < Y_{pl}, Z < Z_{pl}, W_{pl} < W < W_{ph}) = C(v_{pl}, r_{pl}, s_{ph})$$

$$-C(v_{pl}, r_{pl}, s_{pl}) - C(u_{ph}, v_{pl}, r_{pl}, s_{ph}) + C(u_{ph}, v_{pl}, r_{pl}, s_{pl})$$
- 905 (64) The probability of Type [X-L, Y-L, Z-L, W-H] is as follows:
906
$$P(X < X_{pl}, Y < Y_{pl}, Z < Z_{pl}, W > W_{ph}) = C(u_{pl}, v_{pl}, r_{pl})$$

$$-C(u_{pl}, v_{pl}, r_{pl}, s_{ph})$$
- 907 (65) The probability of Type [X-L, Y-L, Z-H, W-L] is as follows:
908
$$P(X < X_{pl}, Y < Y_{pl}, Z > Z_{ph}, W < W_{pl}) = C(u_{pl}, v_{pl}, s_{pl})$$

$$-C(u_{pl}, v_{pl}, r_{ph}, s_{pl})$$
- 909 (66) The probability of Type [X-L, Y-H, Z-L, W-L] is as follows:
910
$$P(X < X_{pl}, Y > Y_{ph}, Z < Z_{pl}, W < W_{pl}) = C(u_{pl}, r_{pl}, s_{pl})$$

$$-C(u_{pl}, v_{ph}, r_{pl}, s_{pl})$$
- 911 (67) The probability of Type [X-H, Y-L, Z-L, W-L] is as follows:
912
$$P(X > X_{ph}, Y < Y_{pl}, Z < Z_{pl}, W < W_{pl}) = C(v_{pl}, r_{pl}, s_{pl})$$

$$-C(u_{ph}, v_{pl}, r_{pl}, s_{pl})$$
- 913 (68) The probability of Type [X-M, Y-M, Z-M, W-L] is as follows:
914
$$P(X_{pl} < X < X_{ph}, Y_{pl} < Y < Y_{ph}, Z_{pl} < Z < Z_{ph}, W < W_{pl})$$

$$= C(u_{ph}, v_{ph}, r_{ph}, s_{pl}) - C(u_{ph}, v_{ph}, r_{pl}, s_{pl}) - C(u_{ph}, v_{pl}, r_{ph}, s_{pl})$$

$$-C(u_{pl}, v_{ph}, r_{ph}, s_{pl}) + C(u_{ph}, v_{pl}, r_{pl}, s_{pl}) + C(u_{pl}, v_{ph}, r_{pl}, s_{pl})$$

$$+C(u_{pl}, v_{pl}, r_{ph}, s_{pl}) - C(u_{pl}, v_{pl}, r_{pl}, s_{pl})$$
- 915 (69) The probability of Type [X-M, Y-M, Z-L, W-M] is as follows:
916
$$P(X_{pl} < X < X_{ph}, Y_{pl} < Y < Y_{ph}, Z < Z_{pl}, W_{pl} < W < W_{ph})$$

$$= C(u_{ph}, v_{ph}, r_{pl}, s_{ph}) - C(u_{ph}, v_{ph}, r_{pl}, s_{pl}) - C(u_{ph}, v_{pl}, r_{pl}, s_{ph})$$

$$-C(u_{pl}, v_{ph}, r_{pl}, s_{ph}) + C(u_{ph}, v_{pl}, r_{pl}, s_{pl}) + C(u_{pl}, v_{ph}, r_{pl}, s_{pl})$$

$$+C(u_{pl}, v_{pl}, r_{pl}, s_{ph}) - C(u_{pl}, v_{pl}, r_{pl}, s_{pl})$$
- 917 (70) The probability of Type [X-M, Y-L, Z-M, W-M] is as follows:
918
$$P(X_{pl} < X < X_{ph}, Y < Y_{pl}, Z_{pl} < Z < Z_{ph}, W_{pl} < W < W_{ph})$$

$$= C(u_{ph}, v_{pl}, r_{ph}, s_{ph}) - C(u_{pl}, v_{pl}, r_{ph}, s_{ph}) - C(u_{ph}, v_{pl}, r_{pl}, s_{ph})$$

$$-C(u_{ph}, v_{pl}, r_{pl}, s_{pl}) + C(u_{ph}, v_{pl}, r_{pl}, s_{pl}) + C(u_{pl}, v_{pl}, r_{ph}, s_{pl})$$

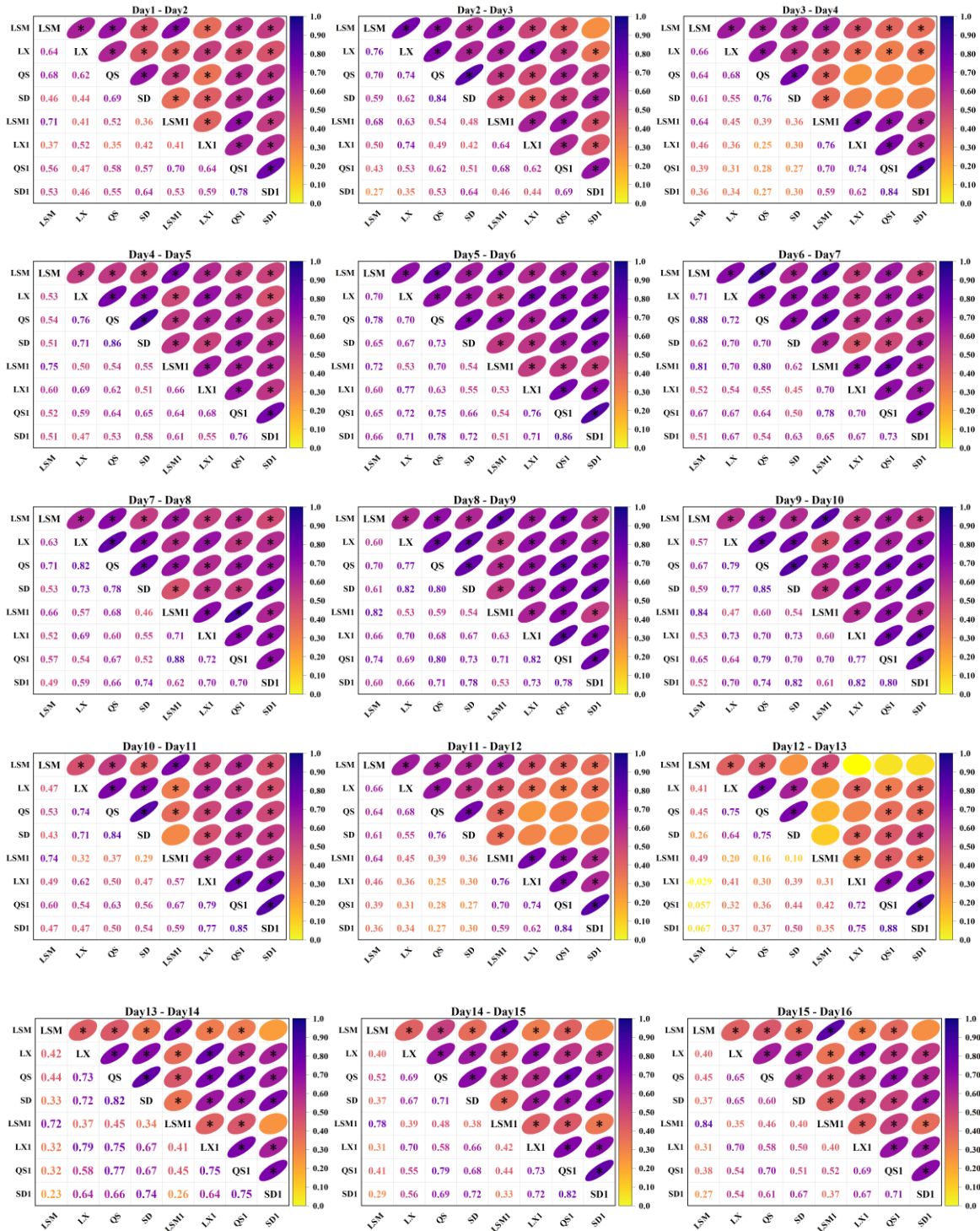
$$+C(u_{pl}, v_{pl}, r_{pl}, s_{ph}) - C(u_{pl}, v_{pl}, r_{pl}, s_{pl})$$
- 919 (71) The probability of Type [X-L, Y-M, Z-M, W-M] is as follows:
920
$$P(X < X_{pl}, Y_{pl} < Y < Y_{ph}, Z_{pl} < Z < Z_{ph}, W_{pl} < W < W_{ph})$$

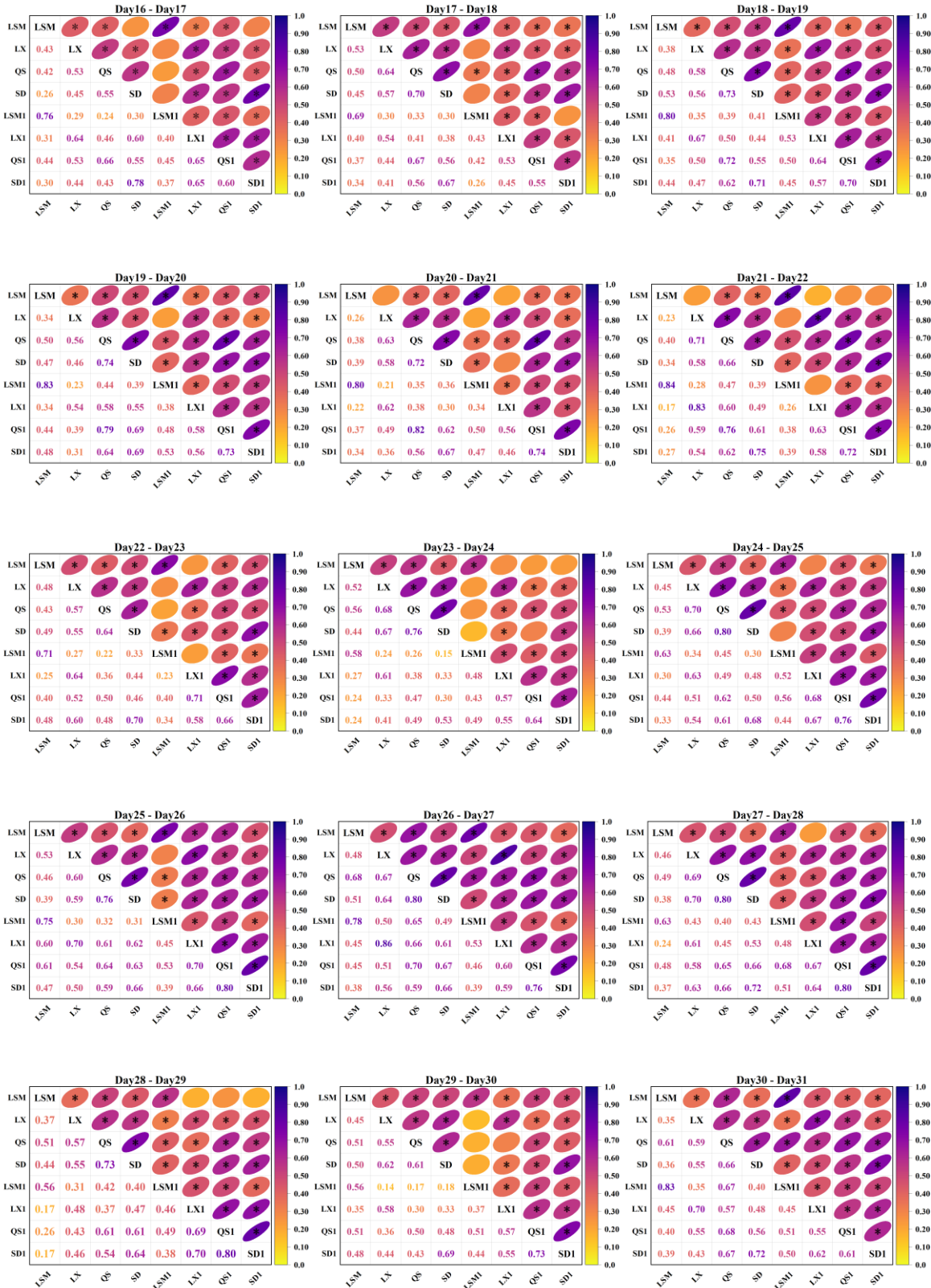
$$= C(u_{pl}, v_{ph}, r_{ph}, s_{ph}) - C(u_{pl}, v_{pl}, r_{ph}, s_{ph}) - C(u_{pl}, v_{ph}, r_{pl}, s_{ph})$$

$$-C(u_{pl}, v_{ph}, r_{ph}, s_{pl}) + C(u_{pl}, v_{ph}, r_{pl}, s_{pl}) + C(u_{pl}, v_{pl}, r_{ph}, s_{pl})$$

$$+C(u_{pl}, v_{pl}, r_{pl}, s_{ph}) - C(u_{pl}, v_{pl}, r_{pl}, s_{pl})$$

- 921 (72) The probability of Type [X-M, Y-M, Z-L, W-L] is as follows:
- $$922 \quad \begin{aligned} & P(X_{pl} < X < X_{ph}, Y_{pl} < Y < Y_{ph}, Z < Z_{pl}, W < W_{pl}) \\ & = C(u_{ph}, v_{ph}, r_{pl}, s_{pl}) - C(u_{ph}, v_{pl}, r_{pl}, s_{pl}) - C(u_{pl}, v_{ph}, r_{pl}, s_{pl}) \\ & \quad + C(u_{pl}, v_{pl}, r_{pl}, s_{pl}) \end{aligned}$$
- 923 (73) The probability of Type [X-M, Y-L, Z-M, W-L] is as follows:
- $$924 \quad \begin{aligned} & P(X_{pl} < X < X_{ph}, Y < Y_{pl}, Z_{pl} < Z < Z_{ph}, W < W_{pl}) \\ & = C(u_{ph}, v_{pl}, r_{ph}, s_{pl}) - C(u_{ph}, v_{pl}, r_{pl}, s_{pl}) - C(u_{pl}, v_{pl}, r_{ph}, s_{pl}) \\ & \quad + C(u_{pl}, v_{pl}, r_{pl}, s_{pl}) \end{aligned}$$
- 925 (74) The probability of Type [X-M, Y-L, Z-L, W-M] is as follows:
- $$926 \quad \begin{aligned} & P(X_{pl} < X < X_{ph}, Y < Y_{pl}, Z < Z_{pl}, W_{pl} < W < W_{ph}) \\ & = C(u_{ph}, v_{pl}, r_{pl}, s_{ph}) - C(u_{ph}, v_{pl}, r_{pl}, s_{pl}) - C(u_{pl}, v_{pl}, r_{pl}, s_{ph}) \\ & \quad + C(u_{pl}, v_{pl}, r_{pl}, s_{pl}) \end{aligned}$$
- 927 (75) The probability of Type [X-L, Y-M, Z-M, W-L] is as follows:
- $$928 \quad \begin{aligned} & P(X < X_{pl}, Y_{pl} < Y < Y_{ph}, Z_{pl} < Z < Z_{ph}, W < W_{pl}) \\ & = C(u_{pl}, v_{ph}, r_{ph}, s_{pl}) - C(u_{pl}, v_{ph}, r_{pl}, s_{pl}) - C(u_{pl}, v_{pl}, r_{ph}, s_{pl}) \\ & \quad + C(u_{pl}, v_{pl}, r_{pl}, s_{pl}) \end{aligned}$$
- 929 (76) The probability of Type [X-L, Y-M, Z-L, W-M] is as follows:
- $$930 \quad \begin{aligned} & P(X < X_{pl}, Y_{pl} < Y < Y_{ph}, Z < Z_{pl}, W_{pl} < W < W_{ph}) \\ & = C(u_{pl}, v_{ph}, r_{pl}, s_{ph}) - C(u_{pl}, v_{ph}, r_{pl}, s_{pl}) - C(u_{pl}, v_{pl}, r_{pl}, s_{ph}) \\ & \quad + C(u_{pl}, v_{pl}, r_{pl}, s_{pl}) \end{aligned}$$
- 931 (77) The probability of Type [X-L, Y-L, Z-M, W-M] is as follows:
- $$932 \quad \begin{aligned} & P(X < X_{pl}, Y < Y_{pl}, Z_{pl} < Z < Z_{ph}, W_{pl} < W < W_{ph}) \\ & = C(u_{pl}, v_{pl}, r_{ph}, s_{ph}) - C(u_{pl}, v_{pl}, r_{pl}, s_{ph}) - C(u_{pl}, v_{pl}, r_{ph}, s_{pl}) \\ & \quad + C(u_{pl}, v_{pl}, r_{pl}, s_{pl}) \end{aligned}$$
- 933 (78) The probability of Type [X-M, Y-L, Z-L, W-L] is as follows:
- $$934 \quad \begin{aligned} & P(X_{pl} < X < X_{ph}, Y < Y_{pl}, Z < Z_{pl}, W < W_{pl}) \\ & = C(u_{ph}, v_{pl}, r_{pl}, s_{pl}) - C(u_{pl}, v_{pl}, r_{pl}, s_{pl}) \end{aligned}$$
- 935 (79) The probability of Type [X-L, Y-M, Z-L, W-L] is as follows:
- $$936 \quad \begin{aligned} & P(X < X_{pl}, Y_{pl} < Y < Y_{ph}, Z < Z_{pl}, W < W_{pl}) \\ & = C(u_{pl}, v_{ph}, r_{pl}, s_{pl}) - C(u_{pl}, v_{pl}, r_{pl}, s_{pl}) \end{aligned}$$
- 937 (80) The probability of Type [X-L, Y-L, Z-M, W-L] is as follows:
- $$938 \quad \begin{aligned} & P(X < X_{pl}, Y < Y_{pl}, Z_{pl} < Z < Z_{ph}, W < W_{pl}) \\ & = C(u_{pl}, v_{pl}, r_{ph}, s_{pl}) - C(u_{pl}, v_{pl}, r_{pl}, s_{pl}) \end{aligned}$$
- 939 (81) The probability of Type [X-L, Y-L, Z-L, W-M] is as follows:
- $$940 \quad \begin{aligned} & P(X < X_{pl}, Y < Y_{pl}, Z < Z_{pl}, W_{pl} < W < W_{ph}) \\ & = C(u_{pl}, v_{pl}, r_{pl}, s_{ph}) - C(u_{pl}, v_{pl}, r_{pl}, s_{pl}) \end{aligned}$$
- 941





943 Figure C1. Results of correlation analysis for daily runoff at multiple sites

944

945 **Appendix D**

946 A total of twelve different distribution functions were employed to fit the daily runoff flows at the four
 947 points for each day in August. ~~For each of the 31 days in August, the preferred marginal distribution~~
 948 ~~functions and their corresponding parameters for each variable can be seen in Table D1.~~ Figure D1 shows
 949 the preferred marginal distribution functions for each variable over month of August.

950 **Table D1 Marginal distributions and parameters preferred for each variable on August 1st-31st**

Date	variable	distribution	shape	loc	scale	mean	rate	meanlog	sdlog	alpha
1	LSM	gamma	0.379	—	—	—	0.106	—	—	—
	LX	gev	0.583	0.246	0.274	—	—	—	—	—
	QS	gev	0.578	1.890	2.056	—	—	—	—	—
	SD	gev	0.643	3.716	3.670	—	—	—	—	—
2	LSM	gev	0.539	0.854	1.434	—	—	—	—	—
	LX	invgauss	0.260	—	—	0.715	—	—	—	—
	QS	gev	0.539	1.964	1.986	—	—	—	—	—
3	SD	llogis	1.527	—	5.206	—	—	—	—	—
	LSM	lnorm	—	—	—	—	—	-0.437	2.817	—
	LX	invgauss	0.182	—	—	1.835	—	—	—	—
	QS	lnorm	—	—	—	—	—	1.166	1.425	—
4	SD	invgauss	3.541	—	—	15.295	—	—	—	—
	LSM	gev	0.646	1.265	2.495	—	—	—	—	—
	LX	lnorm	—	—	—	—	—	-0.664	1.445	—
	QS	gpd	-0.202	-0.715	9.321	—	—	—	—	—
5	SD	gpd	0.000	-0.350	15.000	—	—	—	—	—
	LSM	weibull	0.433	—	3.195	—	—	—	—	—
	LX	gev	0.888	0.250	0.385	—	—	—	—	—
	QS	invgauss	2.133	—	—	8.328	—	—	—	—
6	SD	gev	0.626	4.946	5.406	—	—	—	—	—
	LSM	gamma	0.402	—	—	—	0.090	—	—	—

	LX	llogis	1.277	—	0.324	—	—	—	—	—
	QS	gev	0.688	1.545	1.486	—	—	—	—	—
	SD	llogis	1.495	—	5.761	—	—	—	—	—
	LSM	gev	0.365	1.537	2.783	—	—	—	—	—
7	LX	llogis	1.073	—	0.459	—	—	—	—	—
	QS	lnorm	—	—	—	—	—	1.072	1.567	—
	SD	gev	0.836	4.670	5.745	—	—	—	—	—
	LSM	weibull	0.456	—	4.064	—	—	—	—	—
8	LX	invgauss	0.214	—	—	1.749	—	—	—	—
	QS	llogis	0.977	—	3.253	—	—	—	—	—
	SD	gpd	0.846	-0.712	10.057	—	—	—	—	—
	LSM	weibull	0.438	—	5.072	—	—	—	—	—
9	LX	invgauss	0.211	—	—	3.978	—	—	—	—
	QS	lnorm	—	—	—	—	—	1.368	1.887	—
	SD	lnorm	—	—	—	—	—	2.433	1.905	—
	LSM	weibull	0.358	—	6.476	—	—	—	—	—
10	LX	lnorm	—	—	—	—	—	-0.005	2.051	—
	QS	lnorm	—	—	—	—	—	1.678	2.274	—
	SD	lnorm	—	—	—	—	—	2.720	2.410	—
	LSM	weibull	0.474	—	6.926	—	—	—	—	—
11	LX	lnorm	—	—	—	—	—	0.127	1.718	—
	QS	lnorm	—	—	—	—	—	1.899	1.923	—
	SD	llogis	0.929	—	16.980	—	—	—	—	—
	LSM	llogis	0.885	—	1.786	—	—	—	—	—
12	LX	invgauss	0.542	—	—	1.797	—	—	—	—
	QS	invgauss	2.772	—	—	14.129	—	—	—	—
	SD	invgauss	7.912	—	—	37.729	—	—	—	—
	LSM	gpd	0.216	-0.976	7.565	—	—	—	—	—
13	LX	weibull	0.796	—	1.774	—	—	—	—	—

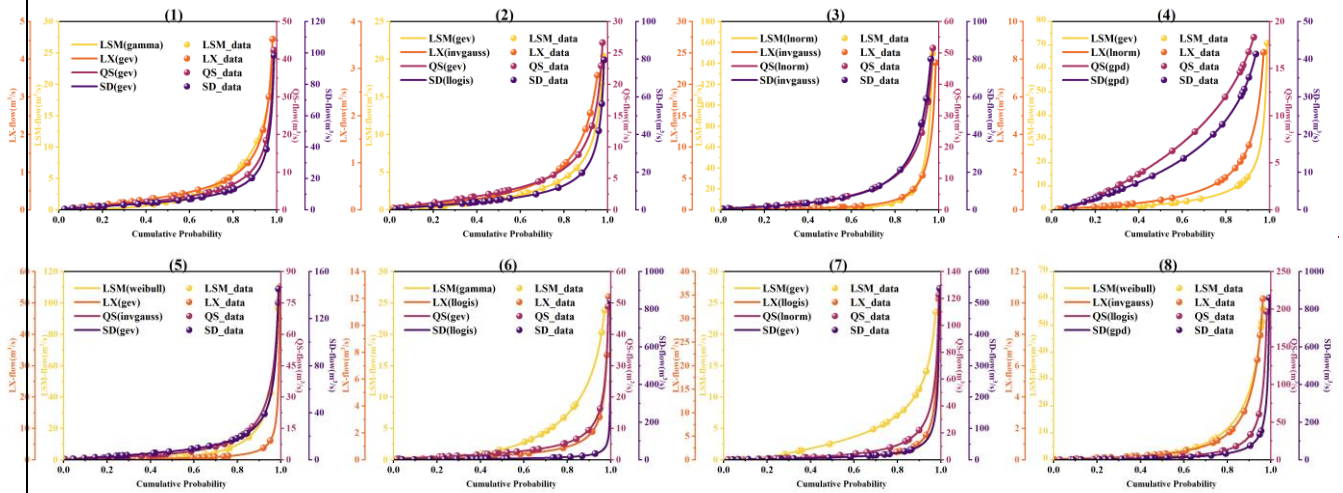
	QS	gpd	0.299	-0.095	10.472	—	—	—	—	—
	SD	invgauss	10.011	—	—	33.990	—	—	—	—
	LSM	gev	0.608	1.580	2.722	—	—	—	—	—
14	LX	invgauss	0.432	—	—	1.527	—	—	—	—
	QS	invgauss	3.695	—	—	14.640	—	—	—	—
	SD	invgauss	8.444	—	—	31.374	—	—	—	—
	LSM	gev	0.436	1.242	2.118	—	—	—	—	—
15	LX	gumbel	—	—	0.655	—	—	—	—	0.515
	QS	invgauss	3.225	—	—	7.595	—	—	—	—
	SD	invgauss	7.520	—	—	18.606	—	—	—	—
	LSM	weibull	0.506	—	2.783	—	—	—	—	—
16	LX	invgauss	0.360	—	—	1.148	—	—	—	—
	QS	invgauss	2.943	—	—	9.336	—	—	—	—
	SD	gpd	0.359	0.529	13.680	—	—	—	—	—
	LSM	weibull	0.479	—	2.907	—	—	—	—	—
17	LX	weibull	0.897	—	0.952	—	—	—	—	—
	QS	gpd	0.385	-0.580	6.729	—	—	—	—	—
	SD	invgauss	6.433	—	—	19.990	—	—	—	—
	LSM	gev	0.552	1.252	2.482	—	—	—	—	—
18	LX	gev	0.492	0.411	0.493	—	—	—	—	—
	QS	gpd	0.300	-0.632	7.393	—	—	—	—	—
	SD	lnorm	—	—	—	—	—	2.290	1.315	—
	LSM	weibull	0.452	—	3.243	—	—	—	—	—
19	LX	invgauss	0.301	—	—	1.595	—	—	—	—
	QS	invgauss	2.268	—	—	14.869	—	—	—	—
	SD	gpd	0.618	-0.297	11.762	—	—	—	—	—
	LSM	lnorm	—	—	—	—	—	-0.048	2.580	—
20	LX	llgis	1.246	—	0.593	—	—	—	—	—
	QS	invgauss	1.989	—	—	25.636	—	—	—	—

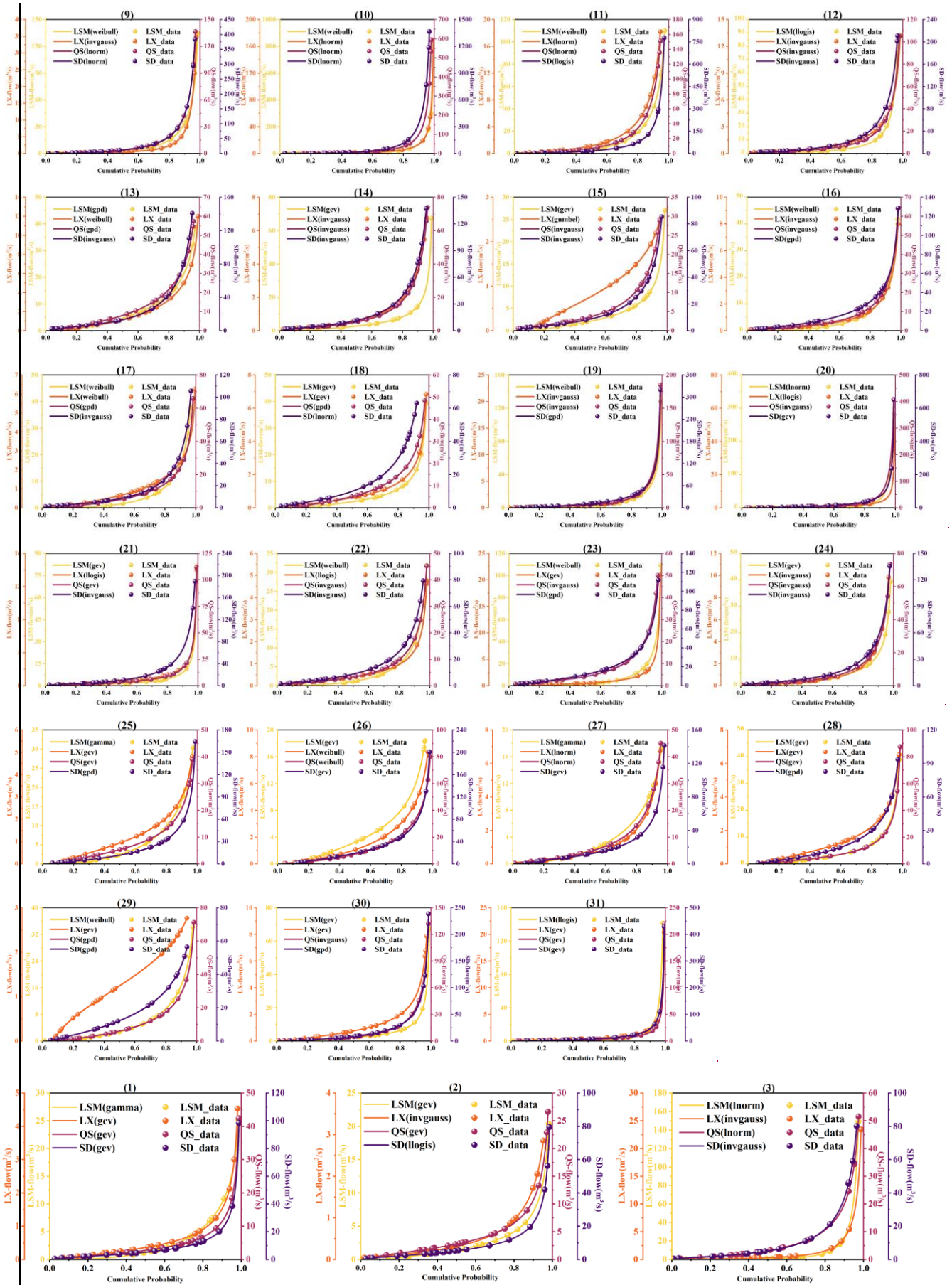
	SD	gev	0.818	6.508	9.642	—	—	—	—	—
	LSM	gev	0.779	0.859	1.315	—	—	—	—	—
21	LX	Hogis	1.522	—	0.528	—	—	—	—	—
	QS	gev	0.738	2.163	2.485	—	—	—	—	—
	SD	invgauss	7.401	—	—	27.102	—	—	—	—
	LSM	weibull	0.521	—	2.298	—	—	—	—	—
22	LX	Hogis	1.595	—	0.402	—	—	—	—	—
	QS	invgauss	2.757	—	—	7.322	—	—	—	—
	SD	invgauss	7.626	—	—	19.094	—	—	—	—
	LSM	weibull	0.460	—	3.114	—	—	—	—	—
23	LX	gev	0.764	0.294	0.402	—	—	—	—	—
	QS	invgauss	3.491	—	—	9.169	—	—	—	—
	SD	gpd	0.345	0.923	13.719	—	—	—	—	—
	LSM	gev	0.619	1.204	2.195	—	—	—	—	—
24	LX	invgauss	0.293	—	—	1.625	—	—	—	—
	QS	invgauss	2.790	—	—	10.814	—	—	—	—
	SD	invgauss	7.810	—	—	23.039	—	—	—	—
	LSM	gamma	0.438	—	—	—	0.073	—	—	—
25	LX	gev	0.238	0.632	0.797	—	—	—	—	—
	QS	gev	0.403	3.483	4.696	—	—	—	—	—
	SD	gpd	0.387	0.057	14.586	—	—	—	—	—
	LSM	gev	0.348	2.009	3.077	—	—	—	—	—
26	LX	weibull	0.789	—	1.674	—	—	—	—	—
	QS	weibull	0.759	—	11.716	—	—	—	—	—
	SD	gev	0.439	12.256	17.061	—	—	—	—	—
	LSM	gamma	0.533	—	—	—	0.127	—	—	—
27	LX	lnorm	—	—	—	—	—	-0.472	1.424	—
	QS	lnorm	—	—	—	—	—	1.549	1.321	—
	SD	gev	0.555	7.945	9.853	—	—	—	—	—

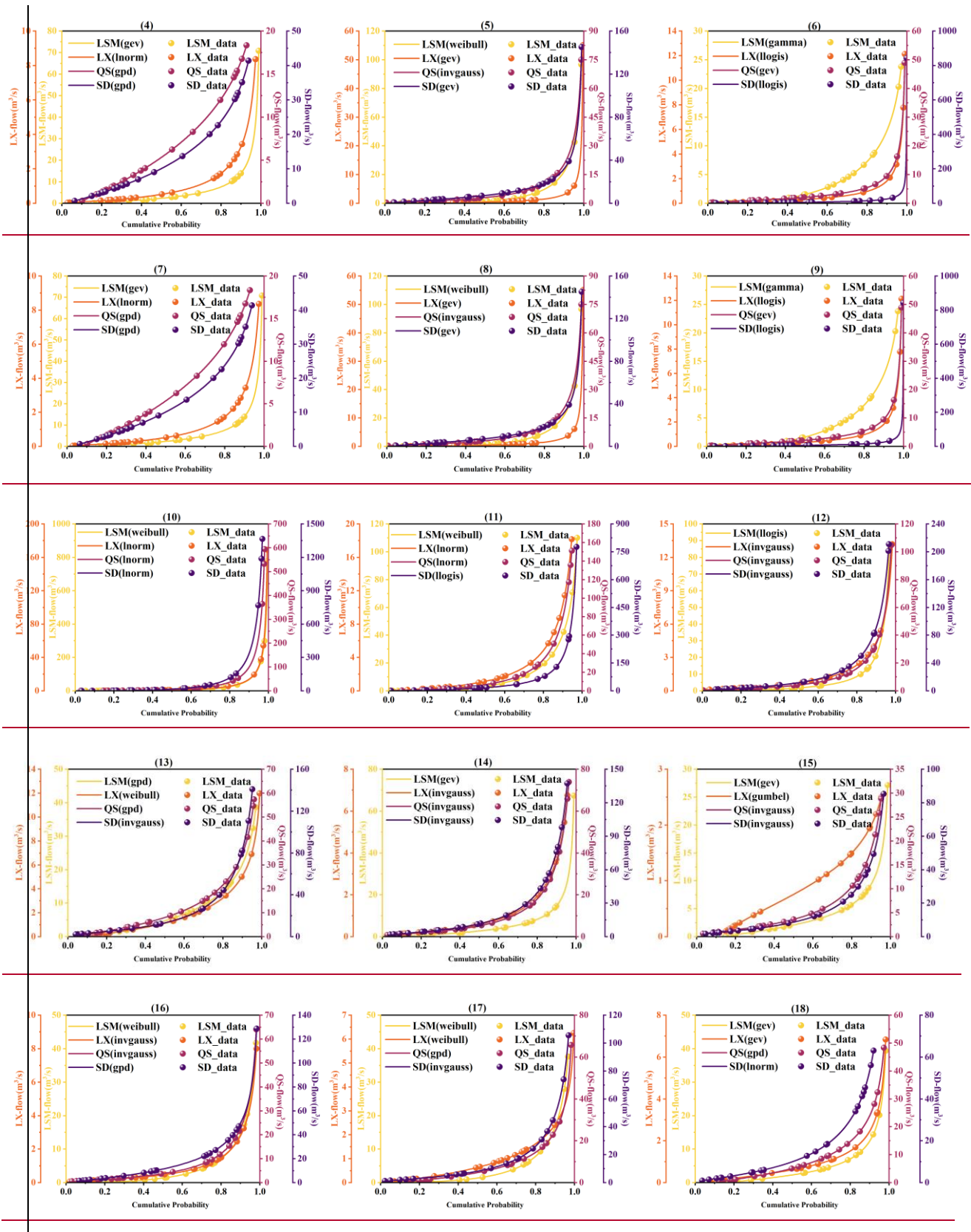
28	LSM	gev	0.604	1.375	2.510	—	—	—	—
	LX	gev	0.318	0.640	0.823	—	—	—	—
	QS	gev	0.605	3.316	4.562	—	—	—	—
	SD	gpd	0.328	-0.247	14.191	—	—	—	—
29	LSM	weibull	0.661	—	4.721	—	—	—	—
	LX	gev	-0.186	0.938	0.851	—	—	—	—
	QS	gpd	0.316	-0.775	8.682	—	—	—	—
30	SD	gpd	0.107	-0.389	17.428	—	—	—	—
	LSM	gev	0.699	1.338	1.895	—	—	—	—
	LX	gev	0.547	0.500	0.639	—	—	—	—
	QS	invgauss	3.152	—	—	15.179	—	—	—
31	SD	gpd	0.651	-0.480	10.676	—	—	—	—
	LSM	llogis	0.868	—	1.232	—	—	—	—
	LX	gev	0.792	0.313	0.325	—	—	—	—
	QS	gev	0.858	1.962	2.066	—	—	—	—
	SD	gev	0.814	4.883	6.333	—	—	—	—

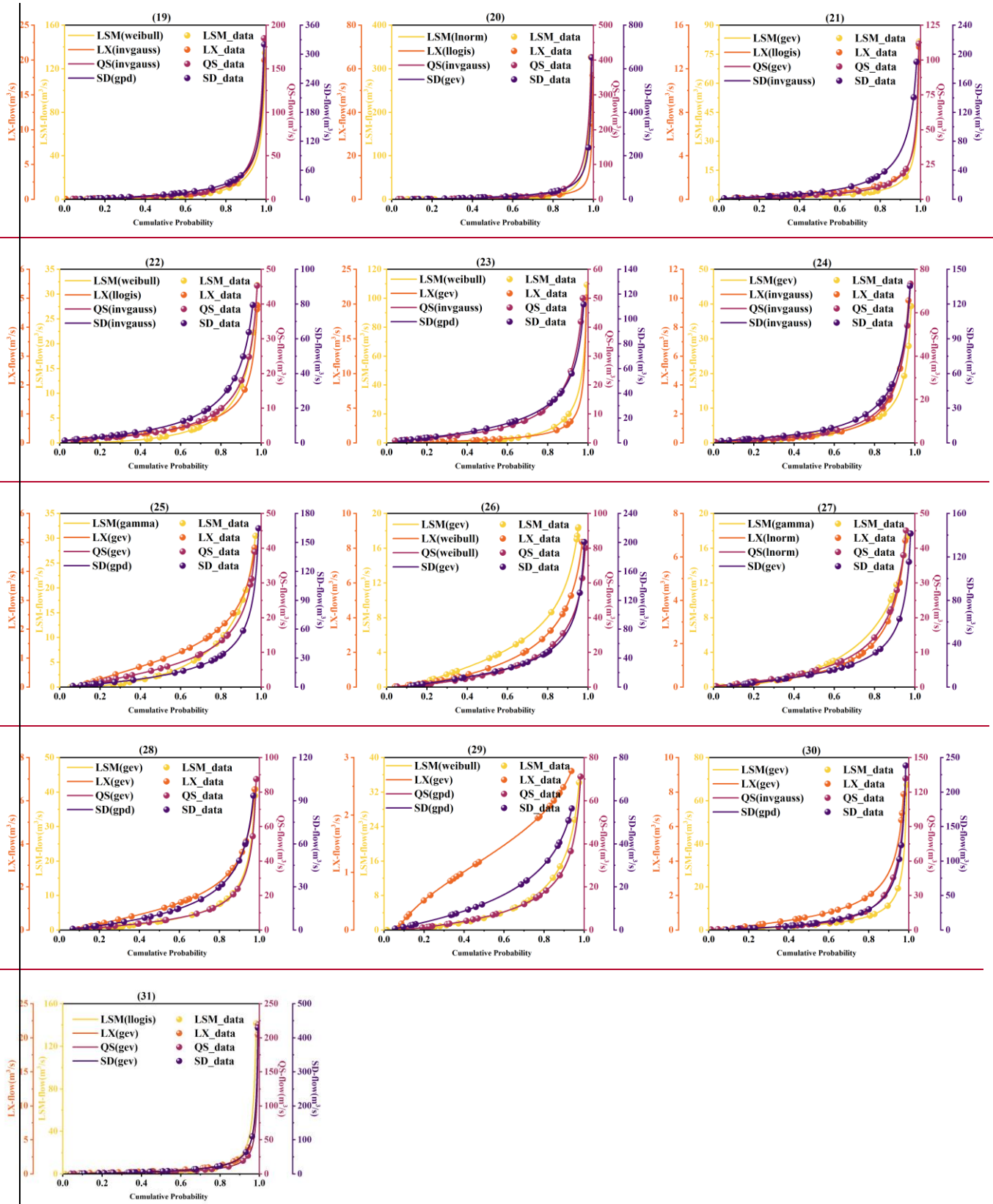
951

952









953 Figure D1. Cumulative probability distribution of the preferred marginal distribution function for runoff

954 on each day throughout August

955 **Code availability**

956 The developed routines for working with conditional joint probability density functions are publicly
957 available via the rvinecopulib R package (<https://github.com/vinecopulib/rvinecopulib>) and
958 CDVineCopulaConditional R package (<https://github.com/cran/CDVineCopulaConditional>). Other
959 codes used to support the findings of this study are available from the authors upon request.

960 **Data Availability**

961 Streamflow can be checked from hydrology information of Taizhou City at
962 <http://www.shui00.com/ZhswFloodWater/web/html/index.html?module=wssyq>. Other data used to
963 support the findings of this study are available from the corresponding author upon request.

964 **Author contribution**

965 XY and YPX designed the research. HG and SC collected and preprocessed the data. XY and YG
966 conducted all the experiments and analyzed the results. SC assisted with the paper's background. XY
967 wrote the first draft of the manuscript with contributions from YPX. YPX supervised the study and edited
968 the manuscript.

969 **Competing interests**

970 At least one of the (co-)authors is a member of the editorial board of Hydrology and Earth System Science.

971 **Disclaimer**

972 Copernicus Publications remains neutral with regard to jurisdictional claims in published maps and
973 institutional affiliations.

974 **Acknowledgments**

975 This study is supported by the Key Research and Development Program of Zhejiang Province

976 (2021C03017), the National Key Research and Development Program of China (2021YFD1700802) and
977 the Natural Science Foundation of Zhejiang Province (LY23E090001). Taizhou Municipal Bureau of
978 Water Resources is greatly acknowledged for providing meteorological and hydrological data used in the
979 study area.

980 Reference

- 981 Aas, K., Czado, C., Frigessi, A., Bakken, H., 2009. Pair-copula constructions of multiple dependence.
982 Insurance: Mathematics and Economics 44, 182–198.
983 <https://doi.org/10.1016/j.insmatheco.2007.02.001>
- 984 Ahn, K.-H., 2021. Streamflow estimation at partially gaged sites using multiple-dependence conditions
985 via vine copulas. Hydrology and Earth System Sciences 25, 4319–4333.
986 <https://doi.org/10.5194/hess-25-4319-2021>
- 987 Bedford, T., Cooke, R.M., 2002. Vines--a new graphical model for dependent random variables. The
988 Annals of Statistics 30, 1031–1068. <https://doi.org/10.1214/aos/1031689016>
- 989 Bedford, T., Cooke, R.M., 2001. Probability Density Decomposition for Conditionally Dependent
990 Random Variables Modeled by Vines. Annals of Mathematics and Artificial Intelligence 32,
991 245–268.
- 992 Bedford, T.J., Cooke, R., 2001. Monte Carlo simulation of vine dependent random variables for
993 applications in uncertainty analysis. Proceedings of Esrel.
- 994 Bekker, P., Wansbeek, T., 2001. A companion to theoretical econometrics. Blackwell publishing.
- 995 Box, G.E.P., Jenkins, G.M., Reinsel, C., 2013. Time series analysis: forecasting and control (third ed).
- 996 Brechmann, E.C., Schepsmeier, U., 2013. Modeling Dependence with C- and D-Vine Copulas: The *R*
997 Package CDVine. J. Stat. Soft. 52. <https://doi.org/10.18637/jss.v052.i03>
- 998 Çekin, S.E., Pradhan, A.K., Tiwari, A.K., Gupta, R., 2020. Measuring co-dependencies of economic
999 policy uncertainty in Latin American countries using vine copulas. The Quarterly Review of
1000 Economics and Finance 76, 207–217. <https://doi.org/10.1016/j.qref.2019.07.004>
- 1001 Chen, L., Singh, V.P., Guo, S., Zhou, J., Zhang, J., 2015. Copula-based method for multisite monthly and
1002 daily streamflow simulation. J. Hydrol. 528, 369–384.
1003 <https://doi.org/10.1016/j.jhydrol.2015.05.018>

1004 Coles, S.G., 2001. An introduction to statistical modeling of extreme values. - springer. An introduction
1005 to statistical modeling of extreme values. - springer.

1006 CredCrunch70.pdf, n.d.

1007 Daneshkhah, A., Remesan, R., Chatrabgoun, O., Holman, I.P., 2016. Probabilistic modeling of flood
1008 characterizations with parametric and minimum information pair-copula model. Journal of
1009 Hydrology 540, 469–487. <https://doi.org/10.1016/j.jhydrol.2016.06.044>

1010 De Michele, C., Salvadori, G., 2003. A Generalized Pareto intensity-duration model of storm rainfall
1011 exploiting 2-Copulas. Journal of Geophysical Research: Atmospheres 108.
1012 <https://doi.org/10.1029/2002JD002534>

1013 Gao, C., Booij, M.J., Xu, Y.-P., 2020. Development and hydrometeorological evaluation of a new
1014 stochastic daily rainfall model: Coupling Markov chain with rainfall event model. J. Hydrol.
1015 589, 125337. <https://doi.org/10.1016/j.jhydrol.2020.125337>

1016 Gao, C., Guan, X., Booij, M.J., Meng, Y., Xu, Y.-P., 2021. A new framework for a multi-site stochastic
1017 daily rainfall model: Coupling a univariate Markov chain model with a multi-site rainfall event
1018 model. J. Hydrol. 598, 126478. <https://doi.org/10.1016/j.jhydrol.2021.126478>

1019 Gao, X., Liu, Y., Sun, B., 2018. Water shortage risk assessment considering large-scale regional transfers:
1020 a copula-based uncertainty case study in Lunan, China. Environ. Sci. Pollut. Res. 25, 23328–
1021 23341. <https://doi.org/10.1007/s11356-018-2408-1>

1022 Gelman, A., Carlin, J.B., Stern, H.S., Rubin, D.B., 2013. Bayesian Data Analysis, Third Edition (Texts
1023 in Statistical Science). Crc Press.

1024 Hao, Z., Singh, V.P., 2013. Modeling multisite streamflow dependence with maximum entropy copula.
1025 Water Resources Research 49, 7139–7143. <https://doi.org/10.1002/wrcr.20523>

1026 Huang, K., Ye, L., Chen, L., Wang, Q., Dai, L., Zhou, J., Singh, V.P., Huang, M., Zhang, J., 2018. Risk
1027 analysis of flood control reservoir operation considering multiple uncertainties. J. Hydrol. 565,
1028 672–684. <https://doi.org/10.1016/j.jhydrol.2018.08.040>

1029 Isaaks, E.H., Srivastava, M.R., 1989. An Introduction to Applied Geostatistics. false.

1030 Khan, M., Chen, L., Markus, M., Bhattarai, R., n.d. A probabilistic approach to characterize the joint
1031 occurrence of two extreme precipitation indices in the upper Midwestern United States. JAWRA
1032 Journal of the American Water Resources Association n/a. <https://doi.org/10.1111/1752->

1033 1688.13187

1034 Li, R., Xiong, L., Jiang, C., Li, W., Liu, C., 2022. Quantifying multivariate flood risk under nonstationary
1035 condition. *Nat Hazards*. <https://doi.org/10.1007/s11069-022-05716-x>

1036 Liu, Z., Cheng, L., Hao, Z., Li, J., Thorstensen, A., Gao, H., 2018. A Framework for Exploring Joint
1037 Effects of Conditional Factors on Compound Floods. *Water Resour. Res.* 54, 2681–2696.
1038 <https://doi.org/10.1002/2017WR021662>

1039 Nazeri Tahroudi, M., Ahmadi, F., Mirabbasi, R., 2023. Performance comparison of IHACRES, random
1040 forest and copula-based models in rainfall-runoff simulation. *Appl Water Sci* 13, 134.
1041 <https://doi.org/10.1007/s13201-023-01929-y>

1042 Nazeri Tahroudi, M., Ramezani, Y., De Michele, C., Mirabbasi, R., 2022. Trivariate joint frequency
1043 analysis of water resources deficiency signatures using vine copulas. *Appl Water Sci* 12, 67.
1044 <https://doi.org/10.1007/s13201-022-01589-4>

1045 Pereira, G., Veiga, Á., 2018. PAR(p)-vine copula based model for stochastic streamflow scenario
1046 generation. *Stoch Environ Res Risk Assess* 32, 833–842. <https://doi.org/10.1007/s00477-017->
1047 1411-2

1048 Prohaska, S., Ilic, A., 2010. Coincidence of Flood Flow of the Danube River and Its Tributaries, in: Brilly,
1049 M. (Ed.), *Hydrological Processes of the Danube River Basin: Perspectives from the Danubian*
1050 *Countries*. Springer Netherlands, Dordrecht, pp. 175–226. <https://doi.org/10.1007/978-90-481->
1051 3423-6_6

1052 Qian, L., Wang, X., Hong, M., Dang, S., Wang, H., 2022. Encounter risk prediction of rich-poor
1053 precipitation using a combined copula. *Theor Appl Climatol* 149, 1057–1067.
1054 <https://doi.org/10.1007/s00704-022-04092-7>

1055 Ren, K., Huang, S., Huang, Q., Wang, H., Leng, G., Fang, W., Li, P., 2020. Assessing the reliability,
1056 resilience and vulnerability of water supply system under multiple uncertain sources. *Journal of*
1057 *Cleaner Production* 252, 119806. <https://doi.org/10.1016/j.jclepro.2019.119806>

1058 Sklar, A., 1959. Fonctions de Repartition a n Dimensions et Leurs Marges. *Publ.inst.statist.univ.paris*.

1059 Stedinger, J.R., Vogel, R.M., Foufoula-Georgiou, E., 1993. *Frequency Analysis of Extreme Events*.
1060 handbook of hydrology.

1061 Szilagyi, J., Balint, G., Csik, A., 2006. Hybrid, Markov Chain-Based Model for Daily Streamflow

1062 Generation at Multiple Catchment Sites. *Journal of Hydrologic Engineering* 11, 245–256.
1063 [https://doi.org/10.1061/\(ASCE\)1084-0699\(2006\)11:3\(245\)](https://doi.org/10.1061/(ASCE)1084-0699(2006)11:3(245))

1064 Tahroudi, M.N., Mohammadi, M., Khalili, K., 2022. The application of the hybrid copula-GARCH
1065 approach in the simulation of extreme discharge values. *Appl. Water Sci.* 12, 274.
1066 <https://doi.org/10.1007/s13201-022-01788-z>

1067 Teng, J., Jakeman, A.J., Vaze, J., Croke, B.F.W., Dutta, D., Kim, S., 2017. Flood inundation modelling:
1068 A review of methods, recent advances and uncertainty analysis. *Environmental Modelling &*
1069 *Software* 90, 201–216. <https://doi.org/10.1016/j.envsoft.2017.01.006>

1070 Tosunoğlu, F., 2018. Accurate estimation of T year extreme wind speeds by considering different model
1071 selection criteria and different parameter estimation methods. *Energy* 162, 813–824.
1072 <https://doi.org/10.1016/j.energy.2018.08.074>

1073 Tosunoglu, F., Gurbuz, F., Ispirli, M.N., 2020. Multivariate modeling of flood characteristics using Vine
1074 copulas. *Environ. Earth Sci.* 79, 459. <https://doi.org/10.1007/s12665-020-09199-6>

1075 Wang, S., Zhong, P.-A., Zhu, F., Xu, C., Wang, Y., Liu, W., 2022. Analysis and Forecasting of Wetness-
1076 Dryness Encountering of a Multi-Water System Based on a Vine Copula Function-Bayesian
1077 Network. *Water* 14, 1701. <https://doi.org/10.3390/w14111701>

1078 Wang, W., Dong, Z., Lall, U., Dong, N., Yang, M., 2019. Monthly Streamflow Simulation for the
1079 Headwater Catchment of the Yellow River Basin With a Hybrid Statistical-Dynamical Model.
1080 *Water Resources Research* 55, 7606–7621. <https://doi.org/10.1029/2019WR025103>

1081 Wang, W., Dong, Z., Zhu, F., Cao, Q., Chen, J., Yu, X., 2018. A Stochastic Simulation Model for Monthly
1082 River Flow in Dry Season. *Water* 10, 1654. <https://doi.org/10.3390/w10111654>

1083 Wang, X., Shen, Y.-M., 2023a. R-statistic based predictor variables selection and vine structure
1084 determination approach for stochastic streamflow generation considering temporal and spatial
1085 dependence. *Journal of Hydrology* 617, 129093. <https://doi.org/10.1016/j.jhydrol.2023.129093>

1086 Wang, X., Shen, Y.-M., 2023b. A Framework of Dependence Modeling and Evaluation System for
1087 Compound Flood Events. *Water Resources Research* 59, e2023WR034718.
1088 <https://doi.org/10.1029/2023WR034718>

1089 Wei, C., Wang, X., Fang, J., Wang, Z., Li, C., Liu, Q., Yu, J., 2023. A new method for estimating multi-
1090 source water supply considering joint probability distributions under uncertainty. *Front. Earth*

1091 Sci. 10. <https://doi.org/10.3389/feart.2022.929613>

1092 Wu, Y., Gao, Y., Li, D., 2015. Error Assessment of Multivariate Random Processes Simulated by a
1093 Conditional-Simulation Method. *Journal of Engineering Mechanics* 141, 04014155.
1094 [https://doi.org/10.1061/\(ASCE\)EM.1943-7889.0000877](https://doi.org/10.1061/(ASCE)EM.1943-7889.0000877)

1095 Xu, P., Wang, D., Wang, Y., Singh, V.P., 2022. A Stepwise and Dynamic C-Vine Copula–Based Approach
1096 for Nonstationary Monthly Streamflow Forecasts. *J. Hydrol. Eng.* 27, 04021043.
1097 [https://doi.org/10.1061/\(ASCE\)HE.1943-5584.0002145](https://doi.org/10.1061/(ASCE)HE.1943-5584.0002145)

1098 Xu, Y., Lu, F., Zhou, Y., Ruan, B., Dai, Y., Wang, K., 2022. Dryness–Wetness Encounter Probabilities’
1099 Analysis for Lake Ecological Water Replenishment Considering Non-Stationarity Effects. *Front.*
1100 *Environ. Sci.* 10. <https://doi.org/10.3389/fenvs.2022.806794>

1101 Yu, R., Yang, R., Zhang, C., Spoljar, M., Kuczynska-Kippen, N., Sang, G., 2020. A Vine Copula-Based
1102 Modeling for Identification of Multivariate Water Pollution Risk in an Interconnected River
1103 System Network. *Water* 12, 2741. <https://doi.org/10.3390/w12102741>

1104 Yu, R., Zhang, C., 2021. Early warning of water quality degradation: A copula-based Bayesian network
1105 model for highly efficient water quality risk assessment. *J. Environ. Manage.* 292, 112749.
1106 <https://doi.org/10.1016/j.jenvman.2021.112749>

1107 Zhang, B., Wang, S., Wang, Y., 2021. Probabilistic Projections of Multidimensional Flood Risks at a
1108 Convection-Permitting Scale. *Water Res* 57. <https://doi.org/10.1029/2020WR028582>

1109 Zhang, S., Kang, Y., Gao, X., Chen, P., Cheng, X., Song, S., Li, L., 2023. Optimal reservoir operation
1110 and risk analysis of agriculture water supply considering encounter uncertainty of precipitation
1111 in irrigation area and runoff from upstream. *Agricultural Water Management* 277, 108091.
1112 <https://doi.org/10.1016/j.agwat.2022.108091>

1113 Zhong, M., Zeng, T., Jiang, T., Wu, H., Chen, X., Hong, Y., 2021. A Copula-Based Multivariate
1114 Probability Analysis for Flash Flood Risk under the Compound Effect of Soil Moisture and
1115 Rainfall. *Water Resour. Manag.* 35, 83–98. <https://doi.org/10.1007/s11269-020-02709-y>

1116